AWARD NUMBER: W81XWH-14-1-0625

TITLE: Plasticity and Activation of Spared Intraspinal Respiratory Circuits Following Spinal Cord Injury

PRINCIPAL INVESTIGATOR: Paul J. Reier, Ph.D.

CONTRACTING ORGANIZATION: University of Florida
Gainesville, FL 32611

REPORT DATE: October 2016

TYPE OF REPORT: Annual

PREPARED FOR: U.S. Army Medical Research and Materiel Command
Fort Detrick, Maryland 21702-5012

REPORT DOCUMENTATION PAGE

Form Approved
OMB No. 0704-0188

1. REPORT DATE	**2. REPORT TYPE**	**3. DATES COVERED**
October 2016	Annual	29Sep2015 - 28Sep2016

4. TITLE AND SUBTITLE
Plasticity and Activation of Spared Intraspinal Respiratory Circuits Following Spinal Cord Injury

5a. CONTRACT NUMBER

5b. GRANT NUMBER
W81XWH-14-1-0625

5c. PROGRAM ELEMENT NUMBER

6. AUTHOR(S)
Paul J. Reier, Ph.D. (P. I.)
David D. Fuller, Ph.D. (Key Co-I)
Chet Moritz, Ph.D. (Univ. Washington subcontract Director)

E-Mail: reier@ufl.edu

5d. PROJECT NUMBER

5e. TASK NUMBER

5f. WORK UNIT NUMBER

7. PERFORMING ORGANIZATION NAME(S) AND ADDRESS(ES)

University of Florida
Gainesville, FL 32611-5500

Subcontract: University of Washington
Seattle, Washington 98195-6490

8. PERFORMING ORGANIZATION REPORT NUMBER

9. SPONSORING / MONITORING AGENCY NAME(S) AND ADDRESS(ES)

U.S. Army Medical Research and Materiel Command
Fort Detrick, Maryland 21702-5012

10. SPONSOR/MONITOR'S ACRONYM(S)

11. SPONSOR/MONITOR'S REPORT NUMBER(S)

12. DISTRIBUTION / AVAILABILITY STATEMENT

Approved for Public Release; Distribution Unlimited

13. SUPPLEMENTARY NOTES

14. ABSTRACT

The goal of this project is to determine whether electrical stimulation of the spinal cord can reduce respiratory dysfunctions occurring after mid-to-high cervical spinal cord injuries (cSCI). Our primary focus is intraspinal microstimulation (ISMS) of the phrenic circuit using physiologically-appropriate, endogenous respiratory signals to trigger activation of the phrenic motoneuron (PhMN) pool following either cSCIs above or at the level of the phrenic nucleus in adult rats. A manuscript providing an important proof of concept demonstration has just been published. Our studies have established that ISMS at the level of the PhMN can effectively activate diaphragm motor units following high cSCI even beyond when stimulation ended. Another manuscript demonstrating independent verification of those findings is to be submitted by our colleagues at the University of Washington. Per comments from our proposal's initial review, we also examined the efficacy of high frequency spinal stimulation. Our data indicate this approach is not effective at selectively activating inspiratory diaphragm (phrenic) motor units. A manuscript describing those results has been accepted pending revisions suggested by the reviewers. We are now testing chronic ISMS for improving breathing and promoting new synaptic connections following cSCI.

15. SUBJECT TERMS
Respiration and cervical spinal cord injury, intraspinal microstimulation, epidural stimulation, Neurochip, phrenic.

16. SECURITY CLASSIFICATION OF:			**17. LIMITATION OF ABSTRACT**	**18. NUMBER OF PAGES**	**19a. NAME OF RESPONSIBLE PERSON**
a. REPORT	**b. ABSTRACT**	**c. THIS PAGE**			USAMRMC
Unclassified	Unclassified	Unclassified	Unclassified	88	**19b. TELEPHONE NUMBER** *(include area code)*

Standard Form 298 (Rev. 8-98)
Prescribed by ANSI Std. Z39.18

Table of Contents

1. INTRODUCTION:

Spinal cord injuries (SCIs) within mid- to upper-neck regions (i.e., at or above the fourth cervical level) often result in severely, if not completely, compromised breathing due to disrupted communication between respiratory centers in the brainstem and circuits in the spinal cord that control ventilatory muscles. The diaphragm, which is often considered the primary muscle of inhalation, receives its motor innervation from the phrenic nucleus located at spinal C3-C5. Interruption of respiratory signals from the brainstem to the phrenic nucleus results in uni- or bilateral paralysis of the diaphragm. Severe impairment of diaphragm function requires individuals to receive some form of assisted ventilatory support (e.g., mechanical, phrenic nerve, or diaphragm pacing). Even if some individuals are weaned, patterns of breathing rarely approximate normal, and pulmonary infection-related hospitalizations and deaths remain common. A need thus exists for interventions that can lead to a greater and more normal restoration of diaphragm and other respiratory muscle functions. Studies being conducted under this Department of Defense award are based upon increasing evidence showing that electrical stimulation of the injured spinal cord can elicit some degree of motor function (e.g., standing, limb movements) in animals and humans even with motor complete SCIs. The most common strategy involves epidural stimulation in which an electrical current is delivered to an electrode array placed on the surface of the spinal cord. Other studies have shown, however, that electrical stimulation via tiny microwires inserted directly into spinal cord tissue (intraspinal microstimulation, ISMS) may produce more natural motor output. Epidural, high frequency spinal stimulation has been shown to offer potential for improving aspects of respiratory function, but it is still dependent upon delivery of programmed signals (i.e., open-loop). We are now proposing to explore the capacity of ISMS to improve diaphragm function when delivered to phrenic circuitry in a more closed-loop-like fashion. An innovative feature of our approach is that a custom-designed microcircuit (i.e., the Neurochip) will be used to capture electromyographic (EMG) signals from unaffected respiratory muscles. Those EMGs will then be used to trigger stimulation of the phrenic circuit in a physiologically-appropriate fashion under normal and more demanding ventilatory conditions after SCI. The intriguing possibility also exists this strategy may lead to persistent recovery by directing functional and anatomical circuit remodeling such that functional improvements will no longer require extrinsic stimulation. We will also compare outcomes via epidural vs. ISMS. Overall, we are proposing the first investigation of a promising approach for stimulating plasticity in respiratory circuits. Success of this project will lead to a significant shift in current approaches for managing respiratory dysfunction following cervical SCIs. Knowledge obtained from this study also may have broader implications related to the use of ISMS for treating other aspects of SCI alone or in combination with other interventions.

2. KEYWORDS:

respiration
cervical spinal cord injury
intraspinal microstimulation
epidural stimulation
Neurochip
phrenic nucleus
phrenic motoneurons
phrenic neurograms
hypoglossal nerve
hypercapnia
hypoxia
neuroplasticity
C2 hemisection
mid-cervical contusion injury
interneurons

3. ACCOMPLISHMENTS:

3.a. Opportunities for Training and Professional Development

This project has provided training opportunities for two postdoctoral fellows (Gonzalez-Rothi, Streeter) and two graduate students (Mercier, Sunshine). In each case, the individuals acquired advanced technical training in neurophysiology and respiratory biology. Individuals were also directly involved in data analysis and manuscript preparation.

3.b. *Dissemination of Results*

Two papers have been published and one is in revision as cited under Item 6 below. PDF copies of the published manuscripts are appended to this document. An overview of the paper being revised is presented below (Item 3.b.2). The paper from the Moritz (Univ. Washington) laboratory is still in preparation and was reviewed extensively in a previous Quarterly Progress Report. Relevant details of the two published and one under revision studies performed at the University of Florida are as follows:

3.b.1. Details for Mercier et al., 2017 publication:

As noted in the last Progress Report, our efforts have been directed primarily at showing initial proof of concept efficacy of naturally-triggered (i.e., closed-loop like) cISMS in the C2Hx model. We have recently published our findings in that regard in the *Journal of Neurophysiology (Mercier et al.,2016)*. A corroborating and complementary study has also been performed at the University of Washington by our subcontract project leader, Dr. Chet Moritz, and a paper describing those results is now being prepared for journal submission (Sunshine et al.).

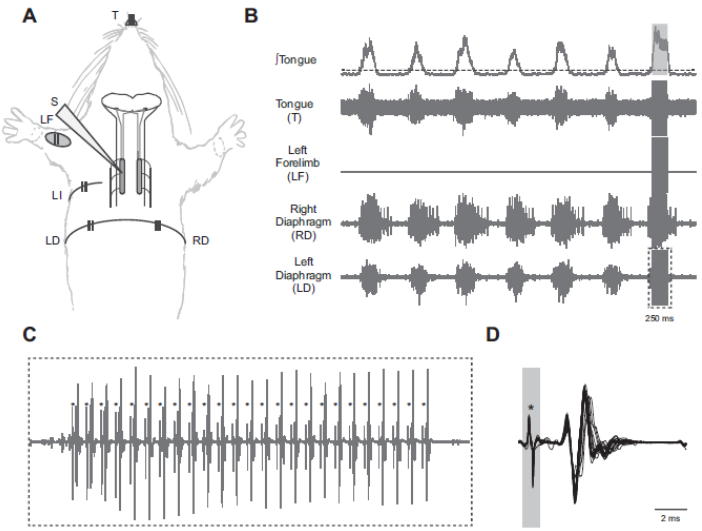

Figure 1. Cervical ISMS activates the ipsilateral diaphragm **A**: schematic diagram illustrates the EMG recording sites relative to the placement of the stimulating electrode (S). The stimulating electrode was placed in the immediate vicinity of the phrenic motor nucleus, and ISMS was initiated via a trigger signal based on inspiratory tongue (genioglossus) EMG activity. LI, left inter-costal. **B**: pre-C2Hx representative EMG recordings from the genioglossus, extensor carpi radialis (ECR), and both sides of the diaphragm showing baseline (prestimulation) activity and a period of genioglossus-triggered cervical ISMS (100 Hz, 200 µA; 0.3-ms pulse duration, 250-ms train duration) represented by a gray box in the tongue trace. **C**: expanded trace of the EMG recording from the left diaphragm during the period of ISMS shows each stimulus artifact, indicated by asterisks, and each subsequent MUAP. **D**: overlay of each elicited MUAP, aligned by the stimulus artifact, demonstrates constant latency and amplitude.

Thirteen female Sprague-Dawley rats (255±16 g; Harlan, Indianapolis, IN) were distributed between two experimental groups: *1*) ISMS after acute SCI, tested before and immediately after lateral hemisection of the spinal cord at C2 (C2Hx) (*n* = 8), and *2*) ISMS after subacute SCI, tested 5–21 days after C2Hx (*n*= 5). All data were collected in terminal procedures using respiratory electrophysiology protocols approved by the Institutional Animal Care and Use Committee at the University of Florida and the US Army Medical Research and Materiel Command Animal Care and Use Review Office. Technical details are in the appended manuscript attached to this document. Emphasis below is on experimental design and results.

The focus of these experiments was on deter-mining whether cISMS-related diaphragm EMG activity could be triggered by an endogenous, spared respiratory signal. For the immediate proof of concept purposes, we used EMG signals from the tongue to trigger cISMS. It is well established that tongue muscle activity is coordinated with respiration. We also investigated whether cISMS would result in off-target, non-respiratory muscle co-activation. One muscle of interest because of proximity of motoneuron pools was the external carpi radialis (ECR) muscle of the forelimb.

Figure 1A shows a representative example of triggered cervical ISMS (directed to the left side of the spinal cord) during the inspiratory phase in a spinal-intact rat. Note that compound MUAPs in the left diaphragm are clearly discernible (Fig. 1*C*) and are entrained to each stimulation pulse (e.g., Fig. 1*D*). In this example, the average latency between stimulus artifact and MUAP (motor unit action potential) peak is 2.14±0.05 ms, which is consistent with a synaptic delay before motor unit activation. In the absence of spontaneous inspiratory EMG activity, it can be appreciated that ISMS targeting the left phrenic motor nucleus evoked a marked response in both the ECR and diaphragm but had minimal impact on the left tongue or right diaphragm.

To confirm that the very small-amplitude EMG signals in the tongue, diaphragm, and intercostals represented activation of motor units, we employed a previously published "detectability index" for evoked potentials. This assessment indicated that ISMS evoked a small but statistically significant increase in entrained and averaged EMG activity in the tongue (5 of 8 animals), left intercostal (8 of 8 animals), and right diaphragm (8 of 8 animals). It should be noted, however, that the amplitudes of these off-target evoked potentials were modest compared with those of the left diaphragm and ECR muscles.

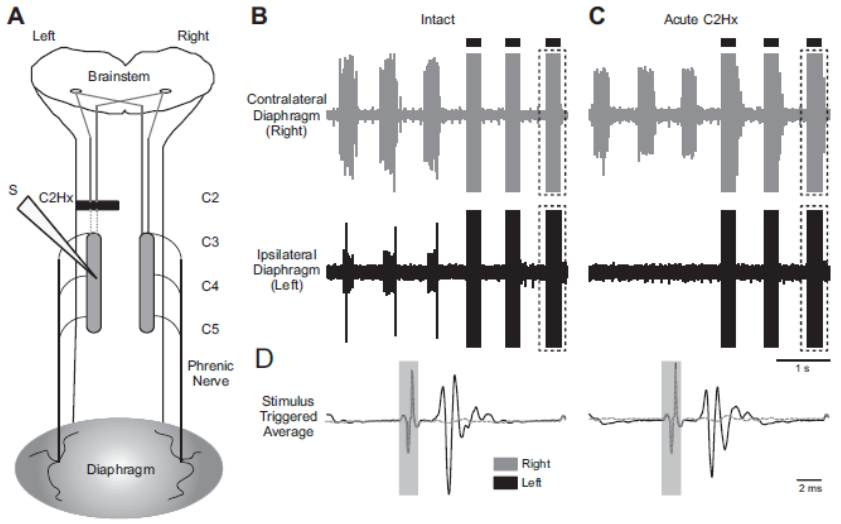

Figure 2. ISMS after acute C2Hx. **A:** illustration of the electrode placement relative to the C2Hx lesion. The solid dark bar represents the injury site; the dashed lines represent severed pathways. **B:** examples of EMG activity in the right and left diaphragm before C2Hx. **C:** Examples of left and right diaphragm EMG activity after acute C2Hx. Note that activity is abolished in the left diaphragm. In B and C, 3 spontaneous breaths are shown followed by 3 breaths during triggered cervical ISMS (solid bars; 100 Hz, 200 A). **D:** stimulus-triggered averages of right and left diaphragm EMG activity obtained from the period of ISMS high-lighted by dashed boxes in B and C. Stimulus-triggered averages were scaled to the same values and represent 25 stimulus triggers. In D, the stimulus artifact is highlighted by the gray boxes. **(Figure 3 in Mercier et al., 2017).**

Experiments were next per-formed immediately after C2Hx (acute injury). The general experi-mental paradigm is illustrated in Fig. 2*A*. Diaphragm MUAPs were first evaluated with the spinal cord intact (Fig. 2*B*). The ISMS-evoked po-tentials in the spinal-intact condition were similar to those described in the preceding section.

Acute C2Hx abolished spon-taneous inspiratory EMG activity in the ipsilateral hemidiaphragm in all animals (Fig. 2*C*). However, cervical ISMS still produced clear MUAPs in the ipsilateral diaphragm after the acute lesion (Fig. 2*D*). Collectively, the data are consistent with a slight reduction in cervical ISMS-evoked MUAP amplitude in most animals after acute C2Hx. The off-target impact of ISMS after C2Hx (i.e., evoked activity in ECR, tongue, and right diaphragm) was indistinguish-able from that reported above for the spinal-intact condition (data not shown).

For the last phase of this study, we tested cISMS in rats that were 5–21 days post-C2Hx (subacute injury). These temporally advanced lesion experiments were performed to determine whether degenerative processes triggered by C2Hx (e.g., axonal retraction) prevented or mitigated the impact of ISMS on diaphragm activation. Spontaneous ipsilateral diaphragm EMG activity was absent in rats studied 5–21 days after C2Hx (Fig. 3*A*), and subsequent histological evaluation of the spinal cord indicated anatomically complete hemilesion in all animals (Fig. 3*B*).

The ISMS procedure evoked clearly discernible MUAPs in the ipsilateral (paralyzed) hemidiaphragm (Fig. 3*C*). Compared with the acute injury group, the only apparent difference in the ISMS responses in the animals with the subacute lesions was a trend for more variable and longer latencies. On average, however, there were no statistical differences between the groups for latency (acute C2Hx: 1.69±0.57 ms, subacute C2Hx: 2.50±0.67 ms), but the increase in latency in the subacute group was close to threshold

for significance (*P* _ 0.065). The MUAP amplitude was variable, but with no evidence for a difference between the two groups (acute C2Hx: 1.62±1.45 mV, subacute C2Hx: 1.76±2.65 mV, *P* _ 0.833).

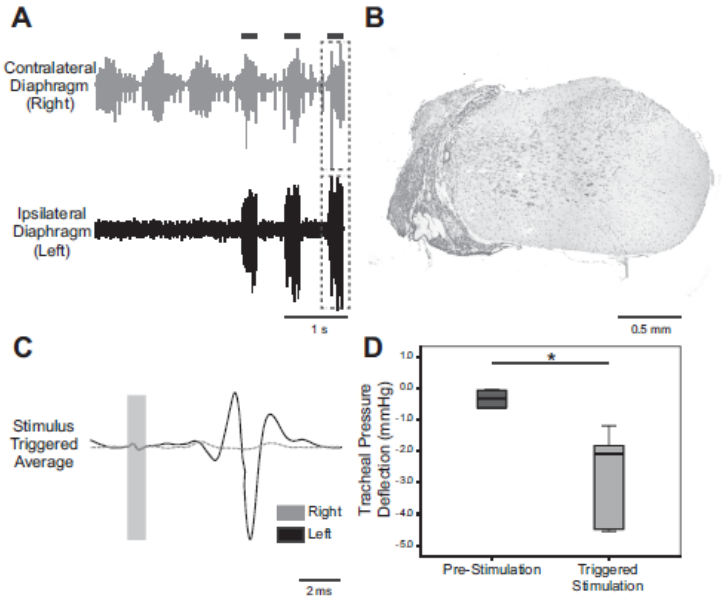

Figure 3. ISMS after subacute C2Hx. **A**: representative diaphragm EMG activity after subacute C2Hx. In the example traces, genio--glossus-triggered ISMS was delivered during the breaths marked by the black bars. **B**: histological section of the C2 spinal cord stained with cresyl violet. The example demonstrates an anatomically complete hemilesion extending to the midline of cervical cord. **C**: stimulus-triggered averages from the ipsilesional (solid line) and contralesional diaphragm (dashed line); data were obtained from the period indicated by the dashed boxes in *A*. These traces illustrate activation of the diaphragm ipsilateral to the C2Hx lesion. **D**: average change in tracheal pressure during lung inflation at prestimulation baseline and during ISMS. **P* <0.05. (Figure 5 in Mercier et al., 2017)

ISMS caused the expected negative deflection in tracheal pressure in the subacute C2Hx animals, thus confirming that there was a biomechanical impact of the stimulation on breathing (Fig. 3*D*). The off-target muscle activation was similar to what was obtained in the spinal-intact and acute C2Hx animals. Thus very small, but statistically significant, changes in EMG activity during ISMS were detected in the tongue (4/5 animals), intercostal (3/4 animals), and right diaphragm (4/5 animals). The left ECR showed greater EMG responses in five of five animals.

While our primary intent was to determine whether ISMS evoked diaphragm activity during the period of stimulation, we noted that spontaneous diaphragm EMG activity often was present after the stimulus was turned off. Thus, in six of eight animals after acute C2Hx, the hemidiaphragm that was electrically silent before ISMS showed both tonic and inspiratory-related activity during and after the 1-min period of stimulation (Fig. 4*A*). In these experiments, "activity" was defined as one or more clearly discernible motor unit potentials that were discharging phasically during the inspiratory period. The duration of the effect was variable and did not persist beyond 2 min in any experiment. On average, ISMS-induced spontaneous diaphragm motor unit activity lasted for 43 ± 38 respiratory cycles after ISMS was terminated. The first breath immediately after cessation of ISMS typically

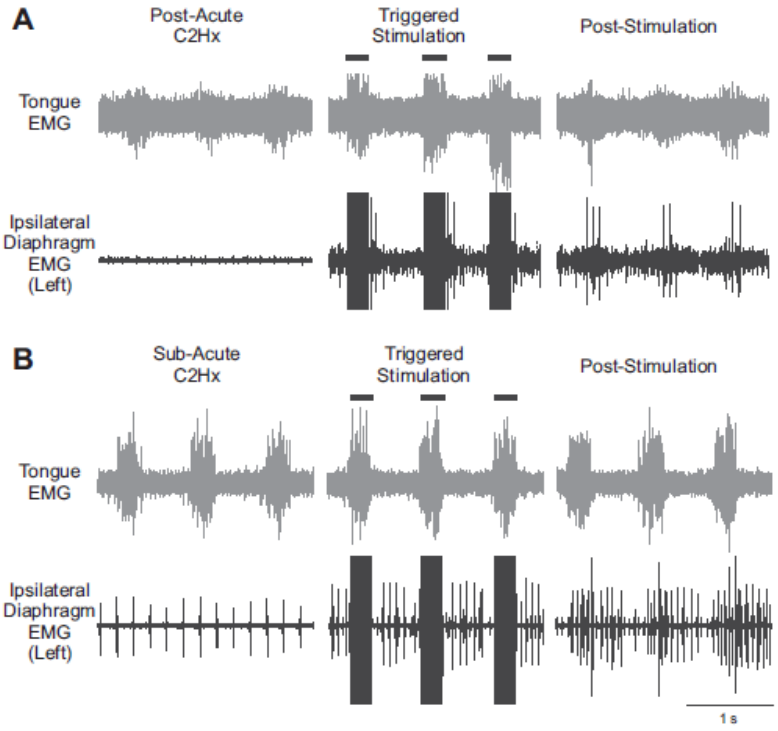

Figure 4. Example recordings illustrate short term potentiation of ipsilateral diaphragm EMG activity following ISMS. ***A***: tongue and ipsilateral (left) diaphragm EMG activity after acute C2Hx, during ISMS, and immediately after cessation of ISMS. Note that clear phasic (inspiratory) activity can be seen after ISMS, whereas the baseline showed no such activity. ***B***: a similar response can be observed in a subacute C2Hx animal. In these examples, the ISMS was triggered by the inspiratory genioglossus EMG signal and was delivered at 100 Hz for 1 min of respiratory efforts (Figure 6 in Mercier et al., 2017).

demonstrated the greatest amount of motor unit recruitment, and this was followed by a gradual decrease in motor unit activity over subsequent respiratory cycles. In addition, we noted an increase in tonic activity (i.e., activity persisting across the entire respiratory cycle) after ISMS that followed a time course similar to the phasically active motor units. A similar response to ISMS was observed in three of five rats after subacute C2Hx injury (Fig. 4*B*).

Conclusions

This study has demonstrated the feasibility of using endogenous medullary output to trigger ISMS to the midcervical spinal cord. The ISMS paradigm was successful in recruiting diaphragm motor units in spinal-intact animals and also after both acute and subacute interruption of bulbospinal inspiratory drive to the phrenic motoneuron pool following high cervical SCI. Further refinement of this approach may enable development of a "respiratory neuroprosthesis" that, by virtue of the endogenous trigger, could adapt to temporally changing metabolic demands. An interesting and potentially important observation that was not part of our original hypothesis was that ISMS-induced inspiratory bursting in the hemiparetic diaphragm persisted for several respiratory cycles after cessation of the stimulation. This occurred in the majority of acute and subacute C2Hx lesions and is similar to the previously described phenomenon of respiratory short-term potentiation (STP) (Lee et al. 2015). Tongue EMG output enabled a rigorous test of the fundamental hypothesis, and we suggest that future work should focus on additional potential sources of respiratory output to serve as endogenous trigger signals or alternative detection algorithms. Future investigations involving awake, spontaneously breathing animals will be crucial for determining whether chronic ISMS delivery will function solely as a neuroprosthetic or can be used short term to promote functional and anatomical neuroplasticity (Moritz et al. 2007) alone or in combination with other therapeutic approaches leading to long-lasting improvement in respiratory function.

3.b.2. Details for Gonzalez-Rothi et al., in revision publication:

Per the recommendations of the panel that reviewed our proposal, we have also explored epidural stimulation, and that has led to a second manuscript which has been tentatively accepted by the *Journal of Neurophysiology* pending minor revisions recommended by the referees.

Overview of Approach. Adult rats were anesthetized and mechanically ventilated and HF-ES (300 Hz) was applied to the ventrolateral C4 or T2 spinal cord ipsilateral to C2Hx for 60-sec at currents from 100-1000 µA via a tungsten microwire. Arterial blood pressure, bilateral phrenic nerve activity, and ipsilateral hypoglossal nerve activity were recorded before and after high frequency epidural stimulation (HF-ES).

Phrenic and XII neural output following cervical HF-ES in rats with C2Hx lesions. Representative traces of phrenic and XII nerve output following brief periods of C4 epidural stimulation are provided in Fig. 5. These examples first illustrate the recording configuration precluded assessment of respiratory nerve activity during the period of stimulation due to a large stimulus artifact that obviated the underlying signal. Second, robust short-term potentiation of the ipsilateral phrenic signal is evident following HF-ES. The lowest current (100 µA) typically evoked minimal if any potentiation of respiratory nerve output, but stimulation at 500 and 1000 µA both resulted in a substantial increase in the overall output of the ipsilateral phrenic nerve. Also, there was no discernable impact on XII or contralateral phrenic output, even at the higher stimulus currents. Superimposition of phrenic waveform averages (not shown), obtained immediately following HF-ES, further illustrates the potentiation of both phasic (inspiratory) and tonic phrenic output that occurred following the higher stimulus currents.

The average changes in phasic, tonic and total activity in the phrenic and XII nerve recordings following C4 HF-ES are presented in Fig. 6. In addition to the mean and standard error, each individual data point is provided in keeping with recent recommendations for data reporting in preclinical research (Landis *et al.* 2012). Evaluation of phasic inspiratory activity in the left (ipsilateral) phrenic nerve revealed a statistical interaction (P=0.028) between the stimulus current (*i.e.*, 100, 500, and 1000 µA) and the time post-injury

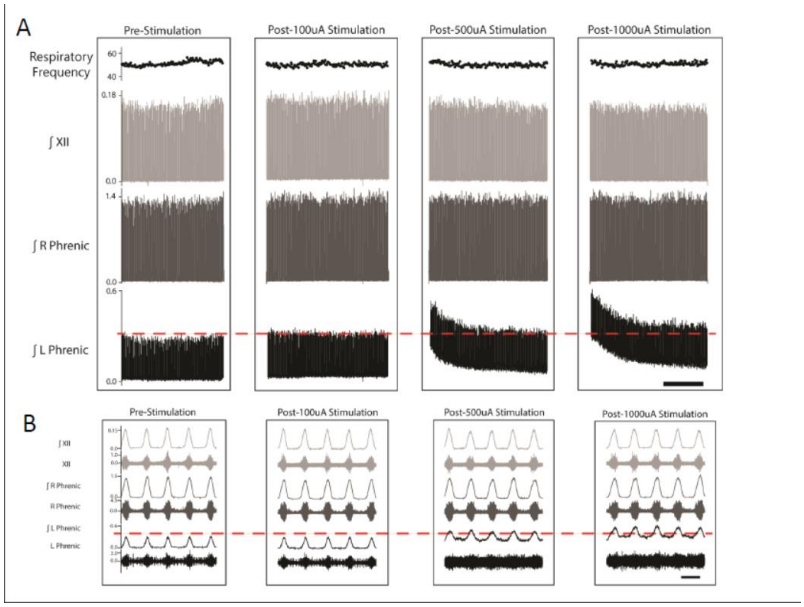

Figure 5. Following a left-sided C2 spinal cord hemisection injury, HF-ES was delivered to the ventrolateral epidural surface of the C4 spinal cord, ipsilateral to the side of injury. **A)** Representative compressed traces depict integrated phrenic and hypoglossal nerve activity prior to and following HF-ES at 100-, 500-, and 1000uA. **B)** Expanded traces depict both raw and integrated phrenic and hypoglossal nerve activity at baseline and following each bout of stimulation. Scale bars represent 1 min (A) and 1 s (B).

(*i.e.*, 2- *vs.* 12-wks post-C2Hx). Thus, higher C4 stimulus currents evoked increases in phasic ipsilateral phrenic activity at 12- but not 2-wks following C2Hx (Fig. 6A). A similar response occurred in the phrenic nerve contralateral to the lesion (P<0.05, Fig. 6B); however, neither the time post-injury (P=0.051) nor the time-stimulus current interaction (P=0.079) reached the threshold for statistical significance. Although there was no significant impact of time post-injury, contralateral phrenic output did increase with stimulus current (P=0.014).

The C4 stimulation paradigm also influenced the medulla as confirmed by small increases in XII motor output following HF-ES. The relative changes were small as compared to the ipsilateral phrenic signal, but the XII inspiratory burst (Fig. 6C) increased with the stimulus current (P=0.027), and potentiation of XII bursting tended to be greater at 12- *vs.* 2-wks post-C2Hx (P=0.070).

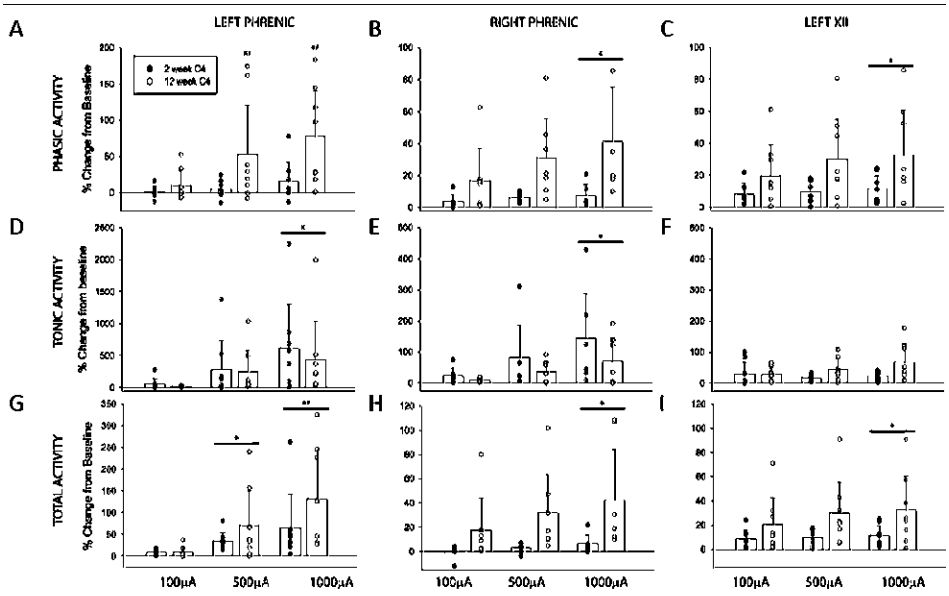

Figure 6. ***Average changes in phrenic and hypoglossal nerve activity following C4 HF-ES.*** Changes in phasic (**A**), tonic (**B**), and total (**C**) phrenic and hypoglossal nerve activity following HF-ES of the C4 spinal cord, delivered at 2 and 12 weeks post-injury. Data were calculated over the three minutes following each bout of stimulation and are represented as a % change from baseline activity. HF-ES delivered to the C4 spinal cord at 12 weeks post-C2Hx resulted in an increase in phasic phrenic activity (*p,<0.05 different from 100µA, #p<0.05 different from 500µA). No other group differences were observed, although dose dependent increases in amplitude (percent change above baseline) resulted following HF-ES, with the greatest amplitude changes occurring following the highest stimulation intensities (500 and 1000µA). Note that profound increases in tonic activity comprised much of the increase in total activity and that the ipsilateral phrenic nerve demonstrated the most dramatic changes in nerve amplitude relative to baseline (Note the scale of the y-axes on the right phrenic and left XII plots is lower than the axes for the L phrenic plots).

The average changes in tonic neural activity following C4 stimulation are provided in Figs. 6D-F. Note that the relative magnitude (%baseline) of the increased tonic dis-charge was considerably greater for tonic as com-pared to phasic output. Both the left (Fig. 5D, P=0.001) the right phrenic nerves (Fig. 5E, P=0.002) showed increases in tonic bursting as the stimulus current increased. The most robust potentiation occurred in the left phrenic nerve with in-creases of approximately 500% of the baseline output at the highest stimulation intensity. There was no evidence for a time-dependent effect in either the left or right phrenic neurogram (*i.e.*, tonic output was similar at 2- and 12-wks post-C2Hx). Tonic XII discharge tended to be greater following C4 stimulation at 12- *vs.* 2-wks, but this was not statistically significant (Fig. 5F, P=0.083). Changes in total phrenic and XII activity (*i.e.*, including both the phasic and tonic components) are presented in Fig. 5G-I. All three recordings showed a progressive

increase in total activity as the stimulus current was increased. Although the XII data suggest an impact of HF-ES on medullary neurons (Fig. 6), no changes in inspiratory burst frequency were observed following stimulation of the cervical spinal cord (Table 1, P=0.402).

Phrenic and XII neural output following thoracic HF-ES. The impact of thoracic (T2) stimulation on phasic, tonic and total activity in left and right phrenic nerves, and the left XII nerve is summarized in Fig. 7. At the 100 µA stimulus current, most rats showed a small increase in phasic discharge in all three motor outputs. The only exception was in the left phrenic recording at the 2-wk time point where only 3 of 6 rats showed an increase in phasic discharge (Fig. 7A). The magnitude of potentiation increased with stimulus current in the left phrenic (Fig. 7A, P=0.004), right phrenic (Fig. 7B, P=0.011) and XII recordings (Fig. 6C, P=0.021). However, time-depend-ent effects (*e.g.*, 2- *vs.* 12-wks) on phasic output were not detected for any of the recordings (all P>0.265).

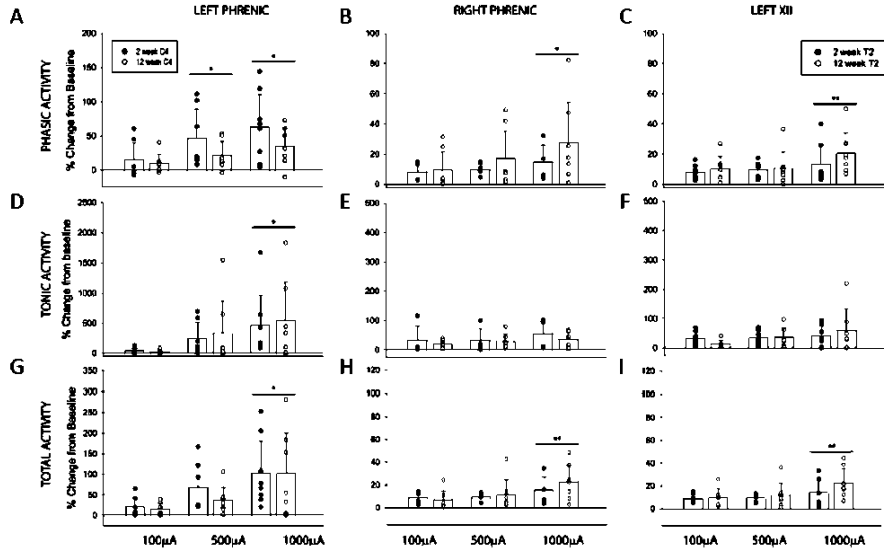

Figure 7. ***Average changes in phrenic and hypoglossal nerve activity following T2 HF-ES.*** Changes in phasic **(A)**, tonic **(B)**, and total **(C)** phrenic and hypoglossal nerve activity following HF-ES of the T2 spinal cord, delivered at 2 and 12 weeks post-injury. Data were calculated over the three minutes following each bout of stimulation and are represented as a % change from baseline activity. A dose-dependent increase in amplitude (percent change above baseline) was observed in all nerves (*p<0.05 different from 100µA, #p<0.05 different from 500 µA) across all outcomes (phasic, tonic, and total nerve activity), with the greatest amplitude changes occurring following the highest stimulation intensities. Note that profound increases in tonic activity comprised much of the increase in total activity and that the ipsilateral phrenic nerve demonstrated the most dramatic changes in nerve amplitude relative to baseline (Note the scale of the y-axes on the right phrenic and left XII plots is lower than the axes for the L phrenic plots). No significant group differences were observed in any nerve in any of the outcomes assessed.

Tonic output was potentiated in all three nerves following T2 stimulation in nearly all experiments at both the 2- and 12-wk time points (Figs. 7D-F). In the left phrenic signal, tonic discharge increased with stimulus intensity (P=0.004), and reached approximately 500% of baseline at the highest stimulus current. Increases in tonic discharge in the right phrenic and left XII recordings were typically in the range of 50-100% (Fig. 6E-F). Time dependent effects on the tonic response to T2 stimulation were not statistically significant for any of the neural outcomes assessed (all P>0.557). The magnitude by which total activity was potentiated increased with stimulus intensity in all recordings (all P<0.007), and there were no significant differences in the total activity between the two time points (all P>0.075).

Similar to the cervical HF-ES data, changes in inspiratory burst frequency were not observed following stimulation of the thoracic spinal cord (Table 1, P=0.281).

Cardiovascular parameters during and following HF-ES. The heart rate (HR) remained stable during all procedures, with the exception of C4 stimulation at 12-wks following C2Hx. Under those conditions, increases in HR ranged from 1-14% of baseline (Fig. 7C), and the mean increase was statistically significant (P<0.001). The mean arterial pressure (MAP) increased during C4 stimulation at 500µA (P=0.033) and 1000 µA (P=0.001), but with no evidence for a time-dependent change between 2- and 12-wks (P-0.259). The MAP also increased during T2 stimulation at 1000 µA (P=0.034); no time-dependent changes were detected. At both 2- and 12-wks, both HR and MAP returned to baseline values following cessation of HF-ES regardless of the level of stimulation (all P>.627).

Arterial blood was assessed for $PaCO_2$, PaO_2, and pH values prior to and following the stimulation protocol. No differences between groups were detected at either time point (all P>0.38). All rats remained

well oxygenated throughout the experimental protocol with PaO_2 values greater than 98 mmHg in all cases.

The impact of the serotonergic receptor agonist quipazine on ipsilateral phrenic output before and after HF-ES. Serotonergic neurons innervate the spinal phrenic circuitry and serotonin is a powerful stimulant of respiratory motor output following SCI. In a subset of experiments, we examined the impact of *i.v.* delivery of the 5-HT receptor agonist quipazine on ipsilateral phrenic motor output before and following HF-ES. Consistent with prior studies of the 5-HT precursor 5-Hydroxytryptophan (Ling *et al.* 1994; Mitchell *et al.* 1992; Zhou and Goshgarian 2000), *i.v.* quipazine triggered a robust increase in both the tonic and total output of the ipsilateral phrenic nerve at both 2- and 12-wks after C2Hx (all $P<0.028$). The relative magnitude of the acute increases following quipazine exceeded the short-term potentiation of ipsilateral phrenic output that was induced by epidural stimulation prior to quipazine. No time-dependent differences in the relative increase in ipsilateral phrenic bursting induced by quipazine (% baseline) were detected across 2- *vs.* 12-wks for either phasic, tonic, or total phrenic output (all $P>0.44$).

Following *i.v.* quipazine, C4 and T2 HF-ES potentiated tonic phrenic output at both 2- and 12-wks post-injury (Fig. 9), and the magnitude of potentiation was dependent upon the stimulus intensity (all $P<0.014$). However, quipazine pretreatment did not enhance the relative magnitude of tonic potentiation following stimulation when compared to the baseline response (*e.g.*, without potentiation without quipazine treatment; $P>0.88$ for all groups). Conversely, the relative increase in phasic inspiratory phrenic bursting that followed epidural stimulation was blunted following quipazine (*i.e.*, reduced potentiation, all $P>0.092$ *vs.* pre-stimulus baseline) in all but the 12-wk T2 group. Thus, the large increase in overall tonic output at this quipazine dose, appears to have largely precluded the ability to detect short-term changes in inspiratory phrenic bursting.

Conclusions

This is the first study to examine the impact of high frequency epidural stimulation (HF-ES) on phrenic motor output following incomplete cervical spinal cord injury. While a detailed head-to-head comparison with ISMS is premature since both approaches have yet to be optimized, we have shown that (High Frequency-Electrical Stimulation) HF-ES of the ventrolateral C4 or T2 spinal cord can cause an increase in phrenic discharge that persists after stimulation. The short-term potentiation of ipsilateral phrenic bursting illustrates the potential for spinal cord stimulation to trigger respiratory plasticity, and this is a concept that could be useful in designing neurorehabilitation paradigms (Kasten et al. 2013; McPherson et al. 2015). However, we also observed large increases in tonic phrenic output with epidural stimulation which indicates that HF-ES is unlikely to have application as a “respiratory neuroprosthesis” for activation of the respiratory muscles after incomplete SCI.

3.b.3. Details for Streeter et al., 2016 publication:

Lastly, as part of Major Task 1 in which we are electrophysiologically mapping changes in phrenic circuitry following cervical SCI, we have just published another paper in the *Journal of Neurophysiology* that describes a method for identifying multi-electrode array recording sites. Several groups have advanced the hypothesis that mid-cervical spinal interneurons can modulate phrenic motoneuron excitability and thereby influence the neural control of the diaphragm. A significant hurdle in testing that hypothesis, however, is the difficulty of studying the “functional connectivity” in diffuse spinal cord networks. A major challenge is to simultaneously record numerous cells. This can be addressed with multi-electrode array (MEA) technology. But histological identification of each recording location (versus the electrode track) while preserving tissue integrity poses a further challenge.

Basic Experimental Approach. Thus, the initial thrust of the current work was modification and validation of a silver labeling technique to enable post-recording deposition of a small amount of silver (i.e., for histological marking) from the tip of each electrode in an MEA. Additionally, we developed an electrical circuit to enable the use of small currents (100 nA) for silver electroplating and deposition to prevent tissue and electrode damage associated with high levels of current. Using the electroplated MEA, we recorded discharge from ensembles of neurons in the mid-cervical (C3-C5) spinal cord in adult rats and demonstrated

a practical application of this technique by “matching” the array electrodes to the corresponding anatomical locations marked by silver.

Most experiments (n=12) were performed with untreated, spinal intact rats. A subset of rats (n=2) received a cervical spinal injury (C3/C4 lateralized contusion, force: 205 KD, displacement: 1225 µm; Infinite Horizon pneumatic impactor, Precision Systems & Instrumentation) using published methods from our group. Spinal injured rats were allowed to recover for 12 weeks prior to electrophysiology. Histological results from spinal injured animals were used to determine effectiveness of silver labeling and to compare micro-motor depths relative to silver labeling depths. Since there is evidence suggesting neurophysiological properties such as connectivity may be altered following SCI, neurophysiological analysis was limited to spinal intact animals (n=4). See appended, published manuscript for methodological details. Images below are from the published manuscript although figure numbers in text differ from those in the publication.

Optimization of Silver Deposition from MEAs and Subsequent Histological Development to Enable Visualization of Recording Locations. We first assessed the impact of two critical variables on the histological appearance of silver in the spinal cord: 1) the duration of deposition current, and 2) the duration of histological development. Consistent and discrete labeling at a resolution between ~25-50 µm was obtained when current used to deposit silver was applied for 50 sec and tissue was developed for 7-10 minutes (Figures 8A and B). When deposition current of less than 50 sec was applied few apparent labels were detected, presumably due to an inadequate amount of silver ions necessary for visualization. In contrast, deposition of 80-100 sec resulted in a “halo effect” which increased the silver labeled area to ~100-150 µm (Figures 8C and D), most likely due to a broad distribution of deposited silver. Similarly, histological development of less than 7 minutes was not long enough to “develop” the deposited silver required to visualize the label; whereas prolonged exposure to the developing solution tended to darken large areas of the section thus confounding differentiation due to insufficient contrast (data not shown).

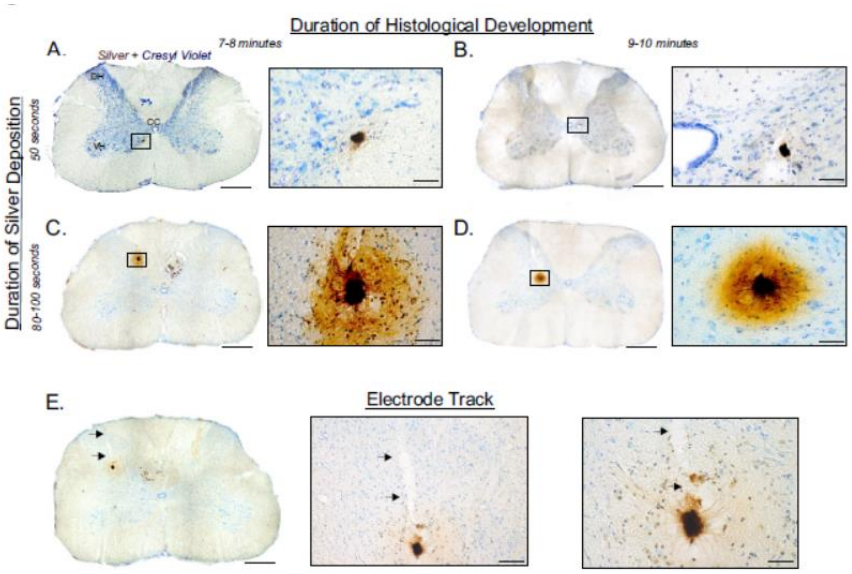

Figure 8. Representative images of silver labeling. A-D: Representative histological sections from the cervical spinal cord containing silver labeled sites counterstained with cresyl violet and high resolution images of the boxed areas. These images depict the variability of silver labeling at different durations of silver deposition (50-100 sec) and histological development (7-10 minutes). **E:** Images of a cervical spinal section depicting an electrode track (black arrows) coursing through the spinal tissue and terminating at the silver labeled site. CC: central canal; DH: dorsal horn; VH: ventral horn. Scale bars: A-D: 0.5 mm and 50 µm (callouts); E: 0.5 mm, 100 µm, and 50 µm, respectively.

We next verified that sites of silver deposition represented the location of the tip (i.e., recording location) of a given electrode. In a subset of animals (n=2 with silver processing, n=1 unprocessed positive control), two of the sixteen silver plated electrodes were coated with the fluorescent lipophilic dye, DiI to visualize the tracks associated with the electrode insertion. While DiI was readily detected in unprocessed tissue (data not shown), DiI could not be detected after the histological processing required for silver labeling. Therefore, we conclude these two techniques are not compatible. However, in several histological sections an “electrode track” could be identified terminating at the silver labeled site (Figure 8E). This is consistent with the interpretation that the silver labeled site is located at the tip of the electrode.

Another objective was to determine if the silver labeling method could be coupled with fluorescent immunohistochemistry (IHC) procedures. Accordingly, we performed IHC with two markers commonly used in the central nervous system (GFAP and NeuN) either prior to, or immediately after histological processing for silver development. These markers were chosen due to their ability to label astrocytes and neurons.

Fluorescent staining was detected in both cases, but was more robust when IHC was performed after the silver staining procedures (data not shown), indicating IHC (at least for these commonly used markers) is compatible with the histological processing steps necessary to "develop" the silver. Using this staining order, we determined the location of deposited silver relative to NeuN positive cells. Representative photomicrographs from a C4 spinal section depicting positive silver labeling in the intermediate gray is shown in Figure 9A. Fluorescent labeling of the same section stained with NeuN and DAPI are shown in Figure 9B. High magnification images of the silver labeled site suggest the recording electrode was in close proximity to a NeuN positive neuron (Figure 9B). These qualitative results demonstrate that the silver labeling technique can be coupled with fluorescent IHC.

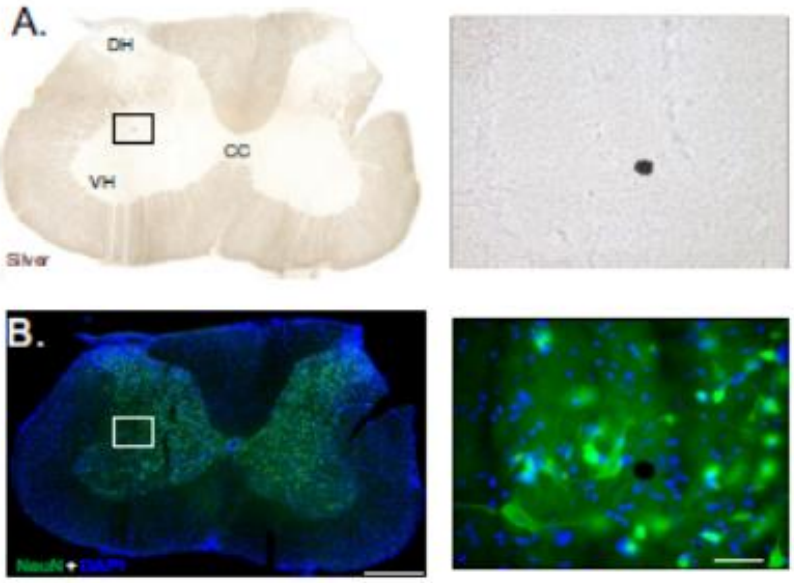

Figure 9. Silver labeling coupled with fluorescent immunohistochemistry. **A:** Representative cervical spinal section of positive silver labeling (*brown/black*) and high resolution image of the boxed area. **B:** Fluorescent labeling of neurons stained with NeuN (*green*) and nuclei stained with DAPI (*blue*) of the same section presented in panel A, and high resolution image of the boxed area illustrating the silver labeled site was in close proximity of a NeuN positive cell. CC: central canal; DH: dorsal horn; VH: ventral horn. Scale bars: 0.5 mm and 50 µm (callouts).

Using Silver Labeling to Identify Anatomical Locations of MEAs. In six animals (n=4 spinal intact and n=2 SCI), we used the optimized deposition and development parameters discussed previously to label select electrodes. Overall, using this approach to identify the anatomical locations of the recording electrodes, we obtained positive labeling in 35 of 39 attempts. This indicates that the silver labeling method can be used to identify the anatomical locations of array electrodes with a success rate of approximately 90%. Positive silver labeling was identified in the spinal gray matter between C3-C5. Silver labeled sites were identified between lamina IV-X, with the greatest number found in lamina VII (Figure 10A). The locations of each silver labeled site in spinal intact and SCI animals was plotted (unilaterally for simplicity) according to their anatomical locations (Figure 10B).

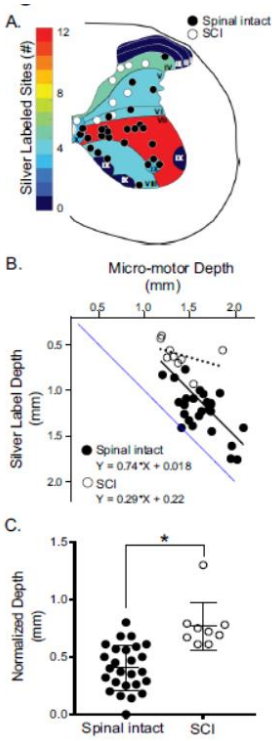

Figure 10. Electrode and silver labeled depth. **A:** Representative C4 section of silver labeled sites in spinally intact (●) and spinally injured (○) animals projected onto one side of the cord for simplicity. Each lamina was shaded according to the number of silver labeled sites within that lamina. **B:** Scatter plot of the micro-motor depths versus the depths of the corresponding silver labeled sites in spinally intact (●) and spinally injured (○) animals. Linear regression analysis was applied to determine the line of best-fit and linear equation for each group. The line of identity is displayed to indicate the location where micro-motor and silver labeling depths are equal. **C:** Normalized depth calculated as the difference between the micro-motor depth silver labeled site for spinally intact (●) and spinally injured (○) animals. * P<0.001 Unpaired T-test.

The success of the discrete silver labeling afforded the chance to compare the intended recording location (i.e., the micro-motor coordinates used during the neurophysiology experiment) with actual the location of the labeling (Figure 10B, C). Each silver labeled site was measured from the dorsal surface of the cord. Based on estimates of prior investigations regarding tissue shrinkage during paraformaldehyde fixation and subsequent tissue processing, the measured histological depth of each silver labeled site was adjusted by 10%. This analyses indicated that the micro-motor depth is likely to overestimate the actual depth of the electrode, and perhaps even more importantly that this relationship is altered by SCI. Linear regression analysis indicated a significant relationship between recording coordinates and histological staining in spinal-intact animals (motor: 1.6 ± 0.04 mm; histological: 1.2 ± 0.05 mm; P = 0.0003), but

not after chronic SCI (motor: 1.4 ± 0.07 mm; histological: 0.6 ± 0.05 mm; P = 0.3014; Figure 10B). The depth of the silver labeled site differed from the micro-motor coordinate in both groups (Figure 10C), but was significantly increased following SCI (0.8 ± 0.07) compared to spinal intact animals (0.4 ± 0.04). These data highlight the need to histologically identify multi-electrode recording sites especially following experimental conditions such as SCI when tissue fibrosis and scarring can be expected to alter electrode movement within the CNS. Future, studies can apply the linear fit as a proxy to more accurately calculate the "actual depth" of the electrode tips.

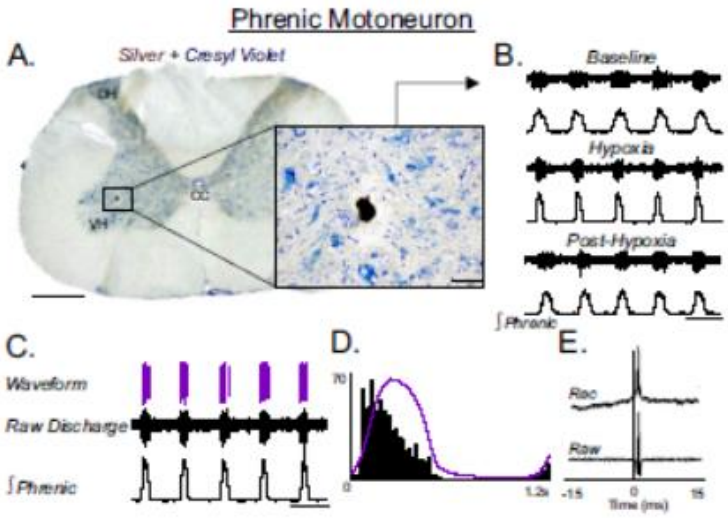

F

Representative C4 section containing a silver labeled site counterstained with cresyl violet and high resolution image containing the silver labeled site located in the medial aspect of the ventral horn in lamina IX (callout). **B:** Corresponding raw spinal discharge and integrated phrenic output during baseline, hypoxia, and post-hypoxia depicting discharge during the inspiratory phase. **C:** Integrated phrenic output, raw neuronal discharge, and sorted spikes (waveform) during hypoxia. **D:** Cycle-triggered histogram during 50 consecutive breaths overlaid with the average integrated phrenic waveform during hypoxia. **E:** Spike-triggered average of the raw and rectified phrenic nerve depicting a delay of 0.76 ms. CC: central canal; DH: dorsal horn; VH: ventral horn. Scale bars: A 0.5mm and 50µm (callout); B, C: 1.5 sec.

Coupling Spinal Discharge with Anatomical Locations. All silver electroplated electrodes could discriminate single units, indicating that the pretreatment had a minimal, if any, impact on the ability to record and discriminate extracellular signals. Three silver labeled sites were identified within lamina IX of the ventral horn (Figure 10A and 11A). Spike-triggered averaging (STA) of the raw and rectified phrenic nerve activity in relation to neuronal discharge produced a distinct peak with an average lag time of 0.45 ± 0.16 ms (Figure 11E), and therefore indicated that the recorded discharge was from phrenic motoneurons. All three of these cells were active primarily during the inspiratory phase (Figure 11B and C), which is the typical firing pattern of phrenic motoneurons in this preparation. The silver labeling data verified that the recordings were from the region of the phrenic motor nucleus. This close matching between neurophys-iological data and anatomical data illustrates the effectiveness of the silver labeling method.

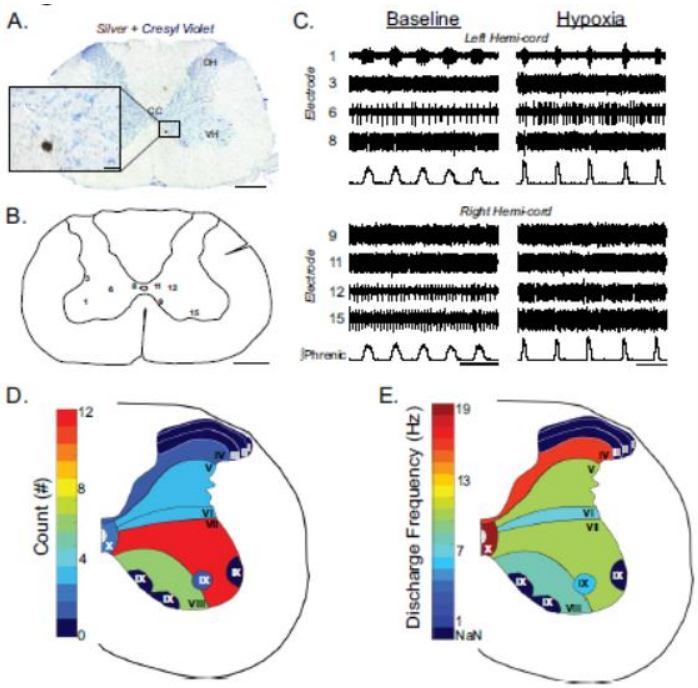

Figure 12. Mapping anatomical locations of mid-cervical spinal neurons. A: Representative photomicrograph of a C4 section containing a silver labeled site (from electrode nine) counterstained with cresyl violet and high resolution image of the silver labeled site (callout). **B:** Camera Lucida-style drawing of the cervical spinal cord summarizing the anatomical locations of eight silver labeled sites obtained in one animal. **C:** Integrated phrenic motor output and mid-cervical spinal discharge on the left and right hemi-cord corresponding to identified silver labeled sites in panel B during baseline and hypoxia. Electrode one recorded phrenic motoneuron discharge and the remaining electrodes recorded interneuron discharge. **D:** Representative C4 section summarizing the total number of silver labeled interneurons within each lamina in spinal intact animals. **E:** Average discharge frequency (Hz) of spinal interneurons within each lamina represented in panel D. CC: central canal; DH: dorsal horn; VH: ventral horn. Scale bars: A, B: 0.5 mm and 50 µm (callout); C: 1.5 sec.

The remaining silver labeled sites were located between laminae IV-X. Spike-triggered averaging provided no evidence of discharge synchrony in relation to phrenic motor output; thus these 28 recordings were considered to represent interneurons (see Figure 7 in appended publication). At baseline, most recorded interneurons (18/28 or 66%) fired tonically throughout the respiratory cycle. These tonically discharging cells were not restricted to a particular lamina, but were instead recorded

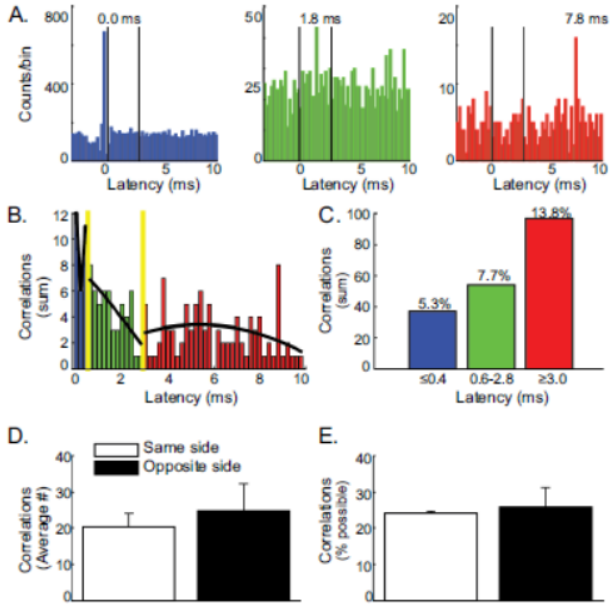

Figure 13. Cross-correlation analysis of mid-cervical spinal interneurons. A: Representative cross-correlations obtained from three pairs of neurons depicting a significant central peak (left), 1.8 ms offset peak (middle), and 7.8 ms offset peak (right). The number of trigger spikes for each correlation: 43,891; 39,208; 3,928; and the detectability index of each correlation: 45.2; 4.3; 5.3, respectively. Black lines plotted at 0.5 and at 2.9 ms to indicate how data was grouped by latency (see panel B). B: A histogram of the latency relative to the trigger for all correlations with a significant peak. The first bar in the histogram is a count of the central peaks (0 ms latency) and each successive bar in the plot represents counts obtained in an increment of 0.2. Yellow bars plotted at 0.5 and at 2.9 ms indicate how data was grouped based on latency. Black lines are 2nd order polynomial fit of the data. C: The sum of significant cross-correlations with latencies ≤ 0.4 ms, between 0.6-2.8 ms, and ≥ 3.0 ms. Percentages reflect the proportion of positive correlations out of the total possible (n=704). D: The average number of positive correlations per animal when both recordings were on the same side of the cord (20 ± 3.9 positive correlations/animal), or on opposite sides of the cord (25 ± 7.5 positive correlations/animal). E: The number of significant correlations expressed as a percent of total possible connections obtained when both recordings were on the same side of the cord (81/332 total possible), or on opposite sides of the cord (89/372 total possible).

throughout the cervical grey matter. A smaller proportion of interneurons (5/28 or 18%) primarily fired during the inspiratory phase, and these cells were found in lamina VI (n=1), VII (n=3), and X (n=1). During hypoxia, two of these neurons (in lamina VII and X) switched to a tonic firing pattern, but then resumed an inspiratory pattern post-hypoxia. Due to phase switching, the proportion of tonic firing interneurons increased to 82% (23/28) during hypoxia and remained elevated post-hypoxia (20/28 or 71%).

Mapping anatomical locations and quantitation of interneuronal discharge across mid-cervical spinal laminae are shown in Figure 12. A representative example from one recording in which silver labeling was used to "map" the anatomical locations of the array electrodes and corresponding electrophysiological data is shown in Figure 12A-C. A Camera Lucida-style drawing of the anatomical locations of eight silver labeled electrodes was constructed (Figure 12B). Numerical identification of the anatomical positions of each electrode corresponds to the schematic presented in Figure 12D and defines the rostral-caudal and medial-lateral positions of the array electrodes.

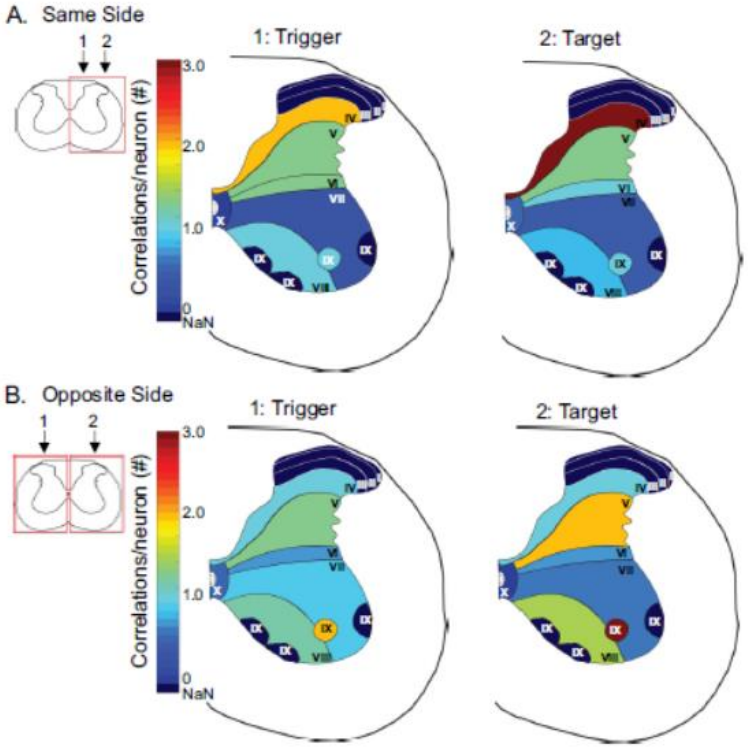

Figure 14. Anatomical locations of functionally connected interneurons. Summary maps of silver labeled interneurons with significant peaks in cross-correlograms. The number of positive correlations in each lamina was normalized to the number of neurons present in the lamina and shaded accordingly. A: When both trigger and target neurons were on the same side of the spinal cord (e.g., unilateral recordings), interneurons in dorsal lamina (i.e., IV, V and VI) made and received the greatest number of excitatory connections. B: When the trigger and target neurons were on opposite sides of the spinal cord (e.g., bilateral recordings), interneurons in lamina V, VIII and IX made and received the most connections.

Corresponding mid-cervical spinal discharge and integrated phrenic nerve activity during baseline and hypoxia on the left and right hemi-cord is shown in Figure 12C. Many these recordings were from tonic firing interneurons (electrodes 3, 8, 9, 11, 12, and 15) and one represented a phase switching (e.g. from tonic at baseline to expiratory during hypoxia) interneuron (electrode 6; Figure 12C). Using this technique, a summary of the anatomical locations of all silver labeled interneurons was constructed (Figure 12D). In addition, the average discharge frequency (Hz) of all silver labeled interneurons was presented in Figure 12E. The results indicate a dorsal-ventral discharge gradient, with higher discharge

rates in lamina IV and X and lower values in lamina VIII and IX. This discharge map of the mid-cervical spinal network demonstrates the utility of using the silver labeling technique to identify the anatomical locations of ensembles of interneurons recorded with a MEA. These results show the utility of using this technique to standardize the sampling distribution of recording locations across experimental groups.

Temporal Relationships between Cervical Interneuron Discharge. Anatomical data indicate that cervical interneurons are part of a diffuse and synaptically coupled propriospinal network, but relatively little is known about functional connectivity between cervical interneurons. Therefore, initial analyses focused on all recorded neurons in spinal intact rats (i.e., silver and non-silver labeled neurons) to screen for short time scale (i.e., 0-10ms) features. Significant features were identified as departures in the cross-correlation histogram $\geq$ 3 standard deviations from the background noise. Using this approach, significant central (i.e., no lag time from zero) and offset correlogram peaks were detected and shown in Figure 13 along with a summary of the latency of significant features relative to the trigger (i.e., time zero).

Neuronal pairs with significant correlogram peaks that were also silver labeled were used to construct correlation summary maps to illustrate the anatomical locations of each neuron (Figure 14). The number of positive correlations within each lamina was normalized to the total number of neurons present in the corresponding lamina. Unilateral neuronal pairs are shown in Figure 14A and bilateral pairs are shown in Figure 14B. Of the positive unilateral correlations, interneurons in dorsal lamina (i.e., IV, V and VI), made and received the greatest number of excitatory connections (Figure 10A). In contrast, when the trigger and target neuron were on opposite sides of the spinal cord, interneurons in lamina V, VIII and IX made and received the most connections (Figure 14B).

Conclusions

To our knowledge, no prior study has comprehensively evaluated the temporal characteristics across multiple mid-cervical neurons using MEA technology. The results presented herein demonstrate a previously unappreciated degree of connectivity and indicate a high prevalence of temporally related discharge patterns between mid-cervical interneurons with characteristics consistent with mono- and polysynaptic connections. Our findings also provide a comprehensive description of a cost-effective histological approach for validating anatomical locations of MEA recording sites with a cost-effective method to identify the anatomical locations of neuronal ensembles recorded with a multi-electrode array during acute preparations without the requirement of specialized array electrodes.

One potential application of MEA technology is to examine how SCI alters the cervical spinal networks. Spinal networks undergo substantial remodeling following SCI and interneurons have been implicated in SCI-induced plasticity and motor recovery. Our results from a small sample of spinal-contused rats demonstrate fundamental feasibility of mapping changes in circuitry; however, we also identified potential caveats that need further investigation to refine methods for spinal injury recordings of this type.

Collective Summary of Papers Submitted or Published To-Date

- We have developed technical approaches to study changes in phrenic circuitry following cervical SCI which may lend to future studies of ISMS.
- Evaluation of activity recorded from silver labeled sites has also revealed a previously unappreciated degree of connectivity between mid-cervical interneurons.
- We have obtained critical proof-of-concept data supporting efficacy of ISMS in reactivating phrenic motor circuitry silenced by SCI.
- This finding has been independently replicated by collaborators at the University of Washington (subcontract).
- Our ISMS data to-date demonstrate the potential for a lasting effect beyond the period of stimulation.
- Our ISMS data also very importantly demonstrate the potential for triggering effective stimulation via spared respiratory activity.
- We performed the first study to examine the impact of high frequency epidural stimulation (HF-ES) on phrenic motor output following incomplete cervical spinal cord injury.
- Short term potentiation of phrenic bursting following HF-ES illustrates the potential for spinal stimulation to induce respiratory neuroplasticity.

- The increases in tonic phrenic output after HF-ES indicate that the continuous stimulation paradigm used here is unlikely to be useful for respiratory muscle activation after spinal cord injury.

Status of Primary SOW Tasks:

Major Task	Status
Major Task 1: To determine chronic changes in neuronal discharge patterns within the phrenic circuit region following a C3/4 lateralized contusion injury.	Analysis continues to be in progress. One publication thus far.
Major Task 2: Terminal electrophysiological comparison of epidural and ISMS stimulation on activation of the phrenic motor circuit after chronic C2 hemisection (C2Hx; one month post-SCI).	Completed. On paper published, another in revision
Major Task 5: Conduct Phase I of closed-loop intraspinal stimulation of phrenic motor neurons (PhMNs) after C2Hx. Contralateral diaphragm EMG triggers intraspinal microstimulation (ISMS) of PhMNs	In progress as part of Major Task 11.
Major Task 6: University of Florida replication of closed-loop/C2Hx (contralateral diaphragm triggered stimulus) results at U.W. and comparison with epidura stimulation.	Will be part of Major Task 11. Partially done via U. W. collaboration. One paper in preparation.
Major Task 7: Conduct Phase II of closed-loop intraspinal stimulation of phrenic motor neurons (PhMNs). Contralateral intercostal EMG triggers intraspinal microstimulation (ISMS) of PhMNs.	Goal is part of Major Task 11.
Major Task 8: Conduct Open-loop intraspinal stimulation of phrenic motor neurons (PhMNs). Average respiratory activity recorded in Phase I & II triggers ISMS	Epidural stimulation results have reduced the immediate need for this study.
Major Task 9: Conduct Phase III of closed-loop intraspinal stimulation of phrenic motor neurons (PhMNs). Repeat most promising closed-loop method (Diaphragm or intercostal triggered ISMS) using mid-cervical contusion model.	Contusion injury will not be done for reasons discussed. Otherwise, goal is linked to Major Task 11
Major Task 11: Neuroanatomical studies on closed-loop and open-loop ISMS treated rats.	In progress

3.c. Plans for Accomplishing Goals:

As far as Major Tasks, Table 1 outlines the current status of the principal Major Tasks proposed (not including basic logistical tasks). We have now been approved for an Extension Without Funds which will be used to complete a major objective of this project – namely, extend our proof of concept study of ISMS to living rats. Specifically, our goal is to determine whether: (a) chronic ISMS delivered to unanesthetized rats with C2Hx injuries will restore diaphragm activity on the side of injury, (b) the effect persists beyond the period of stimulation, and (c) we can demonstrate anatomical neuroplasticity as a result (i.e., Major Task 11). For that purpose, IACUC and ACURO modifications are being prepared at this time, which we hope will not delay us to any significant extent. Given costs of set-ups for this challenging experiment, we are hoping to obtain sufficient data on which to build a future research application to support a larger scale study, while at the same time essentially meeting the original goals of this project. Collaborators at the Univ. Washington are

also ramping up to do chronic ISMS studies as part of the independent replication we proposed. Chronic diaphragm EMG recordings are now being worked out and those signals to trigger ISMS will be tested after C2Hx.

4. Impact:

4.a. Impact on Principal Disciplines:

The results we have obtained to-date provide another dimension to the potential benefits of ISMS on motor function. Up to now, much of what we know about the potential for evoking function from the injured spinal cord with electrical stimulation has derived from studies of epidural stimulation or ISMS targeting other somatic motor systems. Our studies are now moving incrementally, but significantly, towards a better understanding of how ISMS, despite its more invasive nature, may not only restore function but also how it may promote plasticity such that functional recovery can be achieved beyond any need for stimulation via other sources. Electrical modulation of spinal circuits is becoming an area of expanding interest (Samaddar et al. 2016; Song and Martin 2016; Yao and Li 2016).

4.b. Impact on Other Disciplines

Nothing to report

4.c. Impact on Technology Transfer

Nothing to report

4.d. Societal Impact

Nothing to report

5. Changes/Problems

5a. Changes in Approach

We originally proposed to carry out our studies in two different injury models – after C2 hemisection (C2Hx) or a C3-4 lateralized contusion. Given the technical challenges encountered, the decision was made to forgo the contusion injury model for two reasons. First, there is still controversy in the literature related to the type of deficit that occurs following a mid-cervical contusion (Alvarez-Argote et al. 2015; Rana et al. 2016), and it seems that significant respiratory deficits may involve more severe and debilitating injuries than logistically feasible or ethical in experimental animals at this time. At the very least, additional experiments that were not budgeted would be required to support any effect of spinal electrical stimulation. Second, the C2Hx model is often the lesion of choice for studies of cSCIs and respiratory outcomes. Therefore, we feel that all objectives of the original proposal can be adequately addressed with that injury model as it results in a more complete inactivation of the phrenic circuit on the side of injury than even a lateralized contusion can achieve. In sum, our revised plan is not a departure from the original SOW but instead a reorganization of experimental priorities based upon experiences to date. These changes have been indicated in previous Quarterly Reports.

5b. Anticipated Problems and Proposed Corrective Action

None

5c. Changes Affecting Expenditures

None

5d. Changes Affecting Use and Care of Animals

None for this reporting period, but IACUC and ACURO modifications will be submitted for approval for remaining work under the EWOF.

Literature Cited

Alvarez-Argote S, Gransee HM, Mora JC, Stowe JM, Jorgenson AJ, Sieck GC, and Mantilla CB. The Impact of Midcervical Contusion Injury on Diaphragm Muscle Function. *J Neurotrauma* 33: 500-509, 2015.

Kasten MR, Sunshine MD, Secrist ES, Horner PJ, and Moritz CT. Therapeutic intraspinal microstimulation improves forelimb function after cervical contusion injury. *J Neural Eng* 10: 044001, 2013.

Landis SC, Amara SG, Asadullah K, Austin CP, Blumenstein R, Bradley EW, Crystal RG, Darnell RB, Ferrante RJ, Fillit H, Finkelstein R, Fisher M, Gendelman HE, Golub RM, Goudreau JL, Gross RA, Gubitz AK, Hesterlee SE, Howells DW, Huguenard J, Kelner K, Koroshetz W, Krainc D, Lazic SE, Levine MS, Macleod MR, McCall JM, Moxley RT, 3rd, Narasimhan K, Noble LJ, Perrin S, Porter JD, Steward O, Unger E, Utz U, and Silberberg SD. A call for transparent reporting to optimize the predictive value of preclinical research. *Nature* 490: 187-191, 2012.

Lee KZ, Sandhu MS, Dougherty BJ, Reier PJ, and Fuller DD. Hypoxia triggers short term potentiation of phrenic motoneuron discharge after chronic cervical spinal cord injury. *Exp Neurol* 263: 314-324, 2015.

Ling L, Bach KB, and Mitchell GS. Serotonin reveals ineffective spinal pathways to contralateral phrenic motoneurons in spinally hemisected rats. *Exp Brain Res* 101: 35-43, 1994.

McPherson JG, Miller RR, and Perlmutter SI. Targeted, activity-dependent spinal stimulation produces long-lasting motor recovery in chronic cervical spinal cord injury. *Proc Natl Acad Sci U S A* 112: 12193-12198, 2015.

Mitchell GS, Sloan HE, Jiang C, Miletic V, Hayashi F, and Lipski J. 5-Hydroxytryptophan (5-HTP) augments spontaneous and evoked phrenic motoneuron discharge in spinalized rats. *Neuroscience Letters* 141: 75-78, 1992.

Moritz CT, Lucas TH, Perlmutter SI, and Fetz EE. Forelimb movements and muscle responses evoked by microstimulation of cervical spinal cord in sedated monkeys. *J Neurophysiol* 97: 110-120, 2007.

Rana S, Sieck GC, and Mantilla CB. Diaphragm Electromyographic Activity following Unilateral Mid-Cervical Contusion Injury in Rats. *J Neurophysiol* jn.00727.02016, 2016.

Samaddar S, Vazquez K, Ponika D, Toruno P, Sahbani K, Begum S, Abouelela A, Mekhael W, and Ahmed Z. Trans-spinal direct current stimulation modulates migration and proliferation of adult newly-born spinal cells in mice. *J Appl Physiol (1985)* jap.00834.02016, 2016.

Song W, and Martin JH. Spinal cord direct current stimulation differentially modulates neuronal activity in the dorsal and ventral spinal cord. *J Neurophysiol* jn.00584.02016, 2016.

Yao L, and Li Y. The Role of Direct Current Electric Field-Guided Stem Cell Migration in Neural Regeneration. *Stem Cell Rev* 12: 365-375, 2016.

Zhou SY, and Goshgarian HG. 5-Hydroxytryptophan-induced respiratory recovery after cervical spinal cord hemisection in rats. *Journal of applied physiology* 89: 1528-1536, 2000.

6. Products

Manuscripts In Print or Revision (Two published articles (*) appended to this report):

1. *Mercier LM, Gonzalez-Rothi EJ, Streeter KA, et al. Intraspinal microstimulation and diaphragm activation following cervical spinal cord injury. J Neurophysiol. 2016:jn 00721 02016.

2. *Streeter KA, Sunshine MD, Patel SR, et al. Coupling multi-electrode array recordings with silver labeling of recording sites to study cervical spinal network connectivity. J Neurophysiol. 2016:jn 00638 02016.

3. Gonzalez-Rothi EJ, Streeter KA, Hanna MH, Stamas AC, Reier PJ, Baekey DM, Fuller DD. High frequency epidural stimulation evokes short-term potentiation of phrenic discharge after incomplete cervical spinal cord injury. J. Neurophysiol. (in revision).

Manuscript in Preparation:

1. Sunshine, MD, Ganji, CN, Reier, PJ et al. Intraspinal activation of respiratory muscles depends on respiratory cycle phase. In final stages of preparation.

7. Participants & Other Collaborating Organizations

7a. Participating Investigators

Name	Project Role	Nearest Perso Month Worked Equivalents	Contribution to Project
University of Florida			
Paul J. Reier, Ph.D.	Project Director	No change	Oversees entire project; conducts experiments related to Major Task 3
David D. Fuller, Ph.D.	Co-I	No change	Functions as Associate Project Director responsible for overseeing neurophysiology studies and interfacing with Seattle researchers
David Baekey, Ph.D.	Co-I	No change	Multi-electrode array recordings for Maj Task 1
Kristi Streeter, Ph.D.	Post-Doctoral Fellow	4.0	Conducted recordings for Major Task 1
Elisa Gonzalez-Rothi, Ph.D.	Post-Doctoral Fellow	2.0	Epidural stimulation studies for Major Task 2.
Lynne Mercier[2]	Graduate Student	No change	Conducted ISMS proof-of-concept study for Major Task 2.
Lucy Denholtz	Technician	No change	Assists with surgeries and histological procedures.
Savannah Posgai[3]	Technician	Left program to go to medical school.	Assists with surgeries and histological procedures.
Joey Tringali	Technician	0.5	Assists with surgeries and histological procedures. Replaced Ms. Posgai.
University of Washington			
Chet Moritz, Ph.D.	Sub-contract project director	1.73	Oversees project Major Tasks to be done at U. Wash.
Michael Sunshine	Graduate Student	12.0	Primary person responsible for

			carrying out U. Washington studies. He has now come to the Univ. Florida to pursue graduate studies and will assist with the completion of this project. Financial support derived through other sources.

7b. Changes in Active Support/Personnel

No changes during this reporting period.

8. Special Reporting Requirements

8a. Quad Chart (Appendix Attachment)

9. Appendices

See attached PDF files.

Journal of Neurophysiology

Copy of e-mail notification z9k4007

Proof of your article (Manuscript Number: #JN-00721-2016) from "Journal of Neurophysiology" is available for download.

_____

APS-Journal of Neurophysiology z9k-4007

Reprint No: 3959559

Dear Sir or Madam:

Please refer to this URL address http://rapidproof.cadmus.com/RapidProof/retrieval/index.jsp
Login: your e-mail address as listed in the 'to' line of this e-mail message.
Password: 77D9uUVUGFM7

The attached file contains a proof of your article, with query list.

Adobe Acrobat® tools should be used to mark proof; see detailed instructions in this packet.

1) Corrections must be limited. Note that all corrections are subject to evaluation by APS.
2) Answer all author queries (AQ1, AQ2, AQ3, etc.) listed on the last page of the PDF file.
3) Proofread entire document, paying close attention to any tables and equations (these elements often require recreating author's original files).
4) Carefully check any special characters or symbols.
5) Return the corrected set of page proofs WITHIN 2 BUSINESS DAYS to mpasho@the-aps.org.
6) Figures portray those images approved and authorized by the authors at acceptance; hence, changes are not permitted at galley proof stage, except for the most serious of reasons. If an error is discovered, contact me immediately (see below).

Please contact me immediately at mpasho@the-aps.org so that I know you have received this message and have successfully downloaded your PDF proof.

PLEASE INCLUDE YOUR MANUSCRIPT NO. (JN-00721-2016) WITH ALL CORRESPONDENCE.

Maria Pasho
Journal Editorial Supervisor
Journal of Neurophysiology
9650 Rockville Pike, Bethesda, Maryland 20814-3991 (USA)
Email (preferred) mpasho@the-aps.org. Phone (if needed) 301-634-7207

****

REPRINTS: To order reprints of your article, please go to http://www.the-aps.org/Link-Library/Pubs/Reprint-Order-Form.pdf. Then email the completed form to reprints@the-aps.org.

****

Requesting Corrections on Your PDF Proof

To help us facilitate any necessary late-stage corrections, we encourage authors to use the comments and notes features in Adobe Acrobat. The PDF provided has been "comment enabled," which allows the user to utilize the comments and notes features in Adobe Acrobat, even if using only the free Adobe Acrobat reader (see note below regarding acceptable versions). Adobe Acrobat's Help menu provides additional details on the tools. When you open your PDF, the comments/notes/edit tools are clearly shown on the tool bar. The important features to know are the following:

- Note tool (yellow text balloon icon): Click on this feature on the tool bar and then click on a point of the PDF where you would like to make a comment. This feature is useful when providing an instruction to your production contact or to verify a question or change that was posed.

- Text edits ("T" with strike-through and caret icon): The option Insert Text at Cursor allows the user to place the cursor at a point in the text, which will then provide a pop-up box to add the appropriate text to be added to the proof.

- Use the Strike-Out tool to indicate deletions to the text.

As with hand-annotated proof corrections, the important points are to communicate changes clearly and thoroughly, to answer all queries and questions, and to provide complete information for us to make the necessary changes to your article so it is ready for publication.

To use the comments/notes features on this PDF you will need Adobe Reader version 7 or higher. This program is freely available and can be downloaded from http://www.adobe.com/products/acrobat/readstep2.html.

Instructions for Annotating Your .PDF Proof

- Use the Text Boxes and the Callout Tool to indicate changes to the text

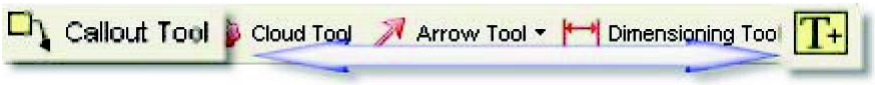

- Use the Strike-Out tool to indicate deletions to the text.

- Use the Highlighting Tool to indicate font problems, bad breaks, and other textual inconsistencies.

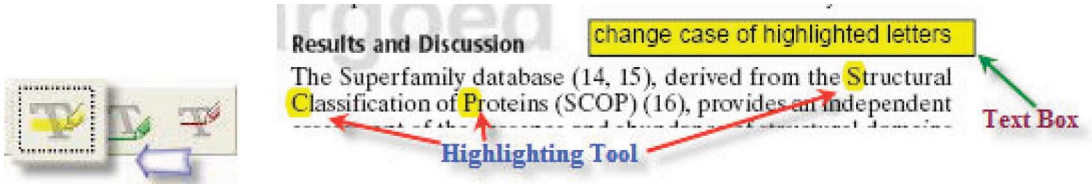

- Clearly indicate where changes need to be made using arrows, lines, and the Call-Out Tool.

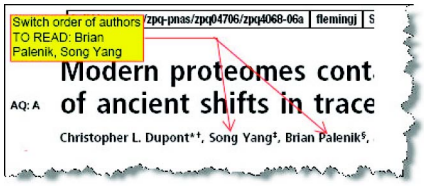

- Mark changes and answer queries in the margins and other areas of white space.

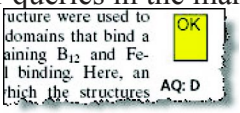

- Avoid obscuring the text with corrections.

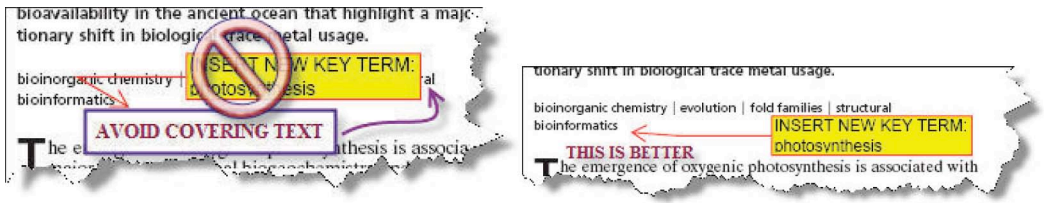

J Neurophysiol 117: 000–000, 2017.
First published November 23, 2016; doi:10.1152/jn.00721.2016.

RESEARCH ARTICLE | *Spinal Control of Motor Outputs*

Intraspinal microstimulation and diaphragm activation after cervical spinal cord injury

L. M. Mercier,[1] E. J. Gonzalez-Rothi,[2] K. A. Streeter,[2] S. S. Posgai,[1] A. S. Poirier,[2] D. D. Fuller,[2] P. J. Reier,[1] and D. M. Baekey[3]

[1]*Department of Neuroscience, University of Florida, Gainesville, Florida;* [2]*Department of Physical Therapy, University of Florida, Gainesville, Florida; and* [3]*Department of Physiological Sciences, University of Florida, Gainesville, Florida*

Submitted 6 September 2016; accepted in final form 21 November 2016

Mercier LM, Gonzalez-Rothi EJ, Streeter KA, Posgai SS, Poirier AS, Fuller DD, Reier PJ, Baekey DM. Intraspinal microstimulation and diaphragm activation after cervical spinal cord injury. *J Neurophysiol* 117: 000–000, 2017. First published November 23, 2016; doi:10.1152/jn.00721.2016.—Intraspinal microstimulation (ISMS) using implanted electrodes can evoke locomotor movements after spinal cord injury (SCI) but has not been explored in the context of respiratory motor output. An advantage over epidural and direct muscle stimulation is the potential of ISMS to selectively stimulate components of the spinal respiratory network. The present study tested the hypothesis that medullary respiratory activity could be used to trigger midcervical ISMS and diaphragm motor unit activation in rats with cervical SCI. Studies were conducted after acute (hours) and subacute (5–21 days) C_2 hemisection (C2Hx) injury in adult rats. Inspiratory bursting in the genioglossus (tongue) muscle was used to trigger a 250-ms train stimulus (100 Hz, 100–200 μA) to the ventral C_4 spinal cord, targeting the phrenic motor nucleus. After both acute and subacute injury, genioglossus EMG activity effectively triggered ISMS and activated diaphragm motor units during the inspiratory phase. The ISMS paradigm also evoked short-term potentiation of spontaneous inspiratory activity in the previously paralyzed hemidiaphragm (i.e., bursting persisting beyond the stimulus period) in ~70% of the C2Hx animals. We conclude that medullary inspiratory output can be used to trigger cervical ISMS and diaphragm activity after SCI. Further refinement of this method may enable "closed-loop-like" ISMS approaches to sustain ventilation after severe SCI.

NEW & NOTEWORTHY We examined the feasibility of using intraspinal microstimulation (ISMS) of the cervical spinal cord to evoke diaphragm activity ipsilateral to acute and subacute hemisection of the upper cervical spinal cord of the rat. This proof-of-concept study demonstrated the efficacy of diaphragm activation, using an upper airway respiratory EMG signal to trigger ISMS at the level of the ipsilesional phrenic nucleus during acute and advanced postinjury intervals.

phrenic motor nucleus; rat; respiration; hypoglossal respiratory activity; diaphragm function

SEVERE RESPIRATORY COMPROMISE often occurs after spinal cord injury (SCI) at upper cervical to midcervical spinal levels (Mansel and Norman 1990; Winslow and Rozovsky 2003). When independent breathing is not possible, positive-pressure mechanical ventilation is often used to sustain alveolar ventilation, but at the risk of potential rapid diaphragm atrophy, atelectasis, and respiratory tract infections (Bezzant and Mortensen 1994; Laghi et al. 2003; Smuder et al. 2016). Diaphragm and phrenic nerve pacing options are clinically available (DiMarco et al. 2005; Glenn and Phelps 1985; Onders et al. 2009), and recent preclinical work has begun exploring high-frequency epidural stimulation of the spinal cord to activate the diaphragm (DiMarco and Kowalski 2013, 2015; Kowalski et al. 2013).

Another approach that may effectively activate respiratory muscles after SCI is intraspinal microstimulation (ISMS). Implementation of this method in motor systems has been demonstrated (Giszter 2015; Kasten et al. 2013; McPherson et al. 2015; Tator et al. 2012), but applications to respiratory motor output after cervical SCI have not been investigated. Potential advantages of ISMS include the ability to deliver currents over a relatively wide range of intensities and with high selectivity for specific motor systems (Mondello et al. 2015; Mushahwar et al. 2000; Sunshine et al. 2013).

The present study was therefore designed to obtain proof-of-concept evidence in support of cervical ISMS as a means of activating diaphragm motor units after cervical SCI. To move toward a "closed-loop-like" design for ISMS, we recorded the inspiratory output of an upper airway muscle (the genioglossus, innervated by cranial nerve XII) and used this to trigger stimulation. Thus cervical ISMS was activated by endogenous inspiratory drive. The data show that a physiologically relevant medullary inspiratory output can be used to trigger cervical ISMS and that this approach can effectively activate diaphragm motor units after acute and subacute SCI.

MATERIALS AND METHODS

Thirteen female Sprague-Dawley rats (255 ± 16 g; Harlan, Indianapolis, IN) were distributed between two experimental groups: *1*) ISMS after acute SCI, tested before and immediately after lateral hemisection of the spinal cord at C_2 (C2Hx) (n = 8), and *2*) ISMS after subacute SCI, tested 5–21 days after C2Hx (n = 5). All data were collected in terminal procedures using protocols approved by the Institutional Animal Care and Use Committee at the University of Florida and the US Army Medical Research and Materiel Command Animal Care and Use Review Office.

Address for reprint requests and other correspondence: D. M. Baekey, Dept. of Physiological Sciences, PO Box 100144, Gainesville, FL 32610-0144 (e-mail: dbaekey@ufl.edu).

C2Hx surgery. For survival surgery, rats were initially anesthetized with isoflurane (3–5% in O_2) in a closed chamber and then anesthesia was maintained via nosecone (1.5–3% in O_2). A dorsal incision was made over the cervical spine, followed by a C_2 laminectomy and durotomy. For acute C2Hx, resection lesions were performed with a needle-blade microknife (Fine Science Tools, Foster City, CA). Subacute C2Hx resection lesions were made with microscissors and fine forceps followed by gentle aspiration of tissue to complete the hemisection (Fuller et al. 2008). The dura and overlying muscles were closed and lactated Ringer solution (5 ml sc) and buprenorphine were administered (0.03 mg/kg sc.; Hospira, Lake Forest, IL). Postoperative care consisted of daily lactated Ringer solution (5 ml/day sc) and oral nutritional supplement (1–3 ml/day; Nutrical, Webster Veterinary). Buprenorphine was given at ~12-h intervals for 2 days after surgery.

General neurophysiology protocols. Rats were anesthetized as above. Rectal temperature was maintained at ~37.5°C by a heating pad (CWE, Ardmore, PA). A femoral artery was catheterized (PE-50) for blood pressure measurements (Statham P-10EZ pressure transducer, CP122 AC/DC strain gauge amplifier; Grass Instruments, West Warwick, RI) and arterial blood samples. The femoral vein of the same hindlimb was also catheterized (PE-50) for supplemental fluid administration and conversion from isoflurane to urethane anesthesia (1.7 g/kg iv; Sigma, St. Louis, MO). Animals received a tracheotomy and were mechanically ventilated (50–65% O_2, balance N_2; 6–7 ml/kg volume; 70–72 bpm frequency; Harvard Apparatus, Holliston, MA) throughout the experimental procedures. Since spontaneously breathing anesthetized rats can rapidly become hypercapnic, we elected to employ mechanical ventilation for these initial experiments in order to keep blood gases stable and remove Pa_{O_2} and/or Pa_{CO_2} fluctuations as confounding variables.

End-tidal CO_2 (Capnogard 1265; Respironics, Wallingford, CT) was continuously monitored, and arterial blood gases (iSTAT1; Abbott, Princeton, NJ) were periodically assessed from 0.1-ml arterial samples. On the basis of these measures, the inspired CO_2 content was adjusted to maintain Pa_{CO_2} at 40 mmHg. If base excess was greater than −3 meq, this was corrected with intravenous administration of sodium bicarbonate solution [8.4%, Hospira; dose (ml) = 0.3·weight (kg)·standard base excess].

Recordings of EMG activity from respiratory-related muscles (i.e., diaphragm, genioglossus, and intercostal) and an off-target, nonrespiratory muscle [i.e., extensor carpi radialis longus (ECR)] were obtained with pairs of Teflon-coated tungsten hooked wires (A-M Systems, Sequim, WA). Recordings of the genioglossus muscle were obtained at the base of the tongue (Fuller et al. 1999; Fuller and Fregosi 2000) and exhibited a centrally driven inspiratory rhythm that was used to trigger ISMS. For intercostal EMG recordings, a small incision lateral to the sternum was made at the T_2 level and wires were placed 1–1.5 cm lateral to the midline.

The spinal cord was exposed via a cervical middorsal incision followed by laminectomy and durotomy from C_2 to C_5. Raw EMG signals were amplified at 100-10K, band-pass filtered at 100 Hz–10 kHz (A-M Systems, Carlsborg, WA), and, in the case of the genioglossus EMG recording, passed through a moving time averager (50 ms time constant; CWE, Ardmore, PA). The moving time average signal was used to trigger the stimulator for ISMS. All EMG signals were digitized at 25 kHz (CED Power 1401) and recorded (Spike2 v8; CED, Cambridge, UK) to a PC and then analyzed off-line.

ISMS at midcervical spinal cord. A tungsten microwire electrode (FHC, Bowdoin, ME) was mounted in a stereotaxic micromanipulator (David Kopf Instruments, Tujunga, CA). The microwire had a 100-μm segment at the tip stripped of all insulation. The electrode was placed above the C_4 segment with the dorsal root entry zone as the lateral anatomical landmark. Electrical activity was initially recorded via the stimulating electrode and assessed visually with Spike2 software and audibly with an AM8 Audio Monitor (Grass Technologies, Quincy, MA). The software program simultaneously displayed the inspiratory diaphragm EMG recording; these procedures enabled placement of the stimulating electrode tip in proximity to inspiratory neurons (i.e., targeting phrenic motoneurons). Inspiratory bursting was absent in rats with subacute C2Hx injury. Therefore, a stimulator and constant-current stimulus isolation unit (S88X and SIU-C; Grass Technologies, Warwick, RI) were used to deliver single pulses (0.3 ms duration) during electrode descent with gradually decreasing currents (200, 100, 50 μA). This approach allowed us to determine a location for ISMS that evoked left diaphragm activation.

Stimulation of the spinal cord was initiated (triggered) with the EMG signal recorded from the genioglossus muscle. Specifically, a "threshold crossing" was established such that when the inspiratory integrated EMG burst (50 ms time constant) reached a preset amplitude the spinal cord was stimulated. All stimulations during the inspiratory phase were made at the onset of the genioglossus inspiratory burst, while stimulations made during expiratory periods were accomplished by adding a 400-ms delay to the trigger.

Experimental group 1: ISMS before and after acute C2Hx. The genioglossus EMG signal was used to trigger ISMS during two consecutive inspiratory cycles, followed by ISMS delivered during two consecutive expiratory cycles. In both cases, repeated 250-ms stimulus trains (200 μA) were delivered with 0.3 ms pulse duration and 100 Hz stimulus frequency. Once these initial stimulations were complete, ISMS was delivered during the inspiratory cycle for 1 min. All of the aforementioned ISMS was done with the spinal cord intact. After C2Hx, the ISMS protocol was repeated, as described above. Subsequent to protocols performed with spinal cord intact or after C2Hx, an additional bout of ISMS was administered after neuromuscular blockade via intravenous pancuronium bromide (2.5 mg/kg; Hospira) to confirm unequivocally that the evoked activity was not contaminated by a stimulus artifact.

Selection of stimulus parameters. Pilot experiments were done with a manually triggered, open-loop approach in spinal-intact animals. Repeated 250-ms trains of ISMS were targeted to the left phrenic motor nucleus, and EMG activity was recorded in both hemidiaphragms, the genioglossus, and ipsilateral intercostal and forelimb (ECR) muscles (see, e.g., Fig. 1). A range of stimulation frequencies (50, 100, 200, 300 Hz) and currents (50–200 μA) were tested to optimize parameters for eliciting compound motor unit action potentials (MUAPs) in the left diaphragm. Activation of the ipsilateral hemidiaphragm was more pronounced when 100-Hz stimulation was used, with stimulation frequencies above 200 Hz ~~thereby~~ producing large ~~contraction~~ of nonrespiratory muscles. Preliminary experiments also indicated that progressive attenuation of ISMS-induced phrenic MUAP amplitude occurred during sustained stimulation (e.g., 1 min) at 200 Hz but not at lower stimulus frequencies (50 Hz, 100 Hz). In the first series of experiments, a stimulus current of 200 μA was used to activate the ipsilateral diaphragm.

Experimental group 2: ISMS after subacute C2Hx. The intraspinal electrode placement was determined as described above. Triggered ISMS was then delivered during two consecutive expiratory periods, followed by one continuous minute of stimulation during the inspiratory phase. In both cases, a continuous 250-ms train was delivered with 0.3-ms pulses at 100 Hz and 100 μA. Stimulations also were repeated after neuromuscular blockade as described above.

Consistent with other reports, we used cessation of the ipsilateral diaphragm inspiratory EMG burst and histology as functional and anatomical verification, respectively, of the subacute C2Hx lesions (Goshgarian 1981). After the electrophysiology protocols, the animals were perfused with saline followed by 4% paraformaldehyde (Sigma). The cervical spinal cords from the subacute C2Hx animals were subsequently harvested, and a tissue block including the C_2 region was paraffin embedded, sectioned (8 μm), and counterstained with cresyl violet.

Biomechanical impact of ISMS. Changes in tracheal pressure were assessed as a crude indicator of the biomechanical impact of ISMS. It should be noted, however, that this was not considered to be a primary

tapraid4/z9k-neurop/z9k-neurop/z9k00217/z9k4007d17z | xppws | S=1 | 1/6/17 | 8:08 | MS: JN-00721-2016 | lni: 02/sa/bew

outcome variable but rather an accessory measurement intended to provide some insight regarding the functional impact of spinal stimulation. The pressures associated with lung inflation and deflation were measured at the tracheal cannula. Measurements were taken continuously and used to compare baseline conditions to stimulation periods. For each period of interest, tracheal pressure deflections for 20 consecutive breaths were averaged and presented in a box and whisker plot (SPSS; IBM, Armonk, NY). Passive tracheal pressure values during exhalation were obtained in each preparation after neuromuscular blockade and thus provided a baseline measurement that was devoid of any respiratory contribution from the animal (for additional details, see RESULTS).

Data acquisition and analyses. For the first group of experiments, results from the spinal-intact condition were compared to data collected 10 min after acute C2Hx. In addition to the evoked responses (i.e., response during ISMS), we also evaluated the impact of the ISMS on spontaneous EMG activity (i.e., following the period of stimulation). To assess ISMS-entrained activation of motor units, the EMG signals were averaged with respect to stimulus pulses within each trial. The resulting stimulus-triggered average (McPherson et al. 2015; Moritz et al. 2007) served to minimize activity unrelated to ISMS. The resultant waveform averages represented ISMS-entrained MUAPs. All data were collected with a CED Spike2 data acquisition system and subsequently analyzed with Spike2 v8 software on a standard PC. Values are reported as means ± SD.

Statistics. A one-way repeated-measures ANOVA followed by the Tukey post hoc test (SigmaPlot; Systat Software, San Jose, CA) was used to compare data collected during baseline vs. ISMS. Dependent variables included the amplitude of MUAPs and spontaneous EMG burst amplitude, blood pressure, tracheal pressure, heart rate, and blood gas data. A "detectability index" statistical test (Aertsen and Gerstein 1985) was used to compare ISMS-evoked MUAP amplitude to background activity in the EMG recordings. We used the modified version of this test with a more stringent value of $D \geq 3$ to prevent "false positives" (Melssen and Epping 1987).

RESULTS

ISMS with spinal cord intact. A representative example of triggered cervical ISMS during the inspiratory phase is provided in Fig. 1. Note that compound MUAPs in the left diaphragm are clearly discernible (Fig. 1*C*) and are entrained to each stimulation pulse (e.g., Fig. 1*D*). In this example, the average latency between stimulus artifact and MUAP peak is

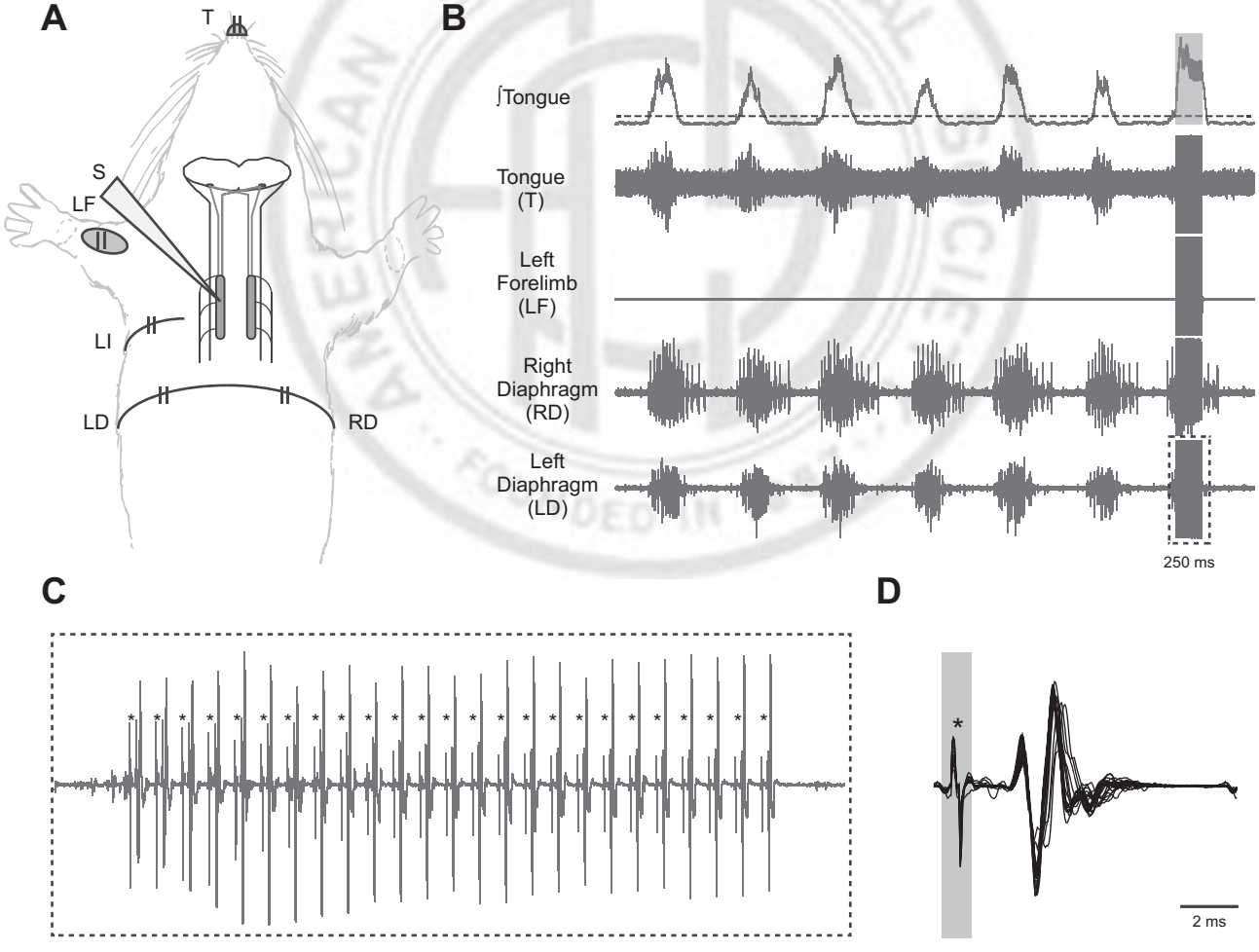

Fig. 1. Cervical ISMS activates the ipsilateral diaphragm *A*: schematic diagram illustrates the EMG recording sites relative to the placement of the stimulating electrode (S). The stimulating electrode was placed in the immediate vicinity of the phrenic motor nucleus, and ISMS was initiated via a trigger signal based on inspiratory tongue (genioglossus) EMG activity. LI, left intercostal. *B*: pre-C2Hx representative EMG recordings from the genioglossus, extensor carpi radialis (ECR), and both sides of the diaphragm showing baseline (prestimulation) activity and a period of genioglossus-triggered cervical ISMS (100 Hz, 200 μA; 0.3-ms pulse duration, 250-ms train duration) represented by a gray ~~bar~~ in the ∫tongue trace. *C*: expanded trace of the EMG recording from the left diaphragm during the period of ISMS shows each stimulus artifact, indicated by asterisks, and each subsequent MUAP. *D*: overlay of each elicited MUAP, aligned by the stimulus artifact, demonstrates constant latency and amplitude.

tapraid4/z9k-neurop/z9k-neurop/z9k00217/z9k4007d17z | xppws | S=1 | 1/6/17 | 8:08 | MS: JN-00721-2016 | Ini: 02/sa/bew

2.14 ± 0.05 ms, which is consistent with a synaptic delay before motor unit activation. An example of ISMS delivered during the expiratory phase is provided in Fig. 2. In the absence of spontaneous inspiratory EMG activity, it can be appreciated that ISMS targeting the left phrenic motor nucleus evoked a marked response in both the ECR and diaphragm but had minimal impact on the left tongue or right diaphragm. To confirm that the very small-amplitude EMG signals in the tongue, diaphragm, and intercostals represented activation of motor units, we employed a previously published "detectability index" for evoked potentials (Aertsen and Gerstein 1985; Melssen and Epping 1987). This assessment indicated that ISMS evoked a small but statistically significant increase in entrained and averaged EMG activity in the tongue (5 of 8 animals), left intercostal (8 of 8 animals), and right diaphragm (8 of 8 animals). It should be noted, however, that the amplitudes of these off-target evoked potentials were modest compared with those of the left diaphragm and ECR muscles. Neuromuscular blockade eliminated evoked potentials, as expected (Fig. 2*C*).

ISMS after high cervical SCI. Experiments were performed immediately after C2Hx (acute injury) and also in rats that were 5–21 days post-C2Hx (subacute injury). These temporally advanced lesion experiments were performed to determine whether degenerative processes triggered by C2Hx (e.g., axonal retraction) prevented or mitigated the impact of ISMS on diaphragm activation. The general experimental paradigm is illustrated in Fig. 3*A*.

In the acute C2Hx experiments, diaphragm MUAPs were first evaluated with the spinal cord intact (Fig. 3*B*). The ISMS-evoked potentials in the spinal-intact condition were similar to those described in the preceding section. Acute C2Hx abolished spontaneous inspiratory EMG activity in the ipsilateral hemidiaphragm in all animals (Fig. 3*C*). However, cervical ISMS still produced clear MUAPs in the ipsilateral diaphragm after the acute lesion (Fig. 3*D*). Before C2Hx, the average latency from stimulus to the peak of the MUAP was 1.99 ± 0.25 ms. After C2Hx the value tended to be reduced (1.69 ± 0.57 ms), but this did not approach statistical significance ($P = 0.190$). In seven of eight experiments, the amplitude of the ISMS-evoked MUAP remained relatively consistent after the acute C2Hx, ranging from 80% to 124% of the preinjury value, with a mean of 94 ± 15% ($P = 0.065$ vs. pre-C2Hx). There was one significant outlier rat (confirmed with Grubbs' outlier test, $P < 0.05$) that demonstrated a profound reduction in MUAP amplitude after acute C2Hx, with

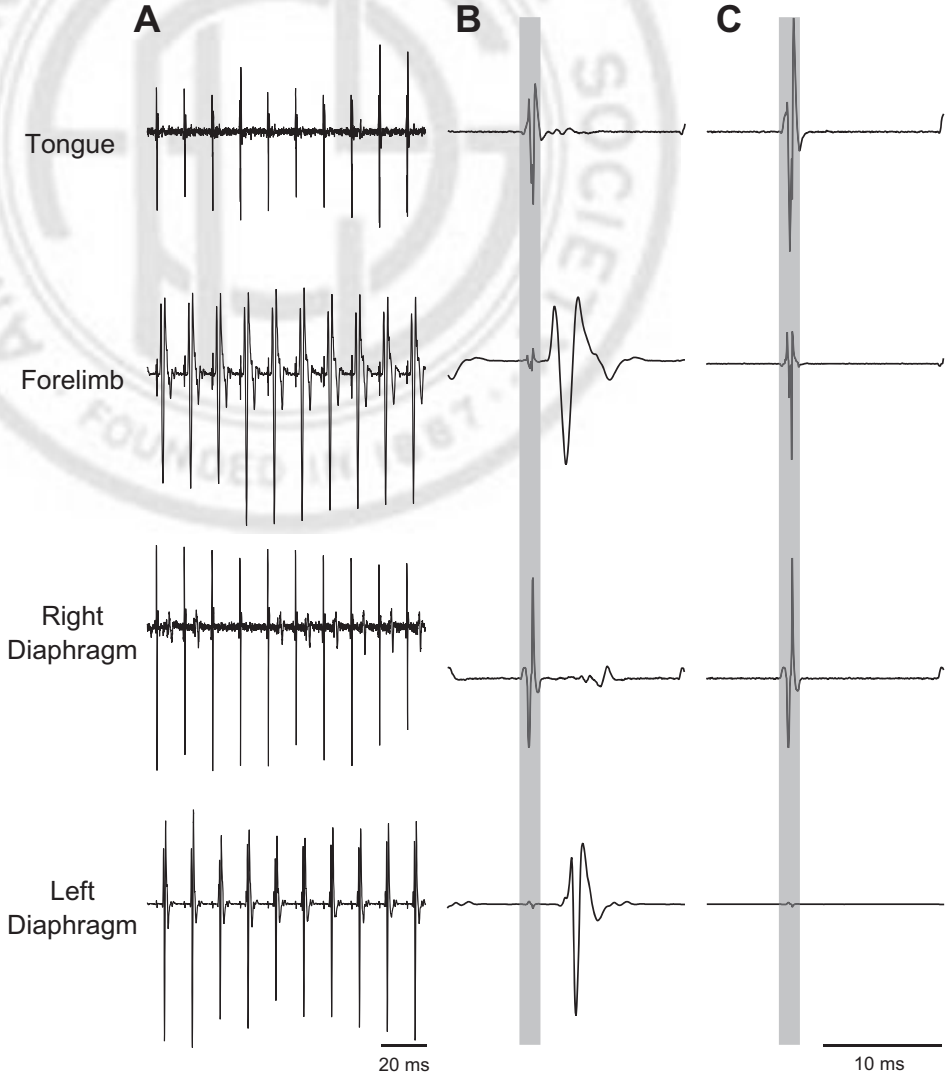

Fig. 2. Examples of raw EMG activity recorded in the tongue (genioglossus), forelimb (ECR), and the left and right hemidiaphragm during ISMS. *A*: representative examples before C2Hx. *B*: stimulus-triggered averages of EMG activity show prominent MUAPs in the forelimb and ipsilateral diaphragm. *C*: stimulus-triggered averages of EMG activity after neuromuscular blockade. In *B* and *C*, the stimulus artifact is highlighted by the gray boxes. Stimulus-triggered averages were scaled to the same values and represent 25 stimulus triggers. In these examples, ISMS was delivered at 100 Hz and 200 μA during expiration.

tapraid4/z9k-neurop/z9k-neurop/z9k00217/z9k4007d17z | xppws | S=1 | 1/6/17 | 8:08 | MS: JN-00721-2016 | Ini: 02/sa/bew

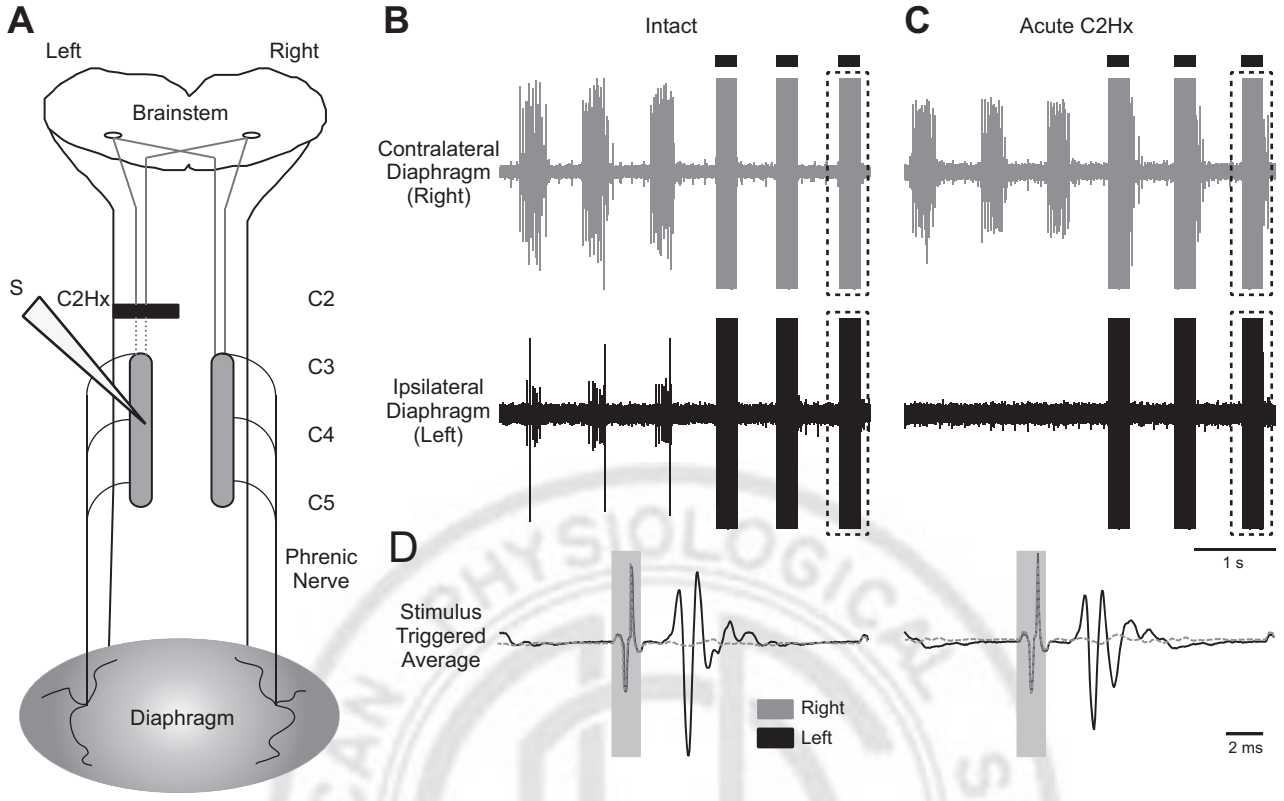

Fig. 3. ISMS after acute C2Hx. *A*: illustration of the electrode placement relative to the C2Hx lesion. The solid dark bar represents the injury site; the dashed lines represent severed pathways. *B*: examples of EMG activity in the right and left diaphragm before C2Hx. *C*: examples of left and right diaphragm EMG activity after acute C2Hx. Note that activity is abolished in the left diaphragm. In *B* and *C*, 3 spontaneous breaths are shown followed by 3 breaths during triggered cervical ISMS (solid bars; 100 Hz, 200 μA). *D*: stimulus-triggered averages of right and left diaphragm EMG activity obtained from the period of ISMS highlighted by dashed boxes in *B* and *C*. Stimulus-triggered averages were scaled to the same values and represent 25 stimulus triggers. In *D*, the stimulus artifact is highlighted by the gray boxes.

AQ: 6

evoked responses reaching only 8% of the preinjury amplitude. If that particular data point is included in the calculation of the overall mean the values after acute C2Hx are 83 ± 35% of the preinjury condition, but the added variance actually produces a higher P value ($P = 0.139$ vs. preinjury). Collectively, the data are consistent with a slight reduction in cervical ISMS-evoked MUAP amplitude in most animals after acute C2Hx. The off-target impact of ISMS after C2Hx (i.e., evoked activity in ECR, tongue, and right diaphragm) was indistinguishable from that reported above for the spinal-intact condition (data not shown).

Tracheal pressures were evaluated to explore the potential of a biomechanical impact of ISMS-induced muscle contraction (Fig. 4, *A* and *B*). Negative pressure swings in tracheal pressure would be expected in this preparation if diaphragm contraction is altering the dimensions of the thoracic cavity. In the spinal-intact condition, genioglossus-triggered cervical ISMS caused a significant negative deflection in tracheal pressure ($P = 0.02$ vs. baseline; Fig. 4*C*), as expected. The acute C2Hx injury resulted in a small, but statistically significant, change in the tracheal pressures that were recorded during ventilator-induced lung inflation (i.e., independent of ISMS; $P = 0.028$; Fig. 4*C*). After acute C2Hx, ISMS also induced a change in tracheal pressure ($P = 0.005$ vs. baseline), thus suggesting a biomechanical impact of the stimulation. However, the relative magnitude of ISMS-induced changes in tracheal pressure were attenuated after C2Hx ($P = 0.038$; Fig. 4*C*).

F4

Spontaneous ipsilateral diaphragm EMG activity was absent in rats studied 5–21 days after C2Hx (Fig. 5*A*), and subsequent histological evaluation of the spinal cord indicated anatomically complete hemilesion in all animals (Fig. 5*B*). The ISMS procedure evoked clearly discernible MUAPs in the ipsilateral (paralyzed) hemidiaphragm (Fig. 5*C*). Compared with the acute injury group, the only apparent difference in the ISMS responses in the animals with the subacute lesions was a trend for more variable and longer latencies. On average, however, there were no statistical differences between the groups for latency (acute C2Hx: 1.69 ± 0.57 ms, subacute C2Hx: 2.50 ± 0.67 ms), but the increase in latency in the subacute group was close to threshold for significance ($P = 0.065$). The MUAP amplitude was variable, but with no evidence for a difference between the two groups (acute C2Hx: 1.62 ± 1.45 mV, subacute C2Hx: 1.76 ± 2.65 mV, $P = 0.833$). ISMS caused the expected negative deflection in tracheal pressure in the subacute C2Hx animals, thus confirming that there was a biomechanical impact of the stimulation (Fig. 5*D*). The off-target muscle activation was similar to what was obtained in the spinal-intact and acute C2Hx animals. Thus very small but statistically significant changes in EMG activity during ISMS were detected in the tongue (4/5 animals), intercostal (3/4 animals), and right diaphragm (4/5 animals). The left ECR showed greater EMG responses in five of five animals.

F5

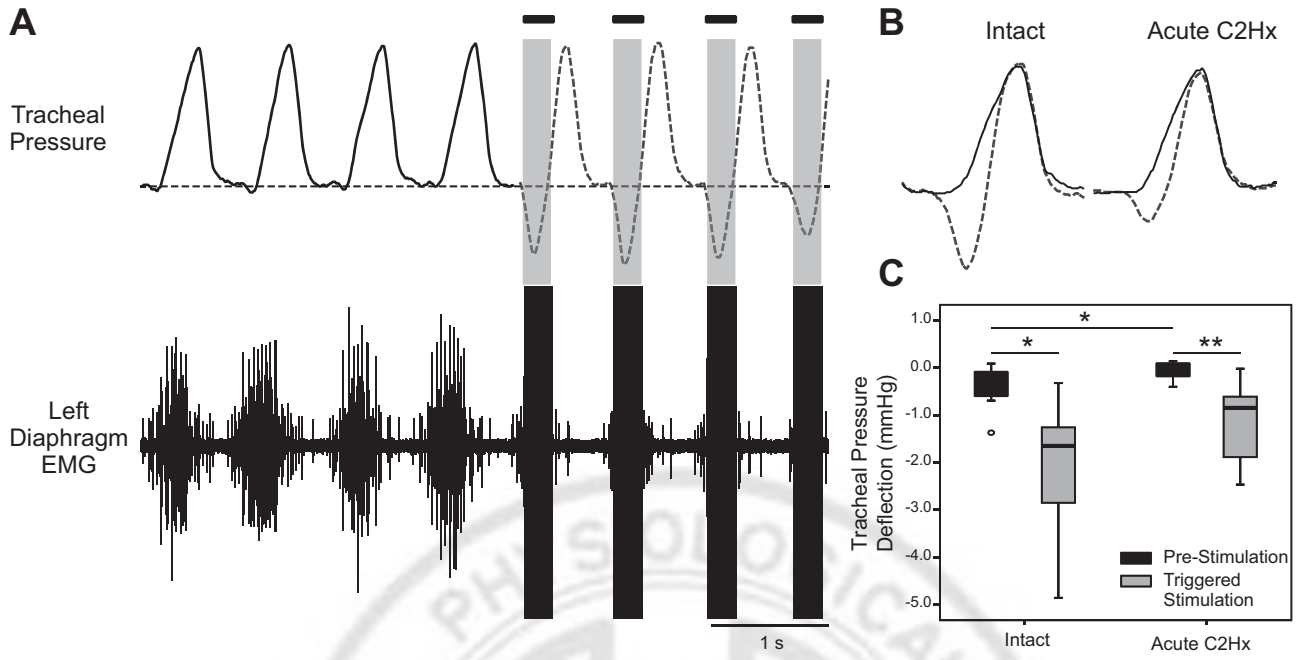

Fig. 4. Impact of ISMS on tracheal pressure. *A*: representative examples of tracheal pressure and left diaphragm EMG activity before and during cervical ISMS (100 Hz, 200 μA). The period of ISMS is indicated by the solid bars. Note the negative deflection in tracheal pressure during ISMS. *B*: overlay plot further illustrates the tracheal pressure before stimulation (solid line) and during ISMS (dashed line). *C*: average change in tracheal pressure during lung inflation at prestimulation baseline and during ISMS. Data are shown for the spinal-intact condition (*left*) and after acute C2Hx (*right*). $*P < 0.05$, $**P < 0.005$.

Inspiratory-related diaphragm EMG bursting is enhanced after ISMS. While our primary intent was to determine whether ISMS evoked diaphragm activity during the period of stimulation, we noted that spontaneous diaphragm EMG activity often was present after the stimulus was turned off. Thus, in six of eight animals after acute C2Hx, the hemidiaphragm that was electrically silent before ISMS showed both tonic and inspiratory-related activity during and after the 1-min period of stimulation (Fig. 6*A*). In these experiments, "activity" was defined as one or more clearly discernible motor unit potentials that were discharging phasically during the inspiratory period. The duration of the effect was variable and did not persist beyond 2 min in any experiment. On average, ISMS-induced spontaneous diaphragm motor unit activity lasted for 43 ± 38

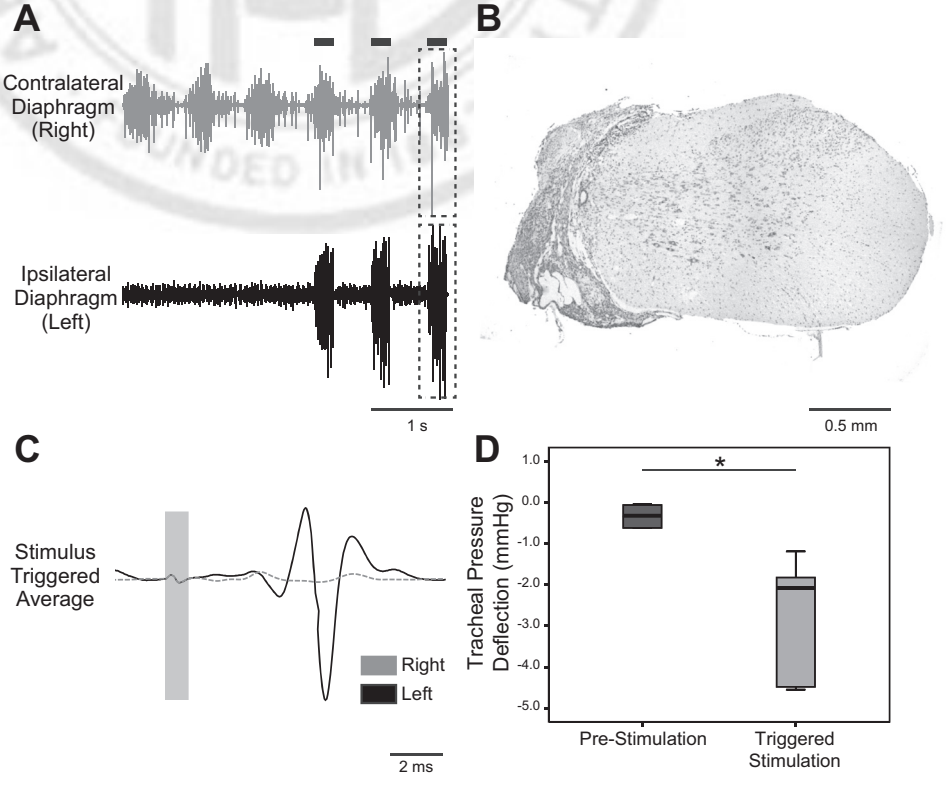

Fig. 5. ISMS after subacute C2Hx. *A*: representative diaphragm EMG activity after subacute C2Hx. In the example traces, genioglossus-triggered ISMS was delivered during the breaths marked by the black bars. *B*: histological section of the C_2 spinal cord stained with cresyl violet. The example demonstrates an anatomically complete hemilesion extending to the midline of cervical cord. *C*: stimulus-triggered averages from the ipsilesional (solid line) and contralesional diaphragm (dashed line); data were obtained from the period indicated by the dashed boxes in *A*. These traces illustrate activation of the diaphragm ipsilateral to the C2Hx lesion. *D*: average change in tracheal pressure during lung inflation at prestimulation baseline and during ISMS. $*P < 0.05$.

tapraid4/z9k-neurop/z9k-neurop/z9k00217/z9k4007d17z | xppws | S=1 | 1/6/17 | 8:08 | MS: JN-00721-2016 | Ini: 02/sa/bew

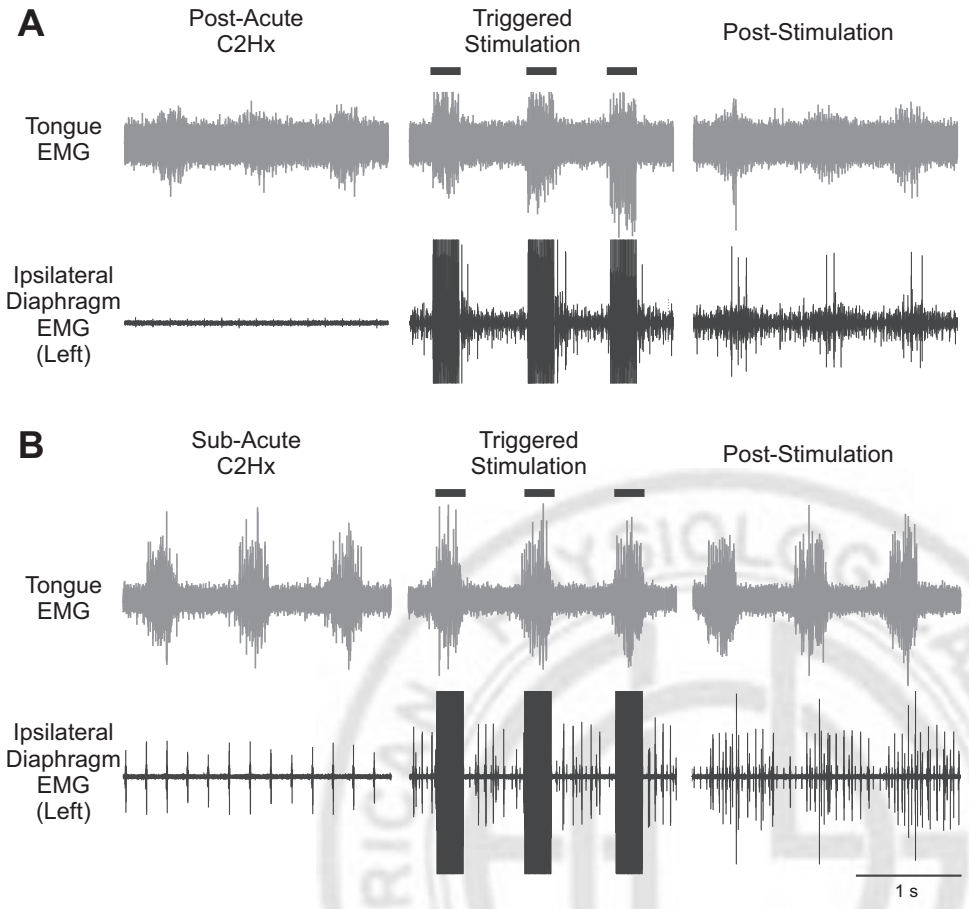

Fig. 6. Example recordings illustrate short-term potentiation of ipsilateral diaphragm EMG activity following ISMS. *A*: tongue and ipsilateral (left) diaphragm EMG activity after acute C2Hx, during ISMS, and immediately after cessation of ISMS. Note that clear phasic (inspiratory) activity can be seen after ISMS, whereas the baseline showed no such activity. *B*: a similar response can be observed in a subacute C2Hx animal. In these examples, the ISMS was triggered by the inspiratory genioglossus EMG signal and was delivered at 100 Hz for 1 min of respiratory efforts.

respiratory cycles after ISMS was terminated. The first breath immediately after cessation of ISMS typically demonstrated the greatest amount of motor unit recruitment, and this was followed by a gradual decrease in motor unit activity over subsequent respiratory cycles. In addition, we noted an increase in tonic activity (i.e., activity persisting across the entire respiratory cycle) after ISMS that followed a time course similar to the phasically active motor units. A similar response to ISMS was observed in three of five rats after subacute C2Hx injury (Fig. 6*B*).

DISCUSSION

This study has demonstrated the feasibility of using endogenous medullary output to trigger ISMS to the midcervical spinal cord. The ISMS paradigm was successful in recruiting diaphragm motor units in spinal-intact animals and also after both acute and subacute interruption of bulbospinal inspiratory drive to the phrenic motoneuron pool following high cervical SCI. Further refinement of this approach may enable development of a "respiratory neuroprosthesis" that, by virtue of the endogenous trigger, could adapt to temporally changing metabolic demands.

Endogenously triggered ISMS induces diaphragm activation. The approach used in this study was a "closed-loop-like" strategy for activating phrenic motoneurons in the cervical spinal cord. As an initial proof of concept, cervical ISMS was triggered from EMG signals recorded from the base of the tongue. Such recordings consist largely of activity from the primary tongue protrudor muscle, the genioglossus (Fuller et al. 1998). Respiratory-related activation of the genioglossus occurs in humans (Mateika et al. 1999; Saboisky et al. 2007) and animal models (Bailey et al. 2005; Fregosi and Fuller 1997) and acts to stiffen and/or dilate the oropharyngeal airway and thus preserve upper airway patency during breathing. The respiratory-related discharge of genioglossus motor units increases during chemoreceptor stimulation in a manner similar to respiratory pump muscles such as the diaphragm (Bailey 2011; Fuller et al. 1998). Genioglossus and tongue muscle output is also subject to vagal modulation, with progressive inhibition occurring as the lung inflates (Bailey et al. 2001; Fukuda and Honda 1982). Collectively, the literature establishes that a complex but coordinated interaction between the genioglossus and the respiratory pump muscles is important for optimizing airway resistance across the respiratory cycle and maintaining upper airway patency. For the present study, the most salient point is that an inspiratory signal was recorded from the genioglossus that provided a marker for the endogenous respiratory rhythm. Thus the animals' own "decision to breathe" triggered the cervical ISMS.

The genioglossus EMG-triggered cervical ISMS approach resulted in diaphragm motor unit activation after both acute (i.e., minutes) and subacute (i.e., days-weeks) C2Hx injury. It was important to repeat the studies under these advanced lesion settings because severed descending pathways have not undergone degeneration after acute injury and therefore could still be capable of conducting action potentials during stimulation

(Gandevia and Kirkwood 2011; Kowalski et al. 2013) as seen in other experimental conditions (Moldovan et al. 2009). Indeed, the latencies of the diaphragm MUAPs in the acute condition (i.e., >1.6 ms) were not consistent with direct phrenic motoneuron activation, and therefore it is likely that synaptic inputs to the phrenic motoneuron pool were being activated via ISMS. Accordingly, it was uncertain if the ISMS approach would be effective at later C2Hx postinjury intervals when degeneration of severed bulbospinal respiratory axons would be well underway. The results showed that diaphragm MUAPs could still be effectively evoked after subacute injury but with a trend toward longer and more variable diaphragm MUAP latencies compared with acute C2Hx animals. In addition, the biomechanical impact of the ISMS (indirectly inferred from changes in tracheal pressure) also appeared to be reduced after subacute vs. acute injury. Refinement of the ISMS method to enable direct phrenic motoneuron stimulation will likely be necessary to optimize diaphragm activation after long-term cervical SCI.

An interesting and potentially important observation that was not part of our original hypothesis was that ISMS-induced inspiratory bursting in the hemiparetic diaphragm persisted for several respiratory cycles after cessation of the stimulation. This occurred in the majority of acute and subacute C2Hx lesions and is similar to the previously described phenomenon of respiratory short-term potentiation (STP) (Lee et al. 2015). Exposure to brief periods of reduced oxygen (hypoxia) triggers phrenic STP, which is manifested as a progressive enhancement of activity followed by a slow decline to baseline levels after removal of the hypoxic stimulus (Lee et al. 2009; Powell et al. 1998). We previously demonstrated that hypoxia can induce STP of phrenic motor output in rats with subacute C2Hx, and the response is greater in the nerve ipsilateral vs. contralateral to the lesion (Lee et al. 2015). The STP in C2Hx rats appeared to reflect recruitment of a population of phrenic motoneurons that had been silenced by injury, which continued to burst beyond the period of hypoxic stimulation. It may be that ISMS can trigger similar STP-like mechanisms of short-term plasticity and ultimately have value in the context of neurorehabilitation. This increased phrenic bursting after cessation of ISMS also may be analogous to longer-duration functional recoveries others have observed with chronic ISMS in other motor systems (Kasten et al. 2013; McPherson et al. 2015).

Methodological caveats including off-target effects of cervical ISMS. The method described here is not truly a "closed-loop" system because the ISMS intensity did not vary with the relative strength of endogenous "respiratory drive." Varying the stimulus intensity or duration in proportion to the relative magnitude of the EMG burst used to trigger ISMS (vs. a simple "onset trigger") could potentially address that issue, but this could also prove problematic since ISMS needs to occur at the onset (vs. peak) of the inspiratory effort. Another caveat is that rats were mechanically ventilated because in our experience spontaneously breathing and anesthetized rats rapidly develop arterial hypercapnia and respiratory acidosis. However, mechanical ventilation will impact endogenous respiratory drive and thereby alter the interactions between spontaneous and ISMS input to the phrenic region. It should also be noted that tongue EMG activity is unlikely to provide an effective ISMS trigger signal in the vagally intact and spontaneously breathing rodent or human. It is possible to record inspiratory-related discharge from the tongue muscles in the awake human and rodent, but available data indicate that tongue EMG may not provide a consistent inspiratory trigger signal (Bailey 2011; Sood et al. 2005). In the present experiments on anesthetized rats, however, the tongue EMG output enabled a rigorous test of the fundamental hypothesis, and we suggest that future work should focus on additional potential sources of respiratory output to serve as endogenous trigger signals or alternative detection algorithms (Dow et al. 2006).

Neural substrate considerations. One of the more challenging issues related to electrical stimulation of the spinal cord is identification of the neural substrate being affected directly or indirectly. Here our immediate goal was to target ISMS of gray matter at the level of the phrenic motor nucleus. Whether phrenic motoneurons are being directly activated by ISMS cannot be determined from the present findings, although latencies in the range of 1.5–2.5 ms suggest indirect stimulation via polysynaptic pathways. In the subacute C2Hx group, stimulation of ipsilateral bulbospinal inputs to phrenic motoneurons can be effectively ruled out because these pathways will be undergoing degeneration. It is possible that ISMS activated commissural bulbospinal projections from the contralateral cord [i.e., pathways associated with the "crossed phrenic phenomenon" (Goshgarian 2003; Goshgarian et al. 1991)]. However, past studies in which intraspinal stimulation of the cervical cord was used to activate crossed phrenic pathways reported latencies of <1 ms (Fuller et al. 2003), and these are considerably shorter than the values reported here. Collectively, the evidence is most consistent with indirect activation of phrenic motoneurons via ISMS, possibly via spinal prephrenic interneurons (Lane 2011) or even ascending afferent projections originating below the injury (Decima and von Euler 1969).

ISMS is capable of discrete activation of circuitry with minimal undesired physiological effects (Pikov et al. 2007). Here we observed clear responses in the ipsilateral diaphragm, as intended, but also off-target motor unit recruitment. Very small and inconsistent activation of the contralateral diaphragm, intercostal muscles, and genioglossus were present during ISMS. This indicates current spread beyond the target region or activation of other circuits via interneurons (Perlmutter et al. 1998). For example, in the case of ISMS-evoked responses in the contralateral diaphragm and intercostal muscles, our previous transneuronal tracing studies provide an interneuronal basis for those off-target responses (Lane et al. 2008). Intercostal and/or contralateral diaphragm recruitment could in fact be advantageous when cervical SCIs involve much larger-scale compromise of diaphragm and inspiratory intercostal function compared with C2Hx. Activation of the genioglossus was barely above the threshold for detection and probably reflected activation of ascending projections to medullary respiratory control neurons. For example, we previously reported that some cervical interneurons associated with the phrenic motor circuit have ascending projections to the medulla (Lane et al. 2008).

The relatively stronger coactivation of forelimb muscles induced by ISMS presents a more challenging technical issue. As with the ipsilateral diaphragm, constant-latency entrainment occurred in the forelimb, and this may reflect overlap of phrenic and forelimb circuits along the rostro-caudal axis

AQ: 4

(Gonzalez-Rothi et al. 2015). ECR motoneurons, however, appear to occupy a more dorso-lateral position than the phrenic motoneuron pool (Tosolini and Morris 2012). This raises the possibility that even if ISMS was precisely restricted to phrenic motoneurons, concomitant excitation of ECR axons as they course toward their ventral roots could still occur. Further investigations are needed to sort out the neuroanatomical basis for direct vs. indirect effects of ISMS. The latter may be especially beneficial by activating desired motoneuron pools in a more natural order than achieved with direct stimulation.

Conclusions. Previous studies directed at spinal cord stimulation and the respiratory system after SCI have focused on epidural stimulation as a means of enhancing abdominal or phrenic motor output. Epidural stimulation has been successful at recruiting diaphragm motor units in animal studies (DiMarco and Kowalski 2009, 2011; Kowalski et al. 2013) and has been used to enhance cough in spinally injured humans (DiMarco et al. 2014). Epidural stimulation also shows promise in the context of locomotor function after SCI in both animals and humans (Edgerton and Harkema 2011; Rejc et al. 2015). Despite these successes, there is unquestionably a need for improvement and refinement of spinal cord stimulation methods. In that regard, the initial findings from our study raise the possibility of utilizing endogenous, physiologically relevant respiratory signals, which entail peripheral and chemosensory feedback, for triggering neuromodulation of the phrenic motor circuit and alleviation of ventilatory insufficiency following mid- to high-cervical SCI. Many ISMS parameters (Bamford and Mushahwar 2011; Giszter 2015; Tator et al. 2012) must be refined, however, before the benefits of invasive ISMS protocols to promote respiratory improvements after cervical SCI can be fully evaluated or compared with other approaches, high-frequency epidural stimulation (Kowalski et al. 2013) in particular. It also is possible that ~~one~~ spinal stimulation approach will be better suited for some SCI cases than ~~others~~. Future investigations involving awake, spontaneously breathing animals will be crucial for determining whether chronic ISMS delivery will function solely as a neuroprosthetic or can be used short term to promote functional and anatomical neuroplasticity (Moritz et al. 2007) alone or in combination with other therapeutic approaches leading to long-lasting improvement in respiratory function.

ACKNOWLEDGMENTS

We thank Dr. Danielle Meola, L. Emma Denholtz, Amy Poirier, Sarah El-Azab, and Alexis Caballero for their technical contributions.

GRANTS

This work was funded by awards from the Department of Defense (W81XWH-14-1-0625; P. J. Reier), the National Institutes of Health (NIH) [R01 NS-054025 (P. J. Reier), R01 NS-080180 (D. D. Fuller)], and the State of Florida Brain and Spinal Cord Injury Research Trust Fund (P. J. Reier, D. D. Fuller, D. M. Baekey). The authors also express their appreciation for the generous support received from the Fraternal Order of Eagles Aerie #3496. L. M. Mercier was supported by a NIH T32 training grant (HD-043730).

DISCLOSURES

No conflicts of interest, financial or otherwise, are declared by the author(s).

AUTHOR CONTRIBUTIONS

L.M.M. and E.J.G.-R. performed experiments; L.M.M., K.A.S., S.S.P., and A.S.P. analyzed data; L.M.M., D.D.F., P.J.R., and D.M.B. interpreted results of experiments; L.M.M. prepared figures; L.M.M. and D.M.B. drafted manuscript; L.M.M., E.J.G.-R., K.A.S., S.S.P., A.S.P., D.D.F., P.J.R., and D.M.B. approved final version of manuscript; D.D.F., P.J.R., and D.M.B. edited and revised manuscript; D.M.B. conceived and designed research.

REFERENCES

Aertsen AM, Gerstein GL. Evaluation of neuronal connectivity: sensitivity of cross-correlation. *Brain Res* 340: 341–354, 1985.

Bailey EF. Activities of human genioglossus motor units. *Respir Physiol Neurobiol* 179: 14–22, 2011.

Bailey EF, Janssen PL, Fregosi RF. PO_2-dependent changes in intrinsic and extrinsic tongue muscle activities in the rat. *Am J Respir Crit Care Med* 171: 1403–1407, 2005.

Bailey EF, Jones CL, Reeder JC, Fuller DD, Fregosi RF. Effect of pulmonary stretch receptor feedback and CO_2 on upper airway and respiratory pump muscle activity in the rat. *J Physiol* 532: 525–534, 2001.

Bamford JA, Mushahwar VK. Intraspinal microstimulation for the recovery of function following spinal cord injury. *Prog Brain Res* 194: 227–239, 2011.

Bezzant TB, Mortensen JD. Risks and hazards of mechanical ventilation: a collective review of published literature. *Dis Mon* 40: 581–638, 1994.

Decima EE, von Euler C. Excitability of phrenic motoneurones to afferent input from lower intercostal nerves in the spinal cat. *Acta Physiol Scand* 75: 580–591, 1969.

DiMarco AF, Kowalski KE. High-frequency spinal cord stimulation of inspiratory muscles in dogs: a new method of inspiratory muscle pacing. *J Appl Physiol (1985)* 107: 662–669, 2009.

DiMarco AF, Kowalski KE. Distribution of electrical activation to the external intercostal muscles during high frequency spinal cord stimulation in dogs. *J Physiol* 589: 1383–1395, 2011.

DiMarco AF, Kowalski KE. Spinal pathways mediating phrenic activation during high frequency spinal cord stimulation. *Respir Physiol Neurobiol* 186: 1–6, 2013.

DiMarco AF, Kowalski KE. Electrical activation to the parasternal intercostal muscles during high-frequency spinal cord stimulation in dogs. *J Appl Physiol (1985)* 118: 148–155, 2015.

DiMarco AF, Kowalski KE, Hromyak DR, Geertman RT. Long-term follow-up of spinal cord stimulation to restore cough in subjects with spinal cord injury. *J Spinal Cord Med* 37: 380–388, 2014.

DiMarco AF, Onders RP, Ignagni A, Kowalski KE, Mortimer JT. Phrenic nerve pacing via intramuscular diaphragm electrodes in tetraplegic subjects. *Chest* 127: 671–678, 2005.

Dow DE, Mantilla CB, Zhan WZ, Sieck GC. EMG-based detection of inspiration in the rat diaphragm muscle. *Conf Proc IEEE Eng Med Biol Soc* 1: 1204–1207, 2006.

Edgerton VR, Harkema S. Epidural stimulation of the spinal cord in spinal cord injury: current status and future challenges. *Expert Rev Neurother* 11: 1351–1353, 2011.

Fregosi RF, Fuller DD. Respiratory-related control of extrinsic tongue muscle activity. *Respir Physiol* 110: 295–306, 1997.

Fukuda Y, Honda Y. Roles of vagal afferents on discharge patterns and CO_2-responsiveness of efferent superior laryngeal, hypoglossal, and phrenic respiratory activities in anesthetized rats. *Jpn J Physiol* 32: 689–698, 1982.

Fuller D, Mateika JH, Fregosi RF. Co-activation of tongue protrudor and retractor muscles during chemoreceptor stimulation in the rat. *J Physiol* 507: 265–276, 1998.

Fuller DD, Doperalski NJ, Dougherty BJ, Sandhu MS, Bolser DC, Reier PJ. Modest spontaneous recovery of ventilation following chronic high cervical hemisection in rats. *Exp Neurol* 211: 97–106, 2008.

Fuller DD, Fregosi RF. Fatiguing contractions of tongue protrudor and retractor muscles: influence of systemic hypoxia. *J Appl Physiol* 88: 2123–2130, 2000.

Fuller DD, Johnson SM, Olson EB Jr, Mitchell GS. Synaptic pathways to phrenic motoneurons are enhanced by chronic intermittent hypoxia after cervical spinal cord injury. *J Neurosci* 23: 2993–3000, 2003.

Fuller DD, Williams JS, Janssen PL, Fregosi RF. Effect of co-activation of tongue protrudor and retractor muscles on tongue movements and pharyngeal airflow mechanics in the rat. *J Physiol* 519: 601–613, 1999.

Gandevia SC, Kirkwood PA. Spinal breathing: stimulation and surprises. *J Neurotrauma* 589: 2661–2662, 2011.

Giszter SF. Spinal primitives and intra-spinal micro-stimulation (ISMS) based prostheses: a neurobiological perspective on the "known unknowns" in ISMS and future prospects. *Front Neurosci* 9: 72, 2015.

Glenn WW, Phelps ML. Diaphragm pacing by electrical stimulation of the phrenic nerve. *Neurosurgery* 17: 974–984, 1985.

Gonzalez-Rothi EJ, Rombola AM, Rousseau CA, Mercier LM, Fitzpatrick GM, Reier PJ, Fuller DD, Lane MA. Spinal interneurons and forelimb plasticity after incomplete cervical spinal cord injury in adult rats. *J Neurotrauma* 32: 893–907, 2015.

Goshgarian HG. The role of cervical afferent nerve fiber inhibition of the crossed phrenic phenomenon. *Exp Neurol* 72: 211–225, 1981.

Goshgarian HG. The crossed phrenic phenomenon: a model for plasticity in the respiratory pathways following spinal cord injury. *J Appl Physiol* 94: 795–810, 2003.

Goshgarian HG, Ellenberger HH, Feldman JL. Decussation of bulbospinal respiratory axons at the level of the phrenic nuclei in adult rats: a possible substrate for the crossed phrenic phenomenon. *Exp Neurol* 111: 135–139, 1991.

Kasten MR, Sunshine MD, Secrist ES, Horner PJ, Moritz CT. Therapeutic intraspinal microstimulation improves forelimb function after cervical contusion injury. *J Neural Eng* 10: 044001, 2013.

Kowalski KE, Hsieh YH, Dick TE, DiMarco AF. Diaphragm activation via high frequency spinal cord stimulation in a rodent model of spinal cord injury. *Exp Neurol* 247: 689–693, 2013.

Laghi F, Cattapan SE, Jubran A, Parthasarathy S, Warshawsky P, Choi YS, Tobin MJ. Is weaning failure caused by low-frequency fatigue of the diaphragm? *Am J Respir Crit Care Med* 167: 120–127, 2003.

Lane MA. Spinal respiratory motoneurons and interneurons. *Respir Physiol Neurobiol* 179: 3–13, 2011.

Lane MA, White TE, Coutts MA, Jones AL, Sandhu MS, Bloom DC, Bolser DC, Yates BJ, Fuller DD, Reier PJ. Cervical prephrenic interneurons in the normal and lesioned spinal cord of the adult rat. *J Comp Neurol* 511: 692–709, 2008.

Lee KZ, Reier PJ, Fuller DD. Phrenic motoneuron discharge patterns during hypoxia-induced short-term potentiation in rats. *J Neurophysiol* 102: 2184–2193, 2009.

Lee KZ, Sandhu MS, Dougherty BJ, Reier PJ, Fuller DD. Hypoxia triggers short term potentiation of phrenic motoneuron discharge after chronic cervical spinal cord injury. *Exp Neurol* 263: 314–324, 2015.

Mansel JK, Norman JR. Respiratory complications and management of spinal cord injuries. *Chest* 97: 1446–1452, 1990.

Mateika JH, Millrood DL, Kim J, Rodriguez HP, Samara GJ. Response of human tongue protrudor and retractors to hypoxia and hypercapnia. *Am J Respir Crit Care Med* 160: 1976–1982, 1999.

McPherson JG, Miller RR, Perlmutter SI. Targeted, activity-dependent spinal stimulation produces long-lasting motor recovery in chronic cervical spinal cord injury. *Proc Natl Acad Sci USA* 112: 12193–12198, 2015.

Melssen WJ, Epping WJ. Detection and estimation of neural connectivity based on crosscorrelation analysis. *Biol Cybern* 57: 403–414, 1987.

Moldovan M, Alvarez S, Krarup C. Motor axon excitability during Wallerian degeneration. *Brain* 132: 511–523, 2009.

Mondello SE, Sunshine MD, Fischedick AE, Moritz CT, Horner PJ. A cervical hemi-contusion spinal cord injury model for the investigation of novel therapeutics targeting proximal and distal forelimb functional recovery. *J Neurotrauma* 32: 1994–2007, 2015.

Moritz CT, Lucas TH, Perlmutter SI, Fetz EE. Forelimb movements and muscle responses evoked by microstimulation of cervical spinal cord in sedated monkeys. *J Neurophysiol* 97: 110–120, 2007.

Mushahwar VK, Collins DF, Prochazka A. Spinal cord microstimulation generates functional limb movements in chronically implanted cats. *Exp Neurol* 163: 422–429, 2000.

Onders RP, Elmo M, Khansarinia S, Bowman B, Yee J, Road J, Bass B, Dunkin B, Ingvarsson PE, Oddsdottir M. Complete worldwide operative experience in laparoscopic diaphragm pacing: results and differences in spinal cord injured patients and amyotrophic lateral sclerosis patients. *Surg Endosc* 23: 1433–1440, 2009.

Perlmutter SI, Maier MA, Fetz EE. Activity of spinal interneurons and their effects on forearm muscles during voluntary wrist movements in the monkey. *J Neurophysiol* 80: 2475–2494, 1998.

Pikov V, Bullara L, McCreery DB. Intraspinal stimulation for bladder voiding in cats before and after chronic spinal cord injury. *J Neural Eng* 4: 356–368, 2007.

Powell FL, Milsom WK, Mitchell GS. Time domains of the hypoxic ventilatory response. *Respir Physiol* 112: 123–134, 1998.

Rejc E, Angeli C, Harkema S. Effects of lumbosacral spinal cord epidural stimulation for standing after chronic complete paralysis in humans. *PLoS One* 10: e0133998, 2015.

Saboisky JP, Gorman RB, De Troyer A, Gandevia SC, Butler JE. Differential activation among five human inspiratory motoneuron pools during tidal breathing. *J Appl Physiol* 102: 772–780, 2007.

Smuder AJ, Gonzalez-Rothi EJ, Kwon OS, Morton AB, Sollanek KJ, Powers SK, Fuller DD. Cervical spinal cord injury exacerbates ventilator-induced diaphragm dysfunction. *J Appl Physiol (1985)* 120: 166–177, 2016.

Sood S, Morrison JL, Liu H, Horner RL. Role of endogenous serotonin in modulating genioglossus muscle activity in awake and sleeping rats. *Am J Respir Crit Care Med* 172: 1338–1347, 2005.

Sunshine MD, Cho FS, Lockwood DR, Fechko AS, Kasten MR, Moritz CT. Cervical intraspinal microstimulation evokes robust forelimb movements before and after injury. *J Neural Eng* 10: 036001, 2013.

Tator CH, Minassian K, Mushahwar VK. Spinal cord stimulation: therapeutic benefits and movement generation after spinal cord injury. *Handb Clin Neurol* 109: 283–296, 2012.

Tosolini AP, Morris R. Spatial characterization of the motor neuron columns supplying the rat forelimb. *Neuroscience* 200: 19–30, 2012.

Winslow C, Rozovsky J. Effect of spinal cord injury on the respiratory system. *Am J Phys Med Rehabil* 82: 803–814, 2003.

AUTHOR QUERIES

AUTHOR PLEASE ANSWER ALL QUERIES 1

AQau—Please confirm the given-names and surnames are identified properly by the colors. ■= Given-Name, ■= Surname

AQ1— AU: Please read entire Proof (including Query page), answer queries, and make essential corrections in Proof margins; return Proof via e-mail or by 1- or 2-day carrier WITHIN TWO BUSINESS DAYS. Please include Query page. IMPORTANT: e-mail (mpasho@the-aps.org) an itemized list of requested changes (these should be essential data error changes and not cosmetic changes, which will not be implemented at this late stage in production). Please do not undo what may have been copy-edited to conform to APS journal style (use of hyphens, quotation marks, italics for certain phrases, non-use of italics for Latin phrases and for emphasis, etc.).

AQ2— AU: Please note that the author list in the abstract line represents the form in which these names will appear in many online databases, such as the NCBI/NIH/NLM PubMed database. Check this carefully, be sure there are no misrepresentations. Please make a note on the proof, if any corrections are needed.

AQ3— AU: Check all figures and legends carefully. Changes to figures will be made only to correct scientifically relevant errors.

AQ4— AU: Journal style does not permit use of italics for emphasis.

AQ5— AU: The text in the DISCLOSURES section reflects your data entry into the Peer Review submission system. Is this still complete, relevant, and accurate?

AQ6— AU: “dashed boxes in *B* and *C*” correct in Figure 3 legend?

AQ7— AU: Please verify accuracy of your e-mail address in the address for correspondence, or delete e-mail address if you do not want it included. (Note: this material is listed as a footnote at bottom of left column of text, on the first page.)

Articles in PresS. J Neurophysiol (December 14, 2016). doi:10.1152/jn.00638.2016

Coupling multi-electrode array recordings with silver labeling of recording sites to study cervical spinal network connectivity

Streeter KA[1], Sunshine MD[1], Patel SR[1], Liddell SS[2], Denholtz LE[2], Reier PJ[2], Fuller DD[1], Baekey DM[3]

[1]Department of Physical Therapy, University of Florida, Gainesville, FL 32610
[2]Department of Neuroscience, University of Florida, Gainesville, FL, 32610
[3]Department of Physiological Sciences, University of Florida, Gainesville, FL 32610

Correspondence:

David M. Baekey, PhD
Department of Physiological Sciences
Box 100144
1333 Center Drive
Gainesville, FL 32610-0144
Phone: (352) 294-4015
Email: dbaekey@ufl.edu

Running Title: Correlating and silver labeling spinal interneurons

Keywords: Spinal cord, Phrenic motor output, Cross-correlation, Functional connectivity, Metal deposition

Acknowledgements: The authors thank Dave Doyle at Bare Electronics (Gainesville, FL) Dr. Nicole Tester, Alexis Caballero, and Kelly Schwanebeck for their technical assistance. This work was supported by funding from the National Institute of Health, grant numbers: 1RO1NS080180-01A1 (DDF), 1F32NS095620-01 (KAS), and T32-ND043730 (MDS). The Department of Defense, grant number W81XWH-14-1-0625 (PJR and DDF).

Abstract

Mid-cervical spinal interneurons form a complex and diffuse network and may be involved in modulating phrenic motor output. The intent of the current work was to enable a better understanding of mid-cervical “network level” connectivity by pairing the neurophysiological multi-electrode array (MEA) data with histological verification of the recording locations. We first developed a method to deliver 100 nA currents to electroplate silver onto and subsequently deposit silver from electrode tips after obtaining mid-cervical (C3-5) recordings using an MEA in anesthetized and ventilated adult rats. Spinal tissue was then fixed, harvested, and histologically processed to “develop” the deposited silver. Histological studies verified that the silver deposition method discretely labeled (50 μm resolution) spinal recording locations between laminae IV-X in cervical segments C3-C5. Using correlative techniques, we next tested the hypothesis that mid-cervical neuronal discharge patterns are temporally linked. Cross correlation histograms produced few positive peaks (5.3%) in the range of 0 - 0.4 ms, but 21.4% of neuronal pairs had correlogram peaks with a lag of ≥ 0.6 ms. These results are consistent with synchronous discharge involving mono- and polysynaptic connections among mid-cervical neurons. We conclude that there is a high degree of synaptic connectivity in the mid-cervical spinal cord, and that the silver labeling method can reliably mark metal electrode recording sites and “map” interneuron populations, thereby providing a low cost and effective tool for use in MEA experiments. We suggest that this method will be useful for further exploration of mid-cervical network connectivity.

New and Noteworthy

We describe a method that reliably identifies the locations of multi-electrode array (MEA) recording sites while preserving the surrounding tissue for immunohistochemistry. To our knowledge, this is the first cost-effective method to identify the anatomical locations of neuronal ensembles recorded with a MEA during acute preparations without the requirement of specialized array electrodes. In addition, evaluation of activity recorded from silver labeled sites revealed a previously unappreciated degree of connectivity between mid-cervical interneurons.

Introduction

Mid-cervical spinal interneurons form a complex and diffuse network that is synaptically coupled to both respiratory and non-respiratory motor pools (Gonzalez-Rothi et al. 2015; Lane 2011; Lane et al. 2008b). Several groups have advanced the hypothesis that mid-cervical spinal interneurons can modulate phrenic motoneuron excitability and thereby influence the neural control of the diaphragm (Bellingham and Lipski 1990; Douse and Duffin 1993; Lane et al. 2008a; Lane et al. 2008b; Palisses et al. 1989). While there is some direct evidence to support this hypothesis (Marchenko et al. 2015; Sandhu et al. 2015), other studies have concluded the opposite (Duffin and Iscoe 1996). A significant hurdle in testing that specific hypothesis, or related hypotheses regarding cervical interneuronal circuits, is the difficulty of studying the "functional connectivity" in diffuse spinal cord networks. One of the foremost challenges is simultaneously recording numerous cells, and this can be addressed through the use of multi-electrode arrays (MEA). The MEA approach enables simultaneous recordings of multiple sites, but histologically identifying each recording location (versus the electrode track) while also preserving tissue integrity, poses a further challenge (Borg et al. 2015; Li et al. 2015; Nuding et al. 2015). Thus, the initial thrust of the current work was modification and validation of a silver labeling technique (Spinelli 1975) to enable post-recording deposition of a small amount of silver (i.e., for histological marking) from the tip of each electrode in an MEA. Additionally, we developed an electrical circuit to enable the use of small currents (100 nA) for silver electroplating and deposition to prevent tissue and electrode damage associated with high levels of current (Fung et al. 1998). Using the electroplated MEA, we recorded discharge from ensembles of neurons in the mid-cervical (C3-C5) spinal cord in adult rats and demonstrated a practical application of this technique by "matching" the array electrodes to the corresponding anatomical locations marked by silver.

The overall intent was to enable a better understanding of mid-cervical spinal discharge and "network level" connectivity by pairing the neurophysiological MEA data with histological verification of the recording locations. Thus, using correlative techniques (Moore et al. 1970), we tested the hypothesis that the discharge patterns of mid-cervical (C3-4) spinal neurons are temporally linked in time domains consistent with mono- and poly-synaptic connections. In addition, mid-cervical neuronal discharge patterns were assessed relative to the endogenous inspiratory pattern – measured via bilateral phrenic nerve recordings – to determine if bursting was temporally linked to phrenic motoneuron activity. To our knowledge, no prior study has comprehensively evaluated the temporal characteristics across multiple mid-cervical neurons using MEA technology. The results presented herein demonstrate a previously unappreciated degree of connectivity and indicate a high prevalence of temporally related discharge patterns between mid-cervical interneurons with characteristics consistent with mono- and polysynaptic connections; and also provides a comprehensive description of a cost-effective histological approach for validating anatomical locations of MEA recording sites.

Materials and Methods

Animals

All experiments were conducted with adult Sprague-Dawley rats obtained from ENVIGO (formally Harlan Laboratories). Most experiments (n=12) were performed with untreated, spinal intact rats. A subset of rats (n=2) received a cervical spinal injury (C3/C4 lateralized contusion, force: 205 KD, displacement: 1225 μm; Infinite Horizon pneumatic impactor, Precision Systems & Instrumentation) using published methods from our group (Lane et al. 2012). Spinal injured rats were allowed to recover for 12 weeks prior to electrophysiology. Histological results from spinal injured animals were used to determine effectiveness of silver labeling and to compare micro-motor depths relative to silver labeling depths. Since there is evidence suggesting

neurophysiological properties such as connectivity may be altered following SCI (Lane et al. 2009; Lane et al. 2008b), analysis of neurophysiology was limited to spinal intact animals (n=4). All rats were housed in pairs in a controlled environment (12h light/dark cycles) with food and water *ad libitum*. All experimental protocols were approved by the Institutional Animal Care and Use Committee at the University of Florida.

In Vivo Electrophysiology

All rats were anesthetized with 3% isoflurane (in 100% O_2) and transferred to a heated station where established surgical methods (Lee and Fuller 2010; Lee et al. 2009; Mahamed et al. 2011; Sandhu et al. 2015; Streeter and Baker-Herman 2014a; b; Strey et al. 2012) were used to set up electrophysiological experiments. Core body temperature was maintained at 37 ± 0.5°C with a servo controlled heating device (CWE, model 700 TC-1000). A tail vein catheter was placed for *i.v* delivery of urethane anesthesia and fluids. The trachea was cannulated (PE-240 tubing) and rats were pump-ventilated (Harvard Apparatus, Rodent Ventilator 683; volume: ~3-2.5 mL; frequency: 70/minute). Once ventilated, CO_2 was added ($FiCO_2$: < 3%) to maintain end-tidal CO_2 ($EtCO_2$) between ~40-50 mmHg throughout the protocol (Capnogard; Respironics, Inc.). Tracheal pressure was monitored and lungs were periodically hyperinflated (2-3 breaths) to prevent atelectasis (~1/hour). A bilateral vagotomy was performed. Rats were slowly converted (6ml/hr; Harvard Apparatus syringe pump) to urethane anesthesia (1.7 g/kg, *i.v.* in distilled water) and isoflurane was withdrawn. A femoral arterial catheter (PE-50 tubing) was placed to monitor blood pressure (CWE, TA-100) and sample blood gases (i-STAT1 Analyzer Abbot) throughout the protocol. Using a dorsal approach, the left and right phrenic nerves were isolated, cut distally, and partially desheathed (~1/2 the length of the exposed nerve). A midline incision extending from the base of the skull to mid-thoracic region was made and spinal vertebrae C3-T2 were exposed. Using a nose clamp and T2 spinous process, the rat was slightly elevated off the table to reduce ventilator induced motion artifact and level the

spinal cord. A laminectomy was performed from C3-C6, the dura was cut and reflected back, and the pia was gently removed at the MEA insertion point. A unilateral pneumothorax was performed to decrease chest wall movement and positive end-expiratory pressure (PEEP) of ~1-2 cm of water was applied to prevent atelectasis. Animals received the neuromuscular paralytic pancuronium bromide (2.5 mg/kg, *i.v.*, Hospira, Inc.) to eliminate spontaneous breathing efforts. Adequate depth of anesthesia was monitored by assessing blood pressure responses to toe-pinch and urethane supplements were given as necessary. Blood pressure and fluid homeostasis were maintained by a slow infusion of a 1:3 solution (8.4% sodium bicarbonate/Lactated Ringers, *i.v.*).

Bilateral phrenic nerve output was recorded using custom made bipolar suction electrodes filled with 0.9% saline. Compound action potentials were amplified (X20 k, Grass Instruments, P511), band-pass filtered (3 Hz to 3 kHz), digitized (16-bit, 25k samples/second/channel; Power1401, Cambridge Electronic Design, Cambridge, UK (CED)), and integrated (time constant: 20ms) in Spike2.v8 software (CED). A custom made MEA similar to that originally designed at the University of South Florida by Lindsey BG and colleagues (Morris 1996) and used in our previous report (Sandhu et al. 2015) was used to record bilateral mid-cervical (C3-C5) spinal activity (Figure 1A). The array contained 16 tungsten electrodes coated with Epoxylite Insulation (impedance: 10 ±1 MΩ; shank diameter 125 µm; tip diameter ≤1 µm; FHC, #UEWLEGSE0N1E) (Figure 1B). A key feature of this array is the ability to independently control the depth of each of the electrodes using micro-motors. This greatly improves the recording yield by allowing the experimenter to “hold” a recording on one electrode while continuing to search for neurons with other electrodes. The array was mounted on a stereotaxic frame and eight electrodes arranged in two staggered rows of four were placed into each hemi-cord at the dorsal root entry zone (indicated by black arrows in Figure 1C). The inner distance between the two sets of eight electrodes was approximately 1 mm, while the distance between electrodes within each row was ~300 µm (Figure 1D). Electrodes tips were maintained

in this “fixed matrix” by the array guide. One by one, electrodes were advanced into the spinal cord while audio was monitored until single units with ~3:1 signal to noise ratio were discriminated. Neural signals from single electrodes were amplified (X5k), band-pass filtered (3-3kHz), digitized (16-bit, 25k samples/second/channel; Power 1401, CED) and recorded with Spike2.v8 software (CED). Once phrenic nerve activity and spinal discharge was stable, “baseline activity” was recorded with FiO_2 set to 0.50. Using experimental procedures similar to our previous studies (Sandhu et al. 2015; Strey et al. 2012), the inspiratory gas mixture was altered using adjustable flow meters to expose rats to a 5 min period of hypoxia (FiO_2: 0.11), followed by 15 min of baseline oxygen levels (FiO_2: 0.50). Silver deposition was performed immediately after the neurophysiology protocol. An arterial blood gas was sampled during baseline and hypoxia to assure blood gases were within physiological limits.

Analysis of Electrophysiological Signals

All electrophysiological data was collected and sorted using Spike2.v8 software (CED). Extracellular action potentials from individual neurons were extracted from continuous recordings and converted to waveforms using spike-sorting tools of the acquisition software. Briefly, spikes were clustered using at least 80% template matching and principle component analyses. Sorted spikes were exported and analyzed using custom MATLAB software (MathWorks R2015a). A standard set of analyses (spike interval histograms, cycle triggered histograms, and spike-triggered averages) were performed to electrophysiologically phenotype each neuron. Interval histograms were created for each spike train to assure only single unit activity was represented in each waveform. Similar to previous studies (Galán et al. 2010; Sandhu et al. 2015), cycle-triggered histograms were used to assess the preferred respiratory modulation of each recorded neuron relative to the phase of the respiratory cycle defined by phrenic nerve activity (Cohen 1968). Using the integrated phrenic nerve output, the beginning and end of the inspiratory, and therefore expiratory phases, were calculated as a departure of

phrenic nerve activity ≥ 15 standard deviations above the average activity during the expiratory phase. Cycle-triggered histograms were constructed for each neuron by dividing the respiratory period into 20 bins of equal size and spikes were counted within each bin and summated over 50 consecutive breaths during baseline, hypoxia, and post-hypoxia. To determine if neurons were respiratory modulated, the spikes occurring during bins of the inspiratory phase were separated from those occurring during the expiratory phase and the Wilcoxon signed-rank test was used to test the null hypothesis (i.e., no difference between inspiration and expiration). Cervical spinal neurons were classified into four categories: 1) neurons that discharged primarily during the inspiratory period (i.e., inspiratory modulated; waveform 1 Figure 7C, D); 2) neurons that discharged primarily during the expiratory period (i.e., expiratory modulated; waveform 1 Figure 7H, I); 3) neurons that discharged without respiratory modulation (i.e., tonic; waveform 2 Figure 7C, D, H, and I); and 4) neurons which ceased firing at time points after baseline were labeled as inactive at that time point.

Spike-triggered averaging of raw and rectified phrenic nerve activity, was used to examine the temporal relationship of neuronal waveforms and phrenic motor output (Lipski et al. 1983). Short-latency, offset peaks in the raw and rectified phrenic nerve average provided evidence that the recorded neuron was a phrenic motoneuron (Christakos et al. 1994). If features were not detected using spike-triggered averaging, the recorded cell was classified as a spinal interneuron. Cross-correlation histograms were constructed for all possible pairs of simultaneously recorded neurons using a bin width of 0.2ms to evaluate functional connectivity (Moore et al. 1970). Similar to published methods (Aertsen and Gerstein 1985), the detectability index (DI) was calculated for each cycle-triggered histogram as the peak relative to average background activity (calculated during the interval -15 to -3 ms prior to zero), divided by the standard deviation. Only significant features occurring with a positive lag (e.g., ≥ 0) were counted. Features were considered significant if the DI was ≥ 3 (Melssen and Epping 1987). Central peaks (0-0.4 ms) between a pair of neurons supported synchronous firing between

neurons; whereas offset peaks (≥ 0.6 ms) indicated functional excitation between the trigger and target neurons.

Plating Electrodes and Depositing Silver

Methods for electroplating and depositing silver described previously (Spinelli 1975) were adapted for use with MEA recordings. For each electrode, silver was electroplated (Figure 2A) and deposited (Figure 2B) using tightly controlled and monitored DC circuits. The circuits consisted of an electrode selection interface (i.e., break out box), two 9V batteries, a custom built µ-current control device (Bare Electronics, Gainesville, FL), a µ-current precision nA current measurement assistant v3 (EEVblog Adafruit Industries, #882), and a digital multimeter (Ideal Industries, #61-340) all connected with copper patch cables. Specifications of the µcurrent control circuit are provided in Figure 2C. Prior to each experiment, 15 of the 16 fine wire tungsten electrodes were electroplated with dissolved silver cations in an electrolyte solution ($AgNO_3$/KCN) and an un-insulated silver wire (100 mm, 0.025 in diameter, A-M Systems, #783500) was used as the anode in the solution (Figure 2A). The electrolyte solution was prepared by mixing equal parts of 1% potassium cyanide and 1% silver nitrate. The circuit was tested before each use by electroplating silver onto copper wire to assure proper connections and current settings. Immediately following the testing procedure, the tip of each individual electrode was introduced to the electrolyte solution (as the cathode) for 100 sec at 100 nA. Electrodes used to deposit silver were re-plated prior to each experiment. In a subset of experiments (n=3), 2 of the 16 electrodes were coated with the lipophilic fluorescent dye, DiI (1,1'-Dioctadecyl-3,3,3',3'-Tetramethylindocarbocyanine Perchlorate ('DiI'; DiIC18(3))) (Thermofisher; #D-282) after electrodes were electroplated with silver and prior to electrophysiology. Each electrode was repeatedly dipped (~10 times) in DiI (50 mg/ml in ethanol) and allowed to dry for 5 sec between each dip (DiCarlo et al. 1996).

Subsequent to ensemble recordings of individual neurons, electrodes were left in place while the MEA was disconnected from the acquisition system and attached to the electrode selection interface (i.e., breakout box) (Figure 2B). Sites to be labeled were chosen based on the quality of the signals during the electrophysiologic recordings. The circuitry was connected as in the plating procedure with the exception that electrode 16 was used as the cathode and the individual electrode chosen for labeling was treated as the anode. Electroplated silver was released from the electrode tip using a 100 nA current for 10-100 sec. Tissue was fixed approximately 15-30 minutes after silver was deposited (described below).

Tissue Preparation

Animals were transcardially perfused with ice cold saline followed by 4% paraformaldehyde (PFA; Electron Microscopy Sciences, #19210) in 1X Dulbecco's phosphate buffered saline (DPBS, Mediatech, Inc., #21-030-CV). Spinal tissue was harvested and post fixed in 4% PFA overnight at 4^{o}C. The cervical spinal cord was subsequently blocked (C3-C6; ~8-9 mm of tissue) and cryoprotected in 30% sucrose in 1X DPBS overnight at 4^{o}C. The spinal cord was embedded in optimal cutting temperature compound (OCT, Fisher Scientific, #23-730-571), flash-frozen using 2-methylbutane and dry ice, and transversely cut at 40 µm on a cryostat (Microm HM 500, GMI). Sections for silver labeling were placed into 12-well trays (Corning®, #3737) containing Corning® Netwell™ inserts (2 sections per well; 15 mm dia., mesh size of 74 µm, Corning®, #3477) filled with glass-distilled water (~4 mL per well). Sections for immunohistochemistry were placed in 96 well plates containing 1X DPBS.

Silver Staining Protocol

Silver staining was performed immediately after sectioning. Due to the sensitivity of the reaction, all trays, glassware, and instruments used for staining protocol were thoroughly acid washed (1% HCl) prior to staining to eliminate contamination and remove non-specific catalysts.

Plastic 12-well trays containing the developer solution were discarded after used for a single tray of tissue, while all other trays were discarded after each animal. Netwell mesh inserts were soaked in bleach between each animal. The deposited silver was “developed” as previously described (Spinelli 1975). Briefly, stock solutions were prepared as outlined in Table 1. The hydrogen peroxide solution was covered in foil throughout entire protocol due to its light sensitivity and the hydroquinone and citric acid solution was made in the same bottle. The developer was made fresh for each 12-well tray of tissue by mixing the three stock solutions (acacia, silver nitrate, and hydroquinone/citric acid) five minutes before use (at the start of step 9). All steps were carried out in a fume hood, and light exposure was limited while mixing developer solution and during “developing” by turning off the fume hood light.

The solutions were poured into either 200 mL glass petri dishes (Corning®, #3160152BO) or 12-well plastic trays according to the step (see Table 1) and arranged in order of the staining sequence. To maintain precision during the staining protocol, staining was performed in “rounds”, where each round contained three trays of tissue (~1 mm tissue/tray). Trays were staggered by 5 min, and all three trays of tissue were stained from start to finish. Rounds were repeated until all tissue was stained. The Netwell mesh inserts were transported through the staining sequence using a Netwell carrier kit with handles (Corning, #3520) to allow simultaneous processing and assure all wells were in each solution for the appropriate time. Following staining, tissue was stored at 4^{o}C in Netwells filled with dH_2O. Sections were mounted onto charged microscope slides (Fisher Scientific™, #12-550-15) using 1X PBS and allowed to dry for 48-72 hrs. Sections were counterstained with cresyl violet covered with mounting medium (Thermo Scientific™, #4111) and coverslipped. Images were captured with bright-field microscopy using a Microscope Axio Imager.A2 (Carl Zeiss Microscopy). Images were stitched and white balanced using Adobe Photoshop. Anatomical locations of the silver labeled sites within the spinal laminae were identified using Sengul, Watson, Tanaka, and Paxinos Atlas of the spinal cord (Sengul et al. 2012). All representative spinal cord images reflect Camera

Lucida-style drawings of our histological images or C4 spinal section in the *Atlas of the spinal cord* (Sengul et al. 2012). The depth of silver labeled sites were determined using 10X photomicrographs and adjusted by 10% to account for tissue contraction during the fixation and histological processing based on estimates of prior investigations (Deutsch and Hillman 1977; Quester and Schröder 1997).

Immunohistochemistry

Initial immunohistochemistry (IHC) experiments determined the order in which IHC should be performed to achieve optimal fluorescent staining using tissue which did not contain deposited silver. IHC was performed either prior to, or immediately after silver staining using two common markers (e.g. GFAP and NeuN). Using the optimal staining order, a subsequent experiment was performed with tissue containing deposited silver. All IHC was performed with free-floating sections in 96 well plates. All tissue was washed with 1X PBS with 0.2% Triton (3 × 5 min). For NeuN staining, tissue was incubated for 40 min at room temp in 10% normal goat serum (NGS) in 1X PBS with 0.2% Triton. Spinal sections were then incubated for 1hr at room temp followed by 72hrs at 4^{o}C in the primary antibody solution: 10% NGS in 1X PBS with 0.2% Triton and NeuN (mouse anti-NeuN, 1:1400; Millipore, #MAB377). Tissue was washed with 1X PBS (3 × 5 min) and incubated in the secondary antibody solution for 1 hr at room temp: 10% NGS in 1X PBS and Alexa Fluor® 488 (goat anti-mouse, 1:500; Invitrogen, #A11029). Following incubation, tissue was washed with 1X PBS (3 × 5 min). For GFAP staining, tissue was incubated for 60 min at room temp in 5% normal goat serum (NGS) in 1X PBS with 0.2% Triton. Spinal sections were then incubated for 1hr at room temp, and overnight at 4^{o}C in the primary antibody solution: 5% NGS in 1X PBS with 0.2% Triton and GFAP (mouse anti-GFAP, 1:200; Sigma-Aldrich, G8393). Tissue was washed with 1X PBS with 0.2% Triton (3 × 5 min) then incubated in the secondary antibody solution for 1hr at room temp: 5% NGS in 1X PBS with 0.2% Triton and Alexa Fluor® 594 (goat anti-mouse 1:500; Life Technologies, #A11005).

Following incubation, tissue was washed with cold 1X PBS (3 × 5 min). Sections were mounted on positively charged glass slides (Fisher Scientific™, #12-550-15), covered with VECTASHIELD Antifade mounting medium (Vector Laboratories, #H1-1200) and cover-slipped. Slides were air-dried and stored at 4°C. All fluorescent images were captured at 10X, 20X and 40X magnification with a Microscope Axio Imager.A2 (Carl Zeiss Microscopy).

Results

Optimization of Silver Deposition from MEAs and Subsequent Histological Development to Enable Visualization of Recording Locations

Initial experiments determined the parameters needed to deposit and identify silver in the spinal cord without emphasis on recording neuronal bursting from the electrodes. As the DC resistance of the commercially purchased recording electrodes was constant and the current used for electroplating silver onto the electrodes was standardized (as described in the methods), we assessed the impact of two critical variables on the histological appearance of silver in the spinal cord: 1) the duration of deposition current, and 2) the duration of histological development. Figure 3 shows representative images of silver labeling obtained at different durations of deposition and histological development which demonstrate the variability of silver staining achieved by altering these parameters. Consistent and discrete labeling at a resolution between ~25-50 μm was obtained when current used to deposit silver was applied for 50 sec and tissue was developed for 7-10 minutes (Figure 3A and B). When deposition current of less than 50 sec was applied few apparent labels were detected, presumably due to an inadequate amount of silver ions necessary for visualization. In contrast, deposition of 80-100 sec resulted in a “halo effect” which increased the silver labeled area to ~100-150 μm (Figure 3C and D), most likely due to a broad distribution of deposited silver. Similarly, histological development of less than 7 minutes was not long enough to “develop” the deposited silver required to visualize

the label; whereas prolonged exposure to the developing solution tended to darken large areas of the section thus confounding differentiation due to insufficient contrast (data not shown).

We next verified that the sites of silver deposition represented the location of the tip (i.e., recording location) of a given electrode. In a subset of animals (n=2 with silver processing, n=1 unprocessed positive control), two of the sixteen silver plated electrodes were coated with the fluorescent lipophilic dye, DiI to visualize the tracks associated with the electrode insertion (DiCarlo et al. 1996; Márton et al. 2016; Naselaris et al. 2005). While DiI was readily detected in unprocessed tissue (data not shown), DiI could not be detected after the histological processing required for silver labeling. Therefore, we conclude these two techniques are not compatible. However, in several histological sections an “electrode track” could be identified terminating at the silver labeled site (Figure 3E). This is consistent with the interpretation that the silver labeled site is located at the tip of the electrode.

Another objective was to determine if the silver labeling method could be coupled with fluorescent immunohistochemistry (IHC) procedures. Accordingly, we performed IHC with two markers commonly used in the central nervous system (GFAP and NeuN) either prior to, or immediately after histological processing for silver development. These markers were chosen due to their ability to label astrocytes (Bignami et al. 1972) and neurons (Wolf et al. 1996). Fluorescent staining was detected in both cases, but was more robust when IHC was performed after the silver staining procedures (data not shown), indicating IHC (at least for these commonly used markers) is compatible with the histological processing steps necessary to “develop” the silver. Using this staining order, we determined the location of deposited silver relative to NeuN positive cells. Representative photomicrographs from a C4 spinal section depicting positive silver labeling in the intermediate gray is shown in Figure 4A. Fluorescent labeling of the same section stained with NeuN and DAPI are shown in Figure 4B. High magnification images of the silver labeled site suggest the recording electrode was in close

proximity to a NeuN positive neuron (Figure 4B). These qualitative results demonstrate that the silver labeling technique can be coupled with fluorescent IHC.

Using Silver Labeling to Identify Anatomical Locations of Metal Array Electrodes

In six animals (n=4 spinal intact and n=2 SCI), we used the optimized deposition and development parameters discussed previously to label select electrodes. Overall, using this approach to identify the anatomical locations of the recording electrodes, we obtained positive labeling in 35 of 39 attempts. This indicates that the silver labeling method can be used to identify the anatomical locations of array electrodes with a success rate of approximately 90%. Positive silver labeling was identified in the spinal gray matter between C3-C5. The locations of each silver labeled site in spinal intact and SCI animals was plotted (unilaterally for simplicity) according to their anatomical locations (Figure 5A). Silver labeled sites were identified between lamina IV-X, with the greatest number found in lamina VII (Figure 5A).

The success of the discrete silver labeling afforded the chance to compare the intended recording location (i.e., the micro-motor coordinates used during the neurophysiology experiment) with actual the location of the labeling (Figure 5B, C). Each silver labeled site was measured from the dorsal surface of the cord. Based on estimates of prior investigations regarding tissue shrinkage during paraformaldehyde fixation and subsequent tissue processing (Deutsch and Hillman 1977; Quester and Schröder 1997), the measured histological depth of each silver labeled site was adjusted by 10%. This analyses indicated that the micro-motor depth is likely to overestimate the actual depth of the electrode, and perhaps even more importantly that this relationship is altered by SCI. Linear regression analysis indicated a significant relationship between recording coordinates and histological staining in spinal-intact animals (motor: 1.6 $\pm$ 0.04 mm; histological: 1.2 $\pm$ 0.05 mm; $P = 0.0003$), but not after chronic SCI (motor: 1.4 $\pm$ 0.07 mm; histological: 0.6 $\pm$ 0.05 mm; $P = 0.3014$; Figure 5B). The depth of the silver labeled site differed from the micro-motor coordinate in both groups (Figure 5C), but

was significantly increased following SCI (0.8 ± 0.07) compared to spinal intact animals (0.4 ± 0.04). These data highlight the need to histologically identify multi-electrode recording sites especially following experimental conditions such as SCI when tissue fibrosis and scarring can be expected to alter electrode movement within the CNS. Future, studies can apply the linear fit as a proxy to more accurately calculate the “actual depth” of the electrode tips.

Coupling Spinal Discharge with Anatomical Locations

All silver electroplated electrodes were capable of discriminating single units, indicating that the pretreatment had a minimal, if any, impact on the ability to record and discriminate extracellular signals. Three silver labeled sites were identified within lamina IX of the ventral horn (Figure 5A and 6A). Spike-triggered averaging (STA) of the raw and rectified phrenic nerve activity in relation to neuronal discharge produced a distinct peak with an average lag time of 0.45 ± 0.16 ms (Figure 6E), and therefore indicated that the recorded discharge was from phrenic motoneurons (Christakos et al. 1994; Mitchell et al. 1992). All three of these cells were active primarily during the inspiratory phase (Figure 6B and C), which is the typical firing pattern of phrenic motoneurons in this preparation (Sandhu et al. 2015). The silver labeling data verified that the recordings were from the region of the phrenic motor nucleus (Furicchia and Goshgarian 1987; Goshgarian and Rafols 1981; Kinkead et al. 1998; Mantilla et al. 2009; Prakash et al. 2000). This close matching between neurophysiological data and anatomical data illustrates the effectiveness of the silver labeling method.

The remaining silver labeled sites were located between laminae IV-X (Figure 7). Spike-triggered averaging provided no evidence of discharge synchrony in relation to phrenic motor output; thus these 28 recordings were considered to represent interneurons (Figure 7E and J). At baseline, most recorded interneurons (18/28 or 66%; Figure 7K) fired tonically throughout the respiratory cycle (e.g., waveform 2 in Figure 7C, D, H and I). These tonically discharging cells were not restricted to a particular lamina, but rather were recorded throughout the cervical grey

matter (Figure 7L). A smaller proportion of interneurons (5/28 or 18%; Figure 7K) primarily fired during the inspiratory phase (waveform 1 in Figure 7C and D), and these cells were found in lamina VI (n=1), VII (n=3), and X (n=1). During hypoxia, two of these neurons (in lamina VII and X) switched to a tonic firing pattern, but then resumed an inspiratory pattern post-hypoxia. In addition, one inspiratory neuron in lamina VII was inspiratory modulated during baseline and hypoxia, but then assumed a tonic firing pattern post-hypoxia. Similarly, during baseline conditions, five cells (5/28 or 18%; Figure 7K) discharged primarily during the expiratory period (e.g., waveform 1 in Figure 7H and I) and were located in lamina VIII (n=3), IX (n=1), and X (n=1). During hypoxia, three of these neurons (in lamina VIII (n=2) and IX (n=1)) switched to a tonic firing pattern which was then maintained post-hypoxia. In addition, one expiratory-modulated neuron in lamina VIII ceased bursting immediately post-hypoxia. Therefore, due to phase switching, the proportion of tonic firing interneurons increased to 82% (23/28) during hypoxia and remained elevated post-hypoxia (20/28 or 71%). Interneuron bursting patterns during baseline, hypoxia and post-hypoxia are summarized in Figure 7K, and the corresponding anatomical locations are provided in Figure 7L. In this sample of neurons, respiratory-related discharge was observed only in the ventral grey matter (i.e., lamina VI, VII, VII, IX and X), and tonic discharge was recorded throughout the mid-cervical grey matter.

Mapping anatomical locations and quantitation of interneuronal discharge across mid-cervical spinal laminae are shown in Figure 8. A representative example from one recording in which silver labeling was used to “map” the anatomical locations of the array electrodes and corresponding electrophysiological data is shown in Figure 8A-C. A Camera Lucida-style drawing of the anatomical locations of eight silver labeled electrodes was constructed (Figure 8B). Numerical identification of the anatomical positions of each electrode corresponds to the schematic presented in Figure 1D and defines the rostral-caudal and medial-lateral positions of the array electrodes. Corresponding mid-cervical spinal discharge and integrated phrenic nerve activity during baseline and hypoxia on the left and right hemi-cord is shown in Figure 8C. The

majority of these recordings were from tonic firing interneurons (electrodes 3, 8, 9, 11, 12, and 15) and one represented a phase switching (e.g. from tonic at baseline to expiratory during hypoxia) interneuron (electrode 6; Figure 8C). Using this technique, a summary of the anatomical locations of all silver labeled interneurons was constructed (Figure 8D). In addition, the average discharge frequency (Hz) of all silver labeled interneurons was presented in Figure 8E. The results indicate a dorsal-ventral discharge gradient, with higher discharge rates in lamina IV and X and lower values in lamina VIII and IX. This discharge map of the mid-cervical spinal network demonstrates the utility of using the silver labeling technique to identify the anatomical locations of ensembles of interneurons recorded with a MEA. These results show the utility of using this technique to standardize the sampling distribution of recording locations across experimental groups.

Temporal Relationships between Cervical Interneuron Discharge

Anatomical data indicate that cervical interneurons are part of a diffuse and synaptically coupled propriospinal network (Lane et al. 2008b), but relatively little is known about functional connectivity between cervical interneurons. Therefore, initial analyses focused on all recorded neurons in spinal intact rats (i.e., silver and non-silver labeled neurons) to screen for short time scale (i.e., 0-10ms) features (Aertsen and Gerstein 1985; Aertsen et al. 1989; Melssen and Epping 1987). Significant features were identified as departures in the cross-correlation histogram ≥ 3 standard deviations from the background noise (Melssen and Epping 1987). Using this approach, significant central (i.e., no lag time from zero) and offset correlogram peaks were detected (Figure 9A). A summary of the latency of significant features relative to the trigger (i.e., time zero) are shown in Figure 9B.

Inspection of the data suggested that latencies for correlogram peaks were distributed in three ranges: 1) ≤ 0.4 ms; 2) 0.6-2.8ms, and 3) ≥ 3.0 ms (discrete integers reflect 0.2ms bins used to construct histograms; Figure 9B and C). Few correlations (37/704 or 5.3% of possible

correlations) had a peak with latency ≤ 0.4 ms which is consistent with excitation from a common synaptic input (Aertsen and Gerstein 1985; Kirkwood 1979; Kirkwood et al. 1991; Melssen and Epping 1987). A greater number of positive correlations had latencies between 0.6-2.8 ms and ≥ 3.0 ms (54/704 or 7.7% and 97/704 or 13.8%, respectively). Correlogram peaks with latencies above 0.6 ms are consistent with the interpretation of functional excitation involving mono-, or polysynaptic connections (Aertsen and Gerstein 1985; Kirkwood 1979; Moore et al. 1970). We next evaluated the number of positive correlations relative to the recording locations. For this, neuronal pairs were classified as “unilateral” (i.e., recordings on the same side of the cord) or “bilateral” (i.e., recordings on opposite sides of the cord). Evaluation of unilateral pairs showed the average number of significant correlogram peaks was 20 ± 3.9 correlations per animal. A similar value was obtained for bilateral neuronal pairs (25 ± 7.5 correlations per animal; Figure 9D). When normalized to the total number of possible unilateral (332) or bilateral (372) correlations, similar values were observed (24 ± 0.5% and 26 ± 5.5% respectively; Figure 9E). No significant differences in latencies were observed when data was separated into unilateral and bilateral neuronal pairs (data not shown).

Neuronal pairs with significant correlogram peaks that were also silver labeled were used to construct correlation summary maps to illustrate the anatomical locations of each neuron (Figure 10). The number of positive correlations within each lamina was normalized to the total number of neurons present in the corresponding lamina. Unilateral neuronal pairs are shown in Figure 10A and bilateral pairs are shown in Figure 10B. Of the positive unilateral correlations, interneurons in dorsal lamina (i.e., IV, V and VI), made and received the greatest number of excitatory connections (Figure 10A). In contrast, when the trigger and target neuron were on opposite sides of the spinal cord, interneurons in lamina V, VIII and IX made and received the most connections (Figure 10B).

We also found 33 troughs in cross-correlograms which were significantly different than background activity using the same criteria used to detect peaks (data not shown). For

comparison purposes, the number of troughs occurring ≤ 0.4 was 20/704 or 2.8%; whereas those between 0.6-2.8 ms was 1/704 or 0.1%; and those ≥ 3.0 ms was 12/704 or 1.7%. Correlogram troughs with these latencies are generally thought to reflect functional inhibition (Aertsen and Gerstein 1985; Kirkwood 1979).

Discussion

Here we describe a silver labeling technique that reliably identifies the position of MEA tips following *in vivo* neurophysiologic recordings. The results indicate that silver labeling can be histologically identified with a resolution of ~50 μm while also preserving the structural integrity of the tissue with a 90% success rate. A practical application of this technique was demonstrated by matching the location of mid-cervical MEA recording sites with neuronal discharge to create maps of bursting patterns (e.g., Figures 7 and 8). Moreover, using correlative techniques, we also provide to our knowledge the first neurophysiological evidence for the presence of extensive connections between interneurons in mid-cervical grey matter (e.g., Figures 9 and 10). Coupling silver labeling with MEA neurophysiology provides a powerful tool to investigate network level properties of the spinal cord.

Commentary Regarding the Silver Labeling Method

The first challenge associated with adapting the silver labeling method (Spinelli 1975) for MEAs was accurately measuring the low currents (nA) needed for electroplating and depositing silver from tungsten array electrodes. Although devices which measure low currents are commercially available (e.g., for patchclamp/iontophoresis), they are expensive and not easily adapted to electroplating or electrodeposition. Additionally, multimeters cannot resolve currents in the nanoamp range and have limited accuracy due to voltage drop caused by current flow through the current measuring device (i.e., “burden voltage”; (Jones 2010). To overcome these limitations, we utilized an EEV precision μ-current assistant which permits nanoamp currents to

be measured on a standard multimeter and also improves the accuracy to 0.2% (Jones 2010). We also designed a μ-current control device capable of generating 100 nA while also allowing current adjustments of less than 1 nA (circuit details provided in Figure 2C). The ability to precisely produce and control this current was critical since passing higher currents can alter electrode impedance and recording characteristics (Fung et al. 1998). The current generating system was specifically designed to be compatible with both single electrodes and MEAs.

Published methods for marking the location of MEAs include iontophoresis of neural tracers (Fekete et al. 2015; Haidarliu et al. 1999; Kovacs et al. 2005), topical application of fluorescent dyes (DiCarlo et al. 1996; Naselaris et al. 2005), lesioning (Brozoski et al. 2006; Townsend et al. 2002) , electrical imaging (Li et al. 2015), and imaging-based approaches (Borg et al. 2015; Fung et al. 1998; Koyano et al. 2011; Matsui et al. 2007). The silver labeling method offers several advantages over these previous techniques. First, this technique can be used with the standard metal electrodes typically used with MEAs (Borg et al. 2015; Cogan 2008). This is in contrast to the specialized electrodes necessary for iontophoresis (Fekete et al. 2015; Kovacs et al. 2005; Naselaris et al. 2005). Second, the silver labeling method does not require implanted electrodes or expensive and often unavailable equipment such as MRI to visualize electrode placement (Borg et al. 2015; Fung et al. 1998; Koyano et al. 2011; Matsui et al. 2007). Third, the histologically identified silver deposition spanned an area of ~50 μm, and this provides an approximately 3X greater resolution as compared to previously published techniques compatible with metal MEAs. For example, MRI based approaches enables visualization of microelectrodes sites at an in-plane resolution of 150-200 μm (Fung et al. 1998; Koyano et al. 2011; Matsui et al. 2007). Fluorescent dyes achieve resolutions between 50-400 μm, but identify electrode track trajectories rather than discrete locations of electrode tips (DiCarlo et al. 1996; Naselaris et al. 2005). Finally, whereas lesioning techniques can damage surrounding tissues (Townsend et al. 2002), low current levels required for silver deposition

553 preserves the integrity of the surrounding tissue. This is a particularly important point since it
554 permits neurochemical phenotyping of neurons at or near the electrode tip.

555 One of the features enabling “matching” of electrophysiological signals with anatomical
556 locations is that the relative position of each electrode was known since the electrodes exist in a
557 fixed matrix (Figure 1D). Nevertheless, with multiple silver labeled sites in a relatively discrete
558 area, matching each silver labeled site with its corresponding recording electrode can pose a
559 challenge. To overcome this hurdle, several safeguards were implemented. First, since
560 recordings were performed with a bilateral recording array, a small longitudinal cut in the dorsal
561 spinal cord was made prior to sectioning to demarcate the left vs. right hemi-cord. Second, the
562 rostral-caudal orientation of spinal sections was maintained throughout the histological process
563 by sectioning sequentially into 12-well plates. Most importantly, the histologically identified silver
564 deposition was linked to the corresponding recording data by using the lateral – medial aspect
565 of the electrode matrix. The phrenic motoneuron data provided further verification of the ability
566 to match silver labeling with the neurophysiology data. The anatomical location of phrenic
567 motoneurons is well defined in rat (Goshgarian and Rafols 1981; Mantilla et al. 2009; Prakash et
568 al. 2000; Zhan et al. 1989), and the electrophysiological analyses (e.g. STA) confirmed an
569 appropriate “match” between the anatomical location of silver labeling (i.e, ventral grey matter,
570 lamina IX) and the recording electrode. Moreover, cells with histological features consistent
571 phrenic motoneurons (Furicchia and Goshgarian 1987; Prakash et al. 2000) were clearly
572 identified near the silver label (~50-100 μm).

573 To assure that our recordings (and silver labeled sites) were from neurons (vs. fibers of
574 passage) in the immediate vicinity of electrode, we used high impedance tungsten wires coated
575 with Epoxylite Insulation with an exposed tip of ≤ 1 μm. We suggest that using these insulated
576 high impedance electrodes, the following assumptions are reasonable: 1) the recorded neural
577 discharge is of somatic origin (*versus axonal*); and 2) the amplitude of the recorded action
578 potentials decrease with distance between the soma and the recording electrode tip. The

reasons for these assumptions are as follows. Extracellular action potentials recorded from axons are very brief (i.e., 0.1-0.3 ms), small, and extremely sensitive to electrode movement (Bellingham and Lipski 1990; Kirkwood et al. 1988). In contrast, action potentials recorded in the current study were broad (i.e., ≥ 1 ms), biphasic, and the recordings were stable as electrodes were moved up to 100 μm. These features are consistent with extracellularly recorded somatic action potentials (Bellingham and Lipski 1990; Nelson 1959). The literature indicates that the amplitude of extracellularly recorded action potentials is inversely proportion to the distance between the soma and the recording electrode (Kirkwood et al. 1988; Nelson 1959). Therefore, by achieving a 3:1 signal-to-noise ratio when placing each electrode, we can be confident that the electrode tip is close to the cell soma generating the largest action potential. Lastly, the electrode design described above reduces the surface area available for silver plating, and thus silver is deposited from only the ~1 μm plated length at each electrode tip.

The silver labeling method was not 100% successful, and we suspect the small number of failures (N=4 of 39 possible sites) occurred due to a lack of deposited silver or tissue damage during histological processing (e.g., tearing of sections or error during the placement of longitudinal notch in the spinal cord). A final methodological commentary relates to the difference between the histologically verified “depth” of the electrode and the coordinates used in the micro-drive while placing each electrode (e.g., Figure 5). The micro-drive coordinates overestimated the actual depth of the recording, and probably reflects some degree of “pillowing” of the tissue as the electrodes were advanced. The most salient point, however, is that the difference between histological and micro-motor coordinates was increased in rats with chronic SCI (e.g., Figure 5C). These data highlight the need to histologically identify multi-electrode recording sites following SCI when tissue fibrosis and scarring can be expected to impede electrode movement within the spinal cord.

Mid-Cervical Spinal Interneurons and Respiratory Motor Output

Several laboratories have suggested that phrenic motoneuron discharge can be modulated by synaptic input from spinal interneurons (Bellingham and Lipski 1990; Davies et al. 1985; Sandhu et al. 2015). Anatomical studies show spinal interneurons are uniquely situated to modulate phrenic motor output sine they are in close opposition with medullary projections (Davies et al. 1985; Fedorko et al. 1983; Hayashi et al. 2003; Lane et al. 2008b) and have synaptic connections to phrenic motoneurons (Dobbins and Feldman 1994; Lane et al. 2009; Lane et al. 2008b; Lois et al. 2009; Yates et al. 1999). Electrophysiological recordings in multiple species have demonstrated that cervical interneurons have respiratory-related discharge patterns (Bellingham and Lipski 1990; Duffin and Iscoe 1996; Marchenko et al. 2015; Palisses et al. 1989; Sandhu et al. 2015) and respond to respiratory stimuli such as phrenic afferent stimulation (Iscoe and Duffin 1996; Speck and Revelette 1987) and hypoxia (Sandhu et al. 2015). Our results add to this literature in two primary ways. First, to our knowledge only one prior study (Marchenko et al. 2015), has combined neurophysiology with the histological identification of the anatomical location of respiratory-related spinal interneurons associated with the phrenic motor pool. Our data show that interneurons with respiratory related discharge are located throughout laminae VI, VII, VII, IX, and X. Second, the current results provide new information regarding the impact of respiratory stimulation with hypoxia on mid-cervical interneuronal discharge patterns. Indeed, during/following hypoxia approximately 29% of spinal interneurons alter their discharge in relation to the respiratory cycle. We noted that both inspiratory and expiratory modulated neurons had a tendency to adopt a tonic firing pattern during hypoxia. However, post-hypoxia interneurons with baseline inspiratory discharge tended to resume an inspiratory firing pattern, whereas the expiratory interneurons maintained the tonic pattern. In addition, we found one example of a tonic firing interneuron during baseline and hypoxia which become inspiratory modulated post-hypoxia. Neurons exhibiting “phase

switching" were located in intermediate and ventral laminae (i.e., VII, VIII and X) rather than dorsal laminae. To our knowledge, this is the first report to describe hypoxia induced phase switching of mid-cervical interneuron bursting patterns. When neuronal discharge frequency was evaluated relative to anatomical locations, higher frequencies were noted in lamina IV and X (e.g., Figure 8E). These results again highlight the importance of matching anatomical location with discharge properties, and show that mid-cervical interneuron discharge varies across cervical lamina which is consistent with previous descriptions of lumbosacral neural activity (Borowska et al. 2013; Ruscheweyh and Sandkühler 2002).

Discharge Synchrony between Mid-Cervical Spinal Interneurons

Despite both historical (Duffin and Iscoe 1996; Palisses et al. 1989) and recent publications (Lane 2011; Marchenko et al. 2015; Sandhu et al. 2015) related to cervical respiratory interneurons, the functional connectivity of mid-cervical spinal circuit remains largely unexplored. This can be attributed to the fact that studies investigating respiratory-related interneurons in the spinal cord have primarily utilized a single unit recording approach (Bellingham and Lipski 1990; Lipski and Duffin 1986; Lipski et al. 1993) and have instead focused on connections between motor- and interneurons (Davies et al. 1985; Duffin and Iscoe 1996; Lipski et al. 1993). In the current study, we utilized cross-correlation analysis to characterize the functional connectivity of pairs of spinal interneurons. Similar to previous studies investigating spinal interneurons in non-respiratory related networks (Brown et al. 1979; Prut and Perlmutter 2003), we found relatively few examples of synchronous discharge consistent with a shared excitatory pre-synaptic input (Aertsen et al. 1989; Kirkwood 1979). That is, when interneuronal pairs were examined, correlogram peaks with latencies between 0 – 0.4 ms were only observed in 5.3% of recordings. In contrast, 21.4% of the total possible positive correlations had latencies ≥ 0.6 ms. These longer latency peaks are consistent with mono- and polysynaptic connections between cervical interneuron pairs. Of the positive correlations

involving neurons on the same side of the spinal cord, interneurons in dorsal lamina (i.e., IV, V and VI), made and received the greatest number of excitatory connections. In contrast, when the trigger and target neuron were on opposite sides of the spinal cord, interneurons in lamina V, VII and IX made and received the most connections. Taken together, our results provide support for the hypothesis that cervical interneurons form a dynamic network which is capable of rapid reconfiguration and modulation of cervical motor outputs. We suggest that the MEA silver labeling method will help advance our understanding of the functional and anatomical correlates of ensembles of spinal neurons.

Application to Spinal Cord Injury

One potential application of MEA technology is to examine how SCI alters the cervical spinal networks. Spinal networks undergo substantial remodeling following SCI (Bareyre et al. 2004; Sperry and Goshgarian 1993) and interneurons have been implicated in SCI-induced plasticity and motor recovery (Alilain et al. 2008; Bareyre et al. 2004; Harkema 2008). However, relatively little is known regarding their contribution to the spontaneous recovery of phrenic output following SCI (Lane et al. 2008b). In the current study, we performed recordings on n=2 rats with chronic cervical SCI. The intent of these experiments was not to “map” changes in the spinal network post-injury, but rather to confirm that the method developed herein could be effectively utilized in rats with SCI. We successfully deposited and detected silver labeling following SCI using the same parameters optimized in spinal intact animals. However, we noted a greater discrepancy between micro-motor and silver labeling depth in spinal injured animals (e.g., Figure 5C). While multiple factors may contribute to this disparity, structural changes resulting from fibrosis and scarring induced following injury (Cregg et al. 2014) may increase electrode drag, thereby reducing the effectiveness of utilizing the electrode micro-motor to predict the actual depth of the electrode tips. Regardless of the specific cause, our results highlight the importance of histologically verifying the locations of recorded neurons, especially

following experimental conditions such as SCI which may alter electrode movement within the CNS. We suggest that future studies utilizing the methods described here will shed light on the contribution of the propriospinal network to the recovery of function following SCI.

Conclusions

The methodology described here provides a solution to the fundamental limitation of using MEAs containing standard metal electrodes by identifying the discrete anatomical locations of the recording sites. Although prior studies have described methods to determine the approximate locations of MEA electrodes (Borg et al. 2015; Brozoski et al. 2006; DiCarlo et al. 1996; Fekete et al. 2015; Haidarliu et al. 1999; Kovacs et al. 2005; Koyano et al. 2011; Naselaris et al. 2005; Townsend et al. 2002), to date labeling the discrete recording locations of non-specialized metal array electrodes in an acute preparation while preserving the surrounding tissue, has only been achieved with single-cell recordings. With MEA recordings, higher order analyses can be used to investigate the functional connectivity of the neural network during physiological stimuli and following neurologic injury (e.g., Figures 9 and 10 also see: (Aertsen and Gerstein 1985; Kirkwood 1979; Melssen and Epping 1987). In this regard, the current results are consistent with a high degree of synaptic connections between mid-cervical neurons. Collectively, our experiments show that 1) MEA silver labeling method enables the electrophysiological output of neural networks to be coupled with histological verification of electrode locations; 2) mid-cervical interneurons are capable of rapid “phase switching” of burst patterns relative to the respiratory cycle during and after hypoxia; and 3) a high percentage of mid-cervical interneuronal pairs have temporally related discharge patterns.

Figure Legends

Figure 1: Multi-electrode array. **A:** Multi-electrode recording array containing 16 tungsten fine wire electrodes each controlled by micro-motors and held in place by the array guide. **B:** High resolution image of the electrode tips maintained in a "fixed matrix" by the array guide. **C:** Image of the electrodes positioned in the dorsal C4 spinal cord at the dorsal root entry zone (e.g., black arrows). **D:** Schematic of the recording matrix consisting of eight electrodes arranged in two staggered rows of four. The inner distance between the two sets of eight electrodes was approximately 1 mm and the distance between electrodes within each row was ~300 µm.

Figure 2: **Silver electroporation and deposition circuits.** Both circuits consisted of an electrode selection interface (*i.e*. breakout box), two 9V batteries connected in series, a custom built µ-current control device (constant current board), a µ-current precision nA current measurement assistant (µ-current Box), and a digital multimeter connected via copper patch cables (thick black lines). **A:** For the silver electroplating circuit, the array was connected as the cathode to the electrode selection box (breakout box) while an un-insulated silver wire was placed in the electrolyte solution ($KCN/AgNO_3$) and used as the anode. The µ-current box was connected to breakout box corresponding to the electrode to be plated (Ch1-15). **B:** For the silver deposition circuit, the polarity of the circuit was reversed with breakout box used to select the reference channel (Cathode/Ch16) and the electrode to be deposited (Anode/Ch1-15). **C:** The µ-current control device utilizes an NPN transistor (Q1 PN2222A) to regulate current from the power source (two 9V batteries; B1 and B2) through a load between J1 and J2. Two small-signal diodes D3 and D4 (1N4148) provide a fixed voltage (~$1.25V_{DC}$) used in parallel with voltage divider (R4). This adjustable voltage divider controls the base current delivered to the transistor so that the emitter current of the transistor produces a stable current of 100nA. As load between J1 and J2 changes, the transistor actively alters the voltage – and therefore

current – drop across collector (C) to emitter (E), maintaining a constant voltage (across R3). Current was monitored by an EEVblog μ-current precision nA current measurement assistant v3 with a consumer grade multi-meter and adjusted to maintain 100 nA.

Figure 3: **Representative images of silver labeling**. **A-D:** Representative histological sections from the cervical spinal cord containing silver labeled sites counterstained with cresyl violet and high resolution images of the boxed areas. These images depict the variability of silver labeling at different durations of silver deposition (50-100 sec) and histological development (7-10 minutes). **E:** Images of a cervical spinal section depicting an electrode track (black arrows) coursing through the spinal tissue and terminating at the silver labeled site. CC: central canal; DH: dorsal horn; VH: ventral horn. Scale bars: A-D: 0.5 mm and 50 μm (callouts); E: 0.5 mm, 100 μm, and 50 μm, respectively.

Figure 4: Silver labeling coupled with fluorescent immunohistochemistry. A: Representative cervical spinal section of positive silver labeling (*brown/black*) and high resolution image of the boxed area. **B:** Fluorescent labeling of neurons stained with NeuN (*green*) and nuclei stained with DAPI (*blue*) of the same section presented in panel A, and high resolution image of the boxed area illustrating the silver labeled site was in close proximity of a NeuN positive cell. CC: central canal; DH: dorsal horn; VH: ventral horn. Scale bars: 0.5 mm and 50 μm (callouts).

Figure 5: Electrode and silver labeled depth. A: Representative C4 section of silver labeled sites in spinally intact (●) and spinally injured (○) animals projected onto one side of the cord for simplicity. Each lamina was shaded according to the number of silver labeled sites within that lamina. **B:** Scatter plot of the micro-motor depths versus the depths of the corresponding silver labeled sites in spinally intact (●) and spinally injured (○) animals. Linear regression analysis

was applied to determine the line of best-fit and linear equation for each group. The line of identity is displayed to indicate the location where micro-motor and silver labeling depths are equal. **C:** Normalized depth calculated as the difference between the micro-motor depth silver labeled site for spinally intact (●) and spinally injured (○) animals. * P<0.001 Unpaired T-test.

Figure 6: Silver labeling of a phrenic motoneuron. A: Representative C4 section containing a silver labeled site counterstained with cresyl violet and high resolution image containing the silver labeled site located in the medial aspect of the ventral horn in lamina IX (callout). **B:** Corresponding raw spinal discharge and integrated phrenic output during baseline, hypoxia, and post-hypoxia depicting discharge during the inspiratory phase. **C:** Integrated phrenic output, raw neuronal discharge, and sorted spikes (waveform) during hypoxia. **D:** Cycle-triggered histogram during 50 consecutive breaths overlaid with the average integrated phrenic waveform during hypoxia. **E:** Spike-triggered average of the raw and rectified phrenic nerve depicting a delay of 0.76 ms. CC: central canal; DH: dorsal horn; VH: ventral horn. Scale bars: A 0.5mm and 50μm (callout); B, C: 1.5 sec.

Figure 7: Silver labeling of mid-cervical spinal interneurons. A: Representative C4 section containing a silver labeled site counterstained with cresyl violet and high resolution image containing the silver labeled site (callout) **B:** Corresponding neuronal output and integrated phrenic output during baseline, hypoxia, and post-hypoxia depicting a single tonic firing neuron at baseline and recruitment of a phasic inspiratory neuron during hypoxia and post-hypoxia. **C:** Integrated phrenic output, raw neuronal discharge, and sorted spikes (waveforms) during hypoxia. **D:** Cycle-triggered histograms of both neurons during 50 consecutive breaths overlaid with the average integrated phrenic waveform during hypoxia. **E:** Spike-triggered average of the raw and rectified phrenic nerve depicting a lack of positive features. **F:** Representative C4 section containing a silver labeled site counterstained with cresyl violet and high resolution

image containing the silver labeled site (callout) **G:** Corresponding neuronal output and integrated phrenic output during baseline, hypoxia, and post-hypoxia depicting an expiratory and tonic firing neuron at baseline and hypoxia, and only the tonic neuron post-hypoxia. **H:** Integrated phrenic output, raw neuronal discharge, and sorted spikes (waveforms) during hypoxia. **I:** Cycle triggered histograms of both neurons during 50 consecutive breaths overlaid with the average integrated phrenic waveform. **J:** Spike triggered average of the raw and rectified phrenic nerve depicting a lack of positive features. **K:** Stacked bar graphs depicting the number of each cell type at baseline, hypoxia, and post-hypoxia each normalized to the total number of interneurons (n=28). **L:** Anatomical location of each silver labeled interneuron projected onto one side of the cord for simplicity, identified by the bursting pattern during baseline. CC: central canal; DH: dorsal horn; VH: ventral horn. Scale bars: A, F, L: 0.5 mm and 50 μm (callouts), B, C, G, H: 1.5 sec.

Figure 8: **Mapping anatomical locations of mid-cervical spinal neurons. A:** Representative photomicrograph of a C4 section containing a silver labeled site (from electrode nine) counterstained with cresyl violet and high resolution image of the silver labeled site (callout). **B:** Camera Lucida-style drawing of the cervical spinal cord summarizing the anatomical locations of eight silver labeled sites obtained in one animal. **C:** Integrated phrenic motor output and mid-cervical spinal discharge on the left and right hemi-cord corresponding to identified silver labeled sites in panel B during baseline and hypoxia. Electrode one recorded phrenic motoneuron discharge and the remaining electrodes recorded interneuron discharge. **D:** Representative C4 section summarizing the total number of silver labeled interneurons within each lamina in spinal intact animals. **E:** Average discharge frequency (Hz) of spinal interneurons within each lamina represented in panel D. CC: central canal; DH: dorsal horn; VH: ventral horn. Scale bars: A, B: 0.5 mm and 50 μm (callout); C: 1.5 sec.

Figure 9: Cross-correlation analysis of mid-cervical spinal interneurons. A: Representative cross-correlations obtained from three pairs of neurons depicting a significant central peak (left), 1.8 ms offset peak (middle), and 7.8 ms offset peak (right). The number of trigger spikes for each correlation: 43,891; 39,208; 3,928; and the detectability index of each correlation: 45.2; 4.3; 5.3, respectively. Black lines plotted at 0.5 and at 2.9 ms to indicate how data was grouped by latency (see panel B). **B:** A histogram of the latency relative to the trigger for all correlations with a significant peak. The first bar in the histogram is a count of the central peaks (0 ms latency) and each successive bar in the plot represents counts obtained in an increment of 0.2. Yellow bars plotted at 0.5 and at 2.9 ms indicate how data was grouped based on latency. Black lines are 2^{nd} order polynomial fit of the data. **C:** The sum of significant cross-correlations with latencies $\leq$ 0.4 ms, between 0.6-2.8 ms, and $\geq$ 3.0 ms. Percentages reflect the proportion of positive correlations out of the total possible (n=704). **D:** The average number of positive correlations per animal when both recordings were on the same side of the cord (20 ± 3.9 positive correlations/animal), or on opposite sides of the cord (25 ± 7.5 positive correlations/animal). **E:** The number of significant correlations expressed as a percent of total possible connections obtained when both recordings were on the same side of the cord (81/332 total possible), or on opposite sides of the cord (89/372 total possible).

Figure 10: Anatomical locations of functionally connected interneurons. Summary maps of silver labeled interneurons with significant peaks in cross-correlograms. The number of positive correlations in each lamina was normalized to the number of neurons present in the lamina and shaded accordingly. **A:** When both trigger and target neurons were on the same side of the spinal cord (e.g., unilateral recordings), interneurons in dorsal lamina (i.e., IV, V and VI) made and received the greatest number of excitatory connections. **B:** When the trigger and target neurons were on opposite sides of the spinal cord (e.g., bilateral recordings), interneurons in lamina V, VIII and IX made and received the most connections.

Table 1: Silver staining protocol. Sequence of solutions necessary to histologically develop the deposited silver adapted from (Spinelli 1975). Solutions were prepared and arranged in the order of the staining sequence in either glass petri dishes or plastic trays. Volumes of solution were calculated for one 12-well tray of tissue (24 sections; ~1 mm of tissue). Shaded text indicates the steps in which solutions were changed after processing one tray of tissue, while remaining non-shaded steps indicate solutions were chanced after processing three trays of tissue.

References

Aertsen AM, and Gerstein GL. Evaluation of neuronal connectivity: sensitivity of cross-correlation. *Brain Res* 340: 341-354, 1985.

Aertsen AM, Gerstein GL, Habib MK, and Palm G. Dynamics of neuronal firing correlation: modulation of "effective connectivity". *J Neurophysiol* 61: 900-917, 1989.

Alilain WJ, Li X, Horn KP, Dhingra R, Dick TE, Herlitze S, and Silver J. Light-induced rescue of breathing after spinal cord injury. *The Journal of neuroscience : the official journal of the Society for Neuroscience* 28: 11862-11870, 2008.

Bareyre FM, Kerschensteiner M, Raineteau O, Mettenleiter TC, Weinmann O, and Schwab ME. The injured spinal cord spontaneously forms a new intraspinal circuit in adult rats. *Nat Neurosci* 7: 269-277, 2004.

Bellingham MC, and Lipski J. Respiratory interneurons in the C5 segment of the spinal cord of the cat. *Brain Res* 533: 141-146, 1990.

Bignami A, Eng LF, Dahl D, and Uyeda CT. Localization of the glial fibrillary acidic protein in astrocytes by immunofluorescence. *Brain Res* 43: 429-435, 1972.

Borg JS, Vu MA, Badea C, Badea A, Johnson GA, and Dzirasa K. Localization of Metal Electrodes in the Intact Rat Brain Using Registration of 3D Microcomputed Tomography Images to a Magnetic Resonance Histology Atlas. *eNeuro* 2: 2015.

Borowska J, Jones CT, Zhang H, Blacklaws J, Goulding M, and Zhang Y. Functional subpopulations of V3 interneurons in the mature mouse spinal cord. *J Neurosci* 33: 18553-18565, 2013.

Brown PB, Koerber HR, and Yezierski RP. Cross-correlation analysis of connectivities among cat lumbosacral dorsal horn cells. *J Neurophysiol* 42: 1199-1211, 1979.

Brozoski TJ, Caspary DM, and Bauer CA. Marking multi-channel silicon-substrate electrode recording sites using radiofrequency lesions. *J Neurosci Methods* 150: 185-191, 2006.

Christakos CN, Cohen MI, Sica AL, Huang WX, See WR, and Barnhardt R. Analysis of recurrent laryngeal inspiratory discharges in relation to fast rhythms. *J Neurophysiol* 72: 1304-1316, 1994.

Cogan SF. Neural Stimulation and Recording Electrodes. *Annu Rev Biomed Eng* 10: 275-309, 2008.

Cohen MI. Discharge patterns of brain-stem respiratory neurons in relation to carbon dioxide tension. *J Neurophysiol* 31: 142-165, 1968.

Cregg JM, DePaul MA, Filous AR, Lang BT, Tran A, and Silver J. Functional regeneration beyond the glial scar. *Exp Neurol* 253: 197-207, 2014.

Davies JG, Kirkwood PA, and Sears TA. The detection of monosynaptic connexions from inspiratory bulbospinal neurones to inspiratory motoneurones in the cat. *J Physiol* 368: 33-62, 1985.

Deutsch K, and Hillman H. The effect of six fixatives on the areas of rabbit neurons and rabbit and rat cerebral slices. *J Microsc* 109: 303-309, 1977.

DiCarlo JJ, Lane JW, Hsiao SS, and Johnson KO. Marking microelectrode penetrations with fluorescent dyes. *J Neurosci Methods* 64: 75-81, 1996.

Dobbins EG, and Feldman JL. Brainstem network controlling descending drive to phrenic motoneurons in rat. *The Journal of comparative neurology* 347: 64-86, 1994.

Douse MA, and Duffin J. Axonal projections and synaptic connections of C5 segment expiratory interneurones in the cat. *The Journal of physiology* 470: 431-444, 1993.

Duffin J, and Iscoe S. The possible role of C5 segment inspiratory interneurons investigated by cross-correlation with phrenic motoneurons in decerebrate cats. *Exp Brain Res* 112: 35-40, 1996.

Fedorko L, Merrill EG, and Lipski J. Two descending medullary inspiratory pathways to phrenic motoneurones. *Neuroscience letters* 43: 285-291, 1983.

Fekete Z, Pálfi E, Márton G, Handbauer M, Zs B, Ulbert I, Pongrácz A, and Négyessy L. In Vivo Iontophoretic BDA Injection through a Buried Microfluidic Channel of a Neural Multielectrode. *Procedia Engineering* 120: 464-467, 2015.

Fung SH, Burstein D, and Born RT. In vivo microelectrode track reconstruction using magnetic resonance imaging. *J Neurosci Methods* 80: 215-224, 1998.

Furicchia JV, and Goshgarian HG. Dendritic organization of phrenic motoneurons in the adult rat. *Exp Neurol* 96: 621-634, 1987.

Galán RF, Dick TE, and Baekey DM. Analysis and modeling of ensemble recordings from respiratory pre-motor neurons indicate changes in functional network architecture after acute hypoxia. *Front Comput Neurosci* 4: 2010.

Gonzalez-Rothi EJ, Rombola AM, Rousseau CA, Mercier LM, Fitzpatrick GM, Reier PJ, Fuller DD, and Lane MA. Spinal interneurons and forelimb plasticity after incomplete cervical spinal cord injury in adult rats. *J Neurotrauma* 32: 893-907, 2015.

Goshgarian HG, and Rafols JA. The phrenic nucleus of th albino rat: a correlative HRP and Golgi study. *J Comp Neurol* 201: 441-456, 1981.

Haidarliu S, Sosnik R, and Ahissar E. Simultaneous multi-site recordings and iontophoretic drug and dye applications along the trigeminal system of anesthetized rats. *J Neurosci Methods* 94: 27-40, 1999.

Harkema SJ. Plasticity of interneuronal networks of the functionally isolated human spinal cord. *Brain research reviews* 57: 255-264, 2008.

Hayashi F, Hinrichsen CF, and McCrimmon DR. Short-term plasticity of descending synaptic input to phrenic motoneurons in rats. *J Appl Physiol* 94: 1421-1430, 2003.

Iscoe S, and Duffin J. Effects of stimulation of phrenic afferents on cervical respiratory interneurones and phrenic motoneurones in cats. *J Physiol* 497 (Pt 3): 803-812, 1996.

Jones DL. The Ucurrent. A professional precision current adapter for Multimeters. http://alternatezone.com/electronics/ucurrent/uCurrentArticle.pdf: 2010.

Kinkead R, Zhan WZ, Prakash YS, Bach KB, Sieck GC, and Mitchell GS. Cervical dorsal rhizotomy enhances serotonergic innervation of phrenic motoneurons and serotonin-dependent long-term facilitation of respiratory motor output in rats. *J Neurosci* 18: 8436-8443, 1998.

Kirkwood PA. On the use and interpretation of cross-correlation measurements in the mammalian central nervous system. *J Neurosci Methods* 1: 107-132, 1979.

Kirkwood PA, Munson JB, Sears TA, and Westgaard RH. Respiratory interneurones in the thoracic spinal cord of the cat. *J Physiol* 395: 161-192, 1988.

Kirkwood PA, Schmid K, Otto M, and Sears TA. Focal blockade of single unit synaptic transmission by iontophoresis of antagonists. *Neuroreport* 2: 185-188, 1991.

Kovacs P, Denes V, Kellenyi L, and Hernadi I. Microiontophoresis electrode location by neurohistological marking: Comparison of four native dyes applied from current balancing electrode channels. *Journal of pharmacological and toxicological methods* 51: 147-151, 2005.

Koyano KW, Machino A, Takeda M, Matsui T, Fujimichi R, Ohashi Y, and Miyashita Y. In vivo visualization of single-unit recording sites using MRI-detectable elgiloy deposit marking. *J Neurophysiol* 105: 1380-1392, 2011.

Lane MA. Spinal respiratory motoneurons and interneurons. *Respir Physiol Neurobiol* 179: 3-13, 2011.

Lane MA, Fuller DD, White TE, and Reier PJ. Respiratory neuroplasticity and cervical spinal cord injury: translational perspectives. *Trends in neurosciences* 31: 538-547, 2008a.

Lane MA, Lee KZ, Fuller DD, and Reier PJ. Spinal circuitry and respiratory recovery following spinal cord injury. *Respir Physiol Neurobiol* 169: 123-132, 2009.

Lane MA, Lee KZ, Salazar K, O'Steen BE, Bloom DC, Fuller DD, and Reier PJ. Respiratory function following bilateral mid-cervical contusion injury in the adult rat. *Experimental neurology* 235: 197-210, 2012.

Lane MA, White TE, Coutts MA, Jones AL, Sandhu MS, Bloom DC, Bolser DC, Yates BJ, Fuller DD, and Reier PJ. Cervical prephrenic interneurons in the normal and lesioned spinal cord of the adult rat. *J Comp Neurol* 511: 692-709, 2008b.

Lee KZ, and Fuller DD. Preinspiratory and inspiratory hypoglossal motor output during hypoxia-induced plasticity in the rat. *J Appl Physiol (1985)* 108: 1187-1198, 2010.

Lee KZ, Reier PJ, and Fuller DD. Phrenic motoneuron discharge patterns during hypoxia-induced short-term potentiation in rats. *Journal of neurophysiology* 102: 2184-2193, 2009.

Li PH, Gauthier JL, Schiff M, Sher A, Ahn D, Field GD, Greschner M, Callaway EM, Litke AM, and Chichilnisky EJ. Anatomical identification of extracellularly recorded cells in large-scale multielectrode recordings. *J Neurosci* 35: 4663-4675, 2015.

Lipski J, and Duffin J. An electrophysiological investigation of propriospinal inspiratory neurons in the upper cervical cord of the cat. *Experimental brain research* 61: 625-637, 1986.

Lipski J, Duffin J, Kruszewska B, and Zhang X. Upper cervical inspiratory neurons in the rat: an electrophysiological and morphological study. *Exp Brain Res* 95: 477-487, 1993.

Lipski J, Kubin L, and Jodkowski J. Synaptic action of R beta neurons on phrenic motoneurons studied with spike-triggered averaging. *Brain research* 288: 105-118, 1983.

Lois JH, Rice CD, and Yates BJ. Neural circuits controlling diaphragm function in the cat revealed by transneuronal tracing. *Journal of applied physiology* 106: 138-152, 2009.

Mahamed S, Strey KA, Mitchell GS, and Baker-Herman TL. Reduced respiratory neural activity elicits phrenic motor facilitation. *Respiratory physiology & neurobiology* 175: 303-309, 2011.

Mantilla CB, Zhan W-Z, and Sieck GC. Retrograde labeling of phrenic motoneurons by intrapleural injection. *J Neurosci Methods* 182: 244-249, 2009.

Marchenko V, Ghali MGZ, and Rogers RF. The role of spinal GABAergic circuits in the control of phrenic nerve motor output. *Am J Physiol Regul Integr Comp Physiol* 308: R916-926, 2015.

Matsui T, Koyano KW, Koyama M, Nakahara K, Takeda M, Ohashi Y, Naya Y, and Miyashita Y. MRI-based localization of electrophysiological recording sites within the cerebral cortex at single-voxel accuracy. *Nat Methods* 4: 161-168, 2007.

Melssen WJ, and Epping WJM. Detection and estimation of neural connectivity based on crosscorrelation analysis. *Biol Cybern* 57: 403-414, 1987.

Mitchell GS, Sloan HE, Jiang C, Miletic V, Hayashi F, and Lipski J. 5-Hydroxytryptophan (5-HTP) augments spontaneous and evoked phrenic motoneuron discharge in spinalized rats. *Neurosci Lett* 141: 75-78, 1992.

Moore GP, Segundo JP, Perkel DH, and Levitan H. Statistical signs of synaptic interaction in neurons. *Biophys J* 10: 876-900, 1970.

Morris KFA, A.Shannon, R. Lindsey, B.G. Long-term facilitation of phrenic nerve activity in the cat: responses and short-time scale correlations of medullary neurones. *Journal of Physiology* 490: 463–480, 1996.

Márton G, Baracskay P, Cseri B, Plósz B, Juhász G, Fekete Z, and Pongrácz A. A silicon-based microelectrode array with a microdrive for monitoring brainstem regions of freely moving rats. *J Neural Eng* 13: 026025, 2016.

Naselaris T, Merchant H, Amirikian B, and Georgopoulos AP. Spatial reconstruction of trajectories of an array of recording microelectrodes. *J Neurophysiol* 93: 2318-2330, 2005.

Nelson JR. Single unit activity in medullary respiratory centers of cat. *J Neurophysiol* 22: 590-598, 1959.

Nuding SC, Segers LS, Iceman KE, O'Connor R, Dean JB, Bolser DC, Baekey DM, Dick TE, Shannon R, Morris KF, and Lindsey BG. Functional connectivity in raphé-pontomedullary circuits supports active suppression of breathing during hypocapnic apnea. *J Neurophysiol* 114: 2162-2186, 2015.

Palisses R, Persegol L, and Viala D. Evidence for respiratory interneurones in the C3-C5 cervical spinal cord in the decorticate rabbit. *Exp Brain Res* 78: 624-632, 1989.

Prakash YS, Mantilla CB, Zhan WZ, Smithson KG, and Sieck GC. Phrenic motoneuron morphology during rapid diaphragm muscle growth. *J Appl Physiol (1985)* 89: 563-572, 2000.

Prut Y, and Perlmutter SI. Firing properties of spinal interneurons during voluntary movement. I. State-dependent regularity of firing. *J Neurosci* 23: 9600-9610, 2003.

Quester R, and Schröder R. The shrinkage of the human brain stem during formalin fixation and embedding in paraffin. *J Neurosci Methods* 75: 81-89, 1997.

Ruscheweyh R, and Sandkühler J. Lamina-specific membrane and discharge properties of rat spinal dorsal horn neurones in vitro. *J Physiol* 541: 231-244, 2002.

Sandhu MS, Baekey DM, Maling NG, Sanchez JC, Reier PJ, and Fuller DD. Midcervical neuronal discharge patterns during and following hypoxia. *J Neurophysiol* 113: 2091-2101, 2015.

Sengul G, Watson C, Tanaka I, and Paxinos G. *Atlas of the Spinal Cord*. Academic Press, 2012, p. 360.

Speck DF, and Revelette WR. Attenuation of phrenic motor discharge by phrenic nerve afferents. *J Appl Physiol* 62: 941-945, 1987.

Sperry MA, and Goshgarian HG. Ultrastructural changes in the rat phrenic nucleus developing within 2 h after cervical spinal cord hemisection. *Experimental neurology* 120: 233-244, 1993.

Spinelli DN. Silver tipped metal microelectrodes: a new method for recording and staining single neurones. *Brain Res* 91: 271-275, 1975.

Streeter KA, and Baker-Herman TL. Decreased spinal synaptic inputs to phrenic motor neurons elicit localized inactivity-induced phrenic motor facilitation. *Exp Neurol* 256: 46-56, 2014a.

Streeter KA, and Baker-Herman TL. Spinal NMDA receptor activation constrains inactivity-induced phrenic motor facilitation in Charles River Sprague Dawley rats. *J Appl Physiol (1985)* 2014b.

Strey KA, Nichols NL, Baertsch NA, Broytman O, and Baker-Herman TL. Spinal atypical protein kinase C activity is necessary to stabilize inactivity-induced phrenic motor facilitation. *J Neurosci* 32: 16510-16520, 2012.

Townsend G, Peloquin P, Kloosterman F, Hetke JF, and Leung LS. Recording and marking with silicon multichannel electrodes. *Brain Res Brain Res Protoc* 9: 122-129, 2002.

Wolf HK, Buslei R, Schmidt-Kastner R, Schmidt-Kastner PK, Pietsch T, Wiestler OD, and Blümcke I. NeuN: a useful neuronal marker for diagnostic histopathology. *J Histochem Cytochem* 44: 1167-1171, 1996.

Yates BJ, Smail JA, Stocker SD, and Card JP. Transneuronal tracing of neural pathways controlling activity of diaphragm motoneurons in the ferret. *Neuroscience* 90: 1501-1513, 1999.

Zhan WZ, Ellenberger HH, and Feldman JL. Monoaminergic and GABAergic terminations in phrenic nucleus of rat identified by immunohistochemical labeling. *Neuroscience* 31: 105-113, 1989.

Figure 1

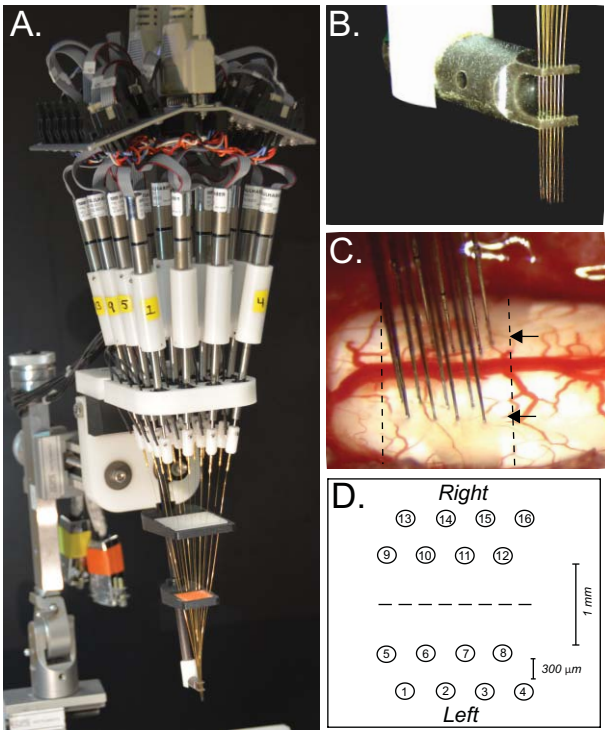

Figure 2

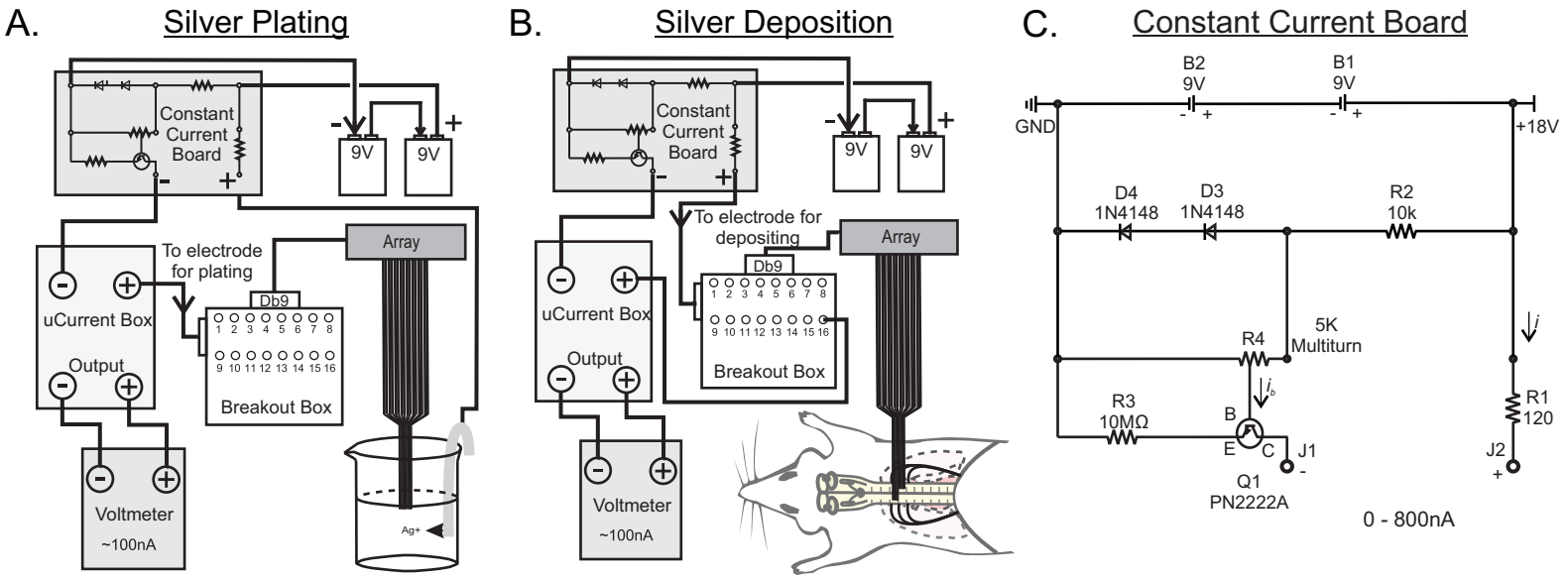
A.
Silver Plating
Constant Current Board
9V
9V
To electrode for plating
Array
uCurrent Box
Output
Db9
1 2 3 4 5 6 7 8
9 10 11 12 13 14 15 16
Breakout Box
Voltmeter
~100nA
Ag+
B.
Silver Deposition
Constant Current Board
9V
9V
To electrode for depositing
Array
Db9
uCurrent Box
Output
Breakout Box
Voltmeter
~100nA
C.
Constant Current Board
B2
9V
B1
9V
GND
+18V
D4
1N4148
D3
1N4148
R2
10k
R4
5K
Multiturn
R3
10MΩ
B
E
C
J1
Q1
PN2222A
R1
120
J2
0 - 800nA

Figure 3

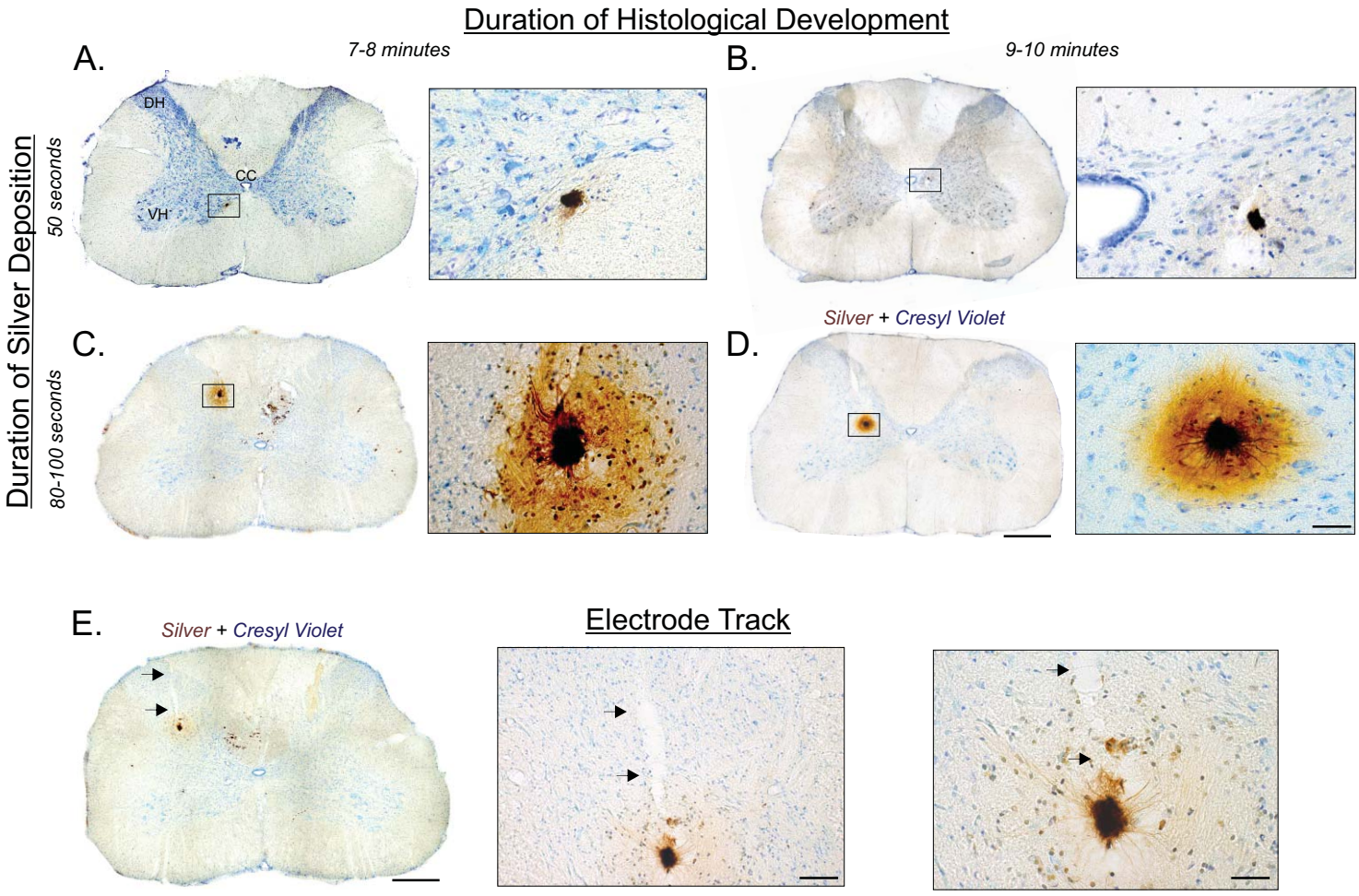
Duration of Histological Development
A.
7-8 minutes
B.
9-10 minutes
Duration of Silver Deposition
50 seconds
80-100 seconds
DH
CC
VH
C.
D.
Silver + Cresyl Violet
E.
Silver + Cresyl Violet
Electrode Track

Figure 4

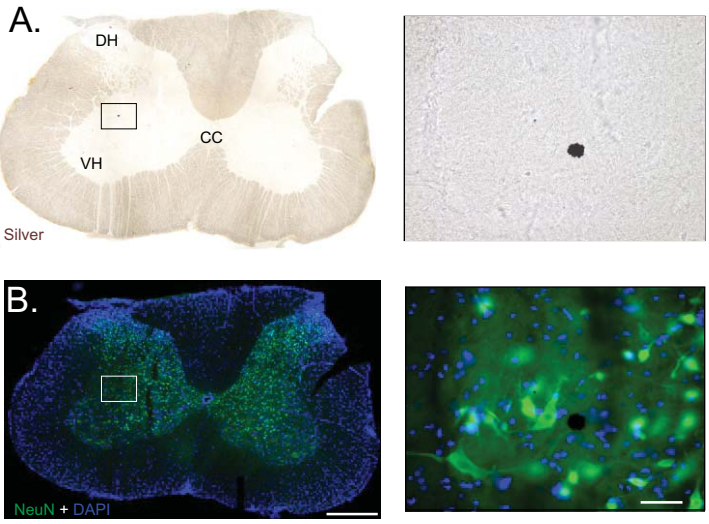

Figure 5

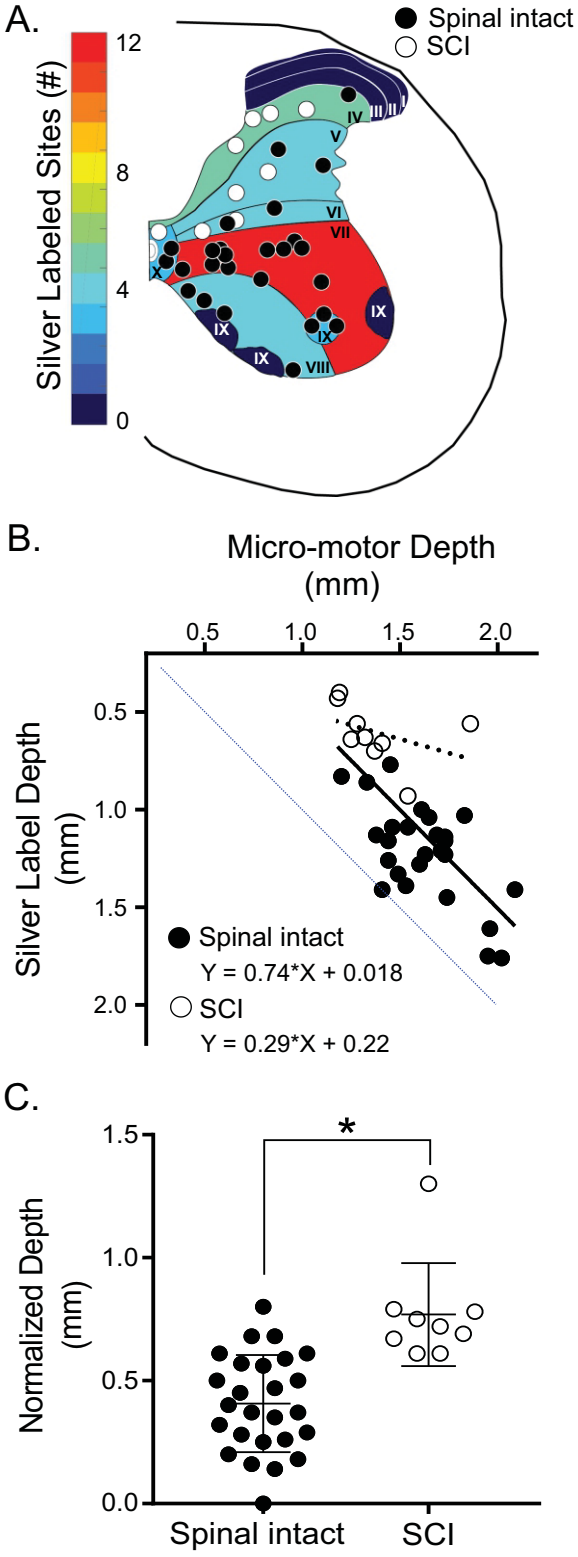
A.
Spinal intact
SCI
Silver Labeled Sites (#)
12
8
4
0
III/II
IV
V
VI
VII
VIII
IX
X
B.
Micro-motor Depth (mm)
0.5
1.0
1.5
2.0
Silver Label Depth (mm)
Spinal intact
Y = 0.74*X + 0.018
SCI
Y = 0.29*X + 0.22
C.
Normalized Depth (mm)
1.5
1.0
0.5
0.0
*
Spinal intact
SCI

Figure 6

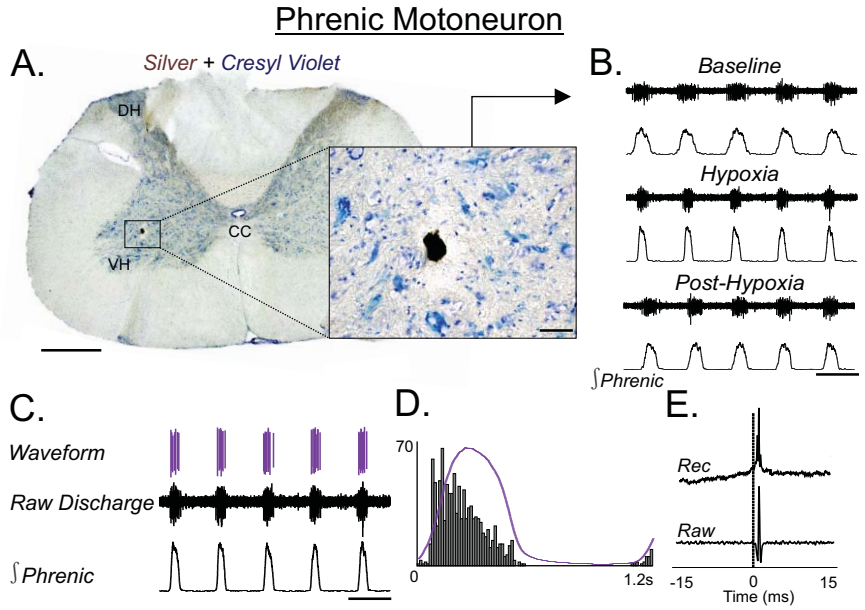
Phrenic Motoneuron
A.
Silver + Cresyl Violet
DH
CC
VH
B.
Baseline
Hypoxia
Post-Hypoxia
∫Phrenic
C.
Waveform
Raw Discharge
∫Phrenic
D.
70
0
1.2s
E.
Rec
Raw
-15
0
15
Time (ms)

Figure 7

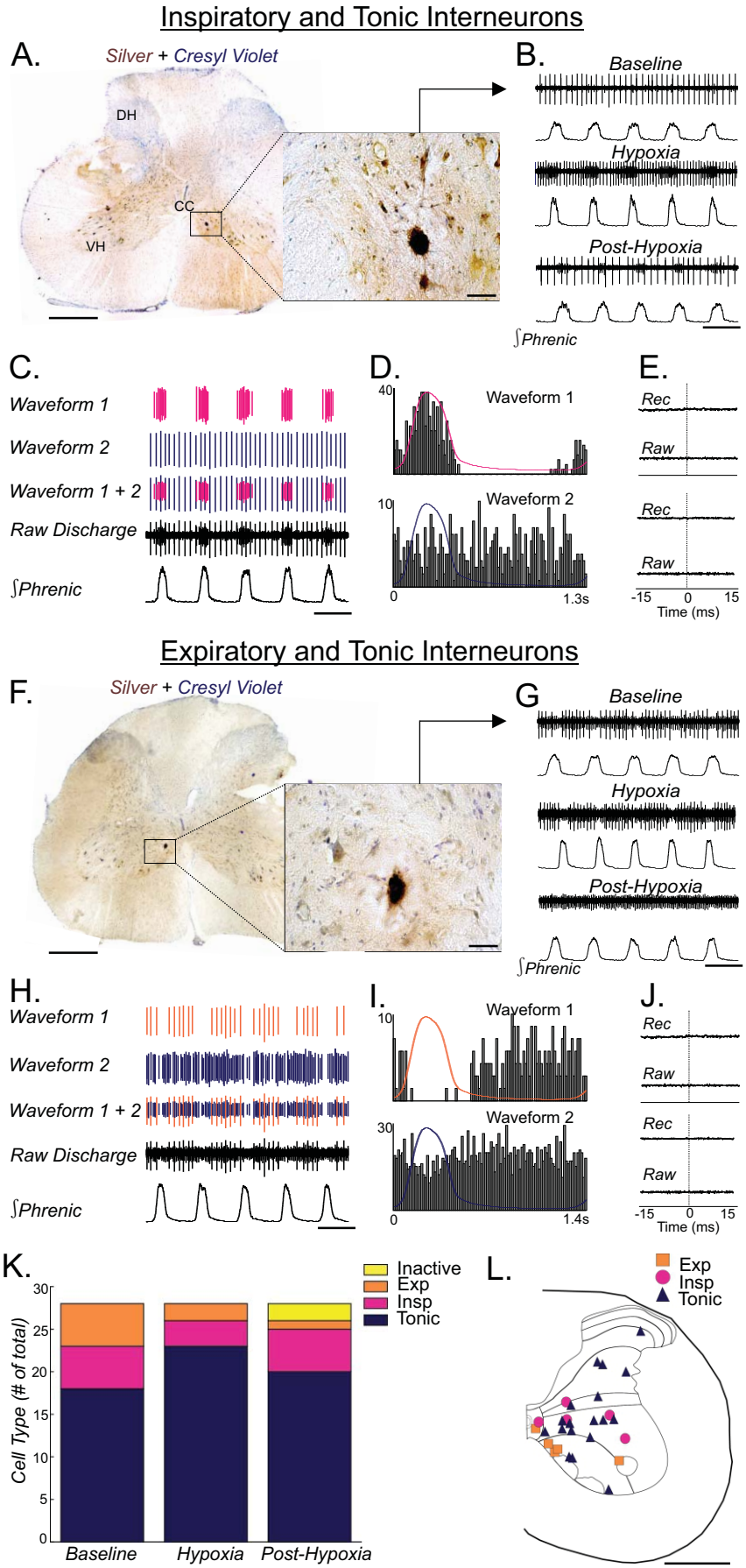
Inspiratory and Tonic Interneurons
A.
Silver + Cresyl Violet
DH
CC
VH
B.
Baseline
Hypoxia
Post-Hypoxia
∫Phrenic
C.
Waveform 1
Waveform 2
Waveform 1 + 2
Raw Discharge
∫Phrenic
D.
40
Waveform 1
10
Waveform 2
0
1.3s
E.
Rec
Raw
Rec
Raw
-15
0
15
Time (ms)
Expiratory and Tonic Interneurons
F.
Silver + Cresyl Violet
G.
Baseline
Hypoxia
Post-Hypoxia
∫Phrenic
H.
Waveform 1
Waveform 2
Waveform 1 + 2
Raw Discharge
∫Phrenic
I.
10
Waveform 1
30
Waveform 2
0
1.4s
J.
Rec
Raw
Rec
Raw
-15
0
15
Time (ms)
K.
Inactive
Exp
Insp
Tonic
Cell Type (# of total)
30
25
20
15
10
5
0
Baseline
Hypoxia
Post-Hypoxia
L.
Exp
Insp
Tonic

Figure 8

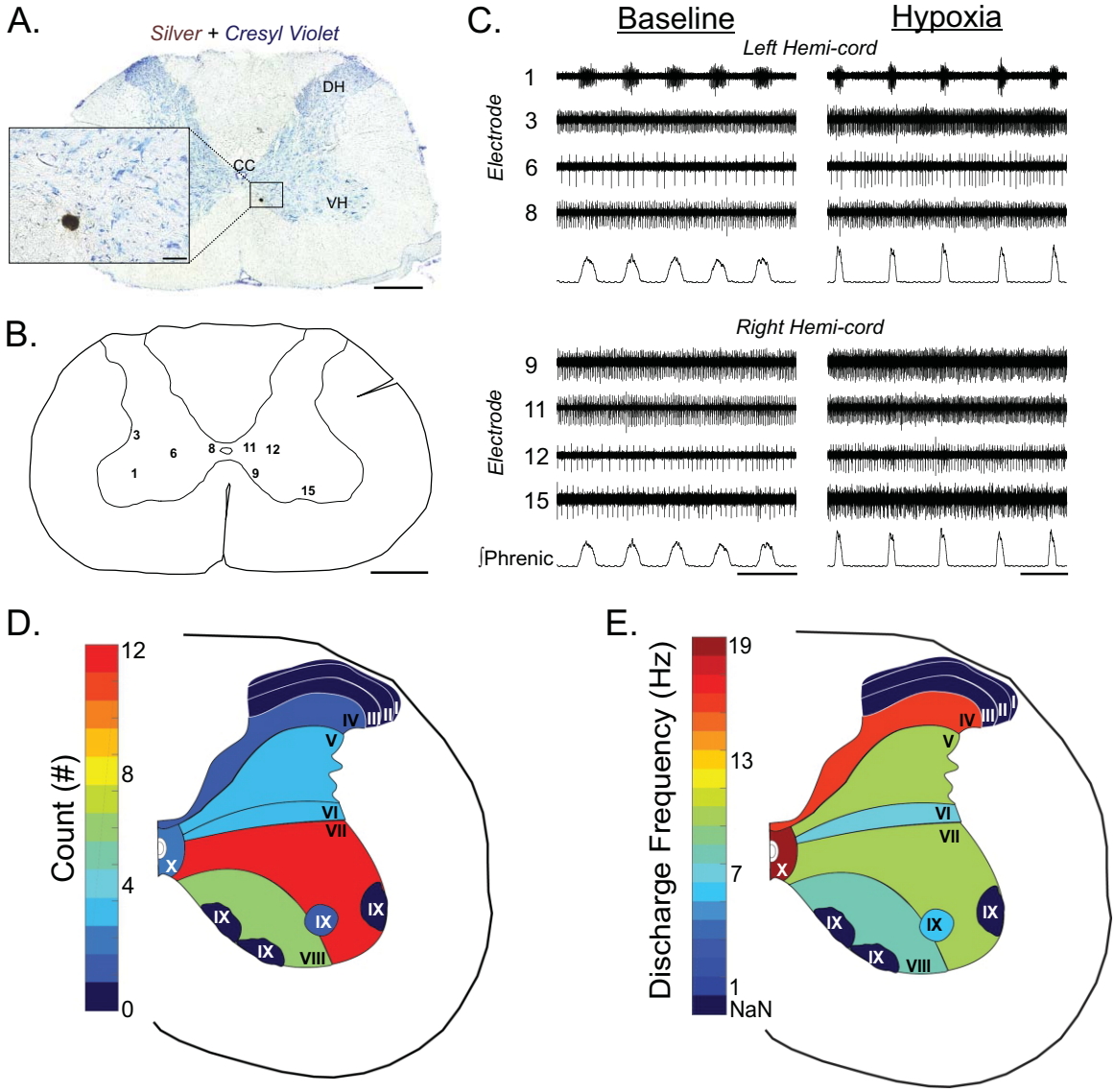
A.
Silver + Cresyl Violet
DH
CC
VH
B.
3
6
8
11
12
1
9
15
C.
Baseline
Hypoxia
Left Hemi-cord
Electrode
1
3
6
8
Right Hemi-cord
Electrode
9
11
12
15
∫Phrenic
D.
Count (#)
12
8
4
0
IV
III
II
V
VI
VII
X
IX
IX
IX
IX
VIII
E.
Discharge Frequency (Hz)
19
13
7
1
NaN
IV
III
II
V
VI
VII
X
IX
IX
IX
IX
VIII

Figure 9

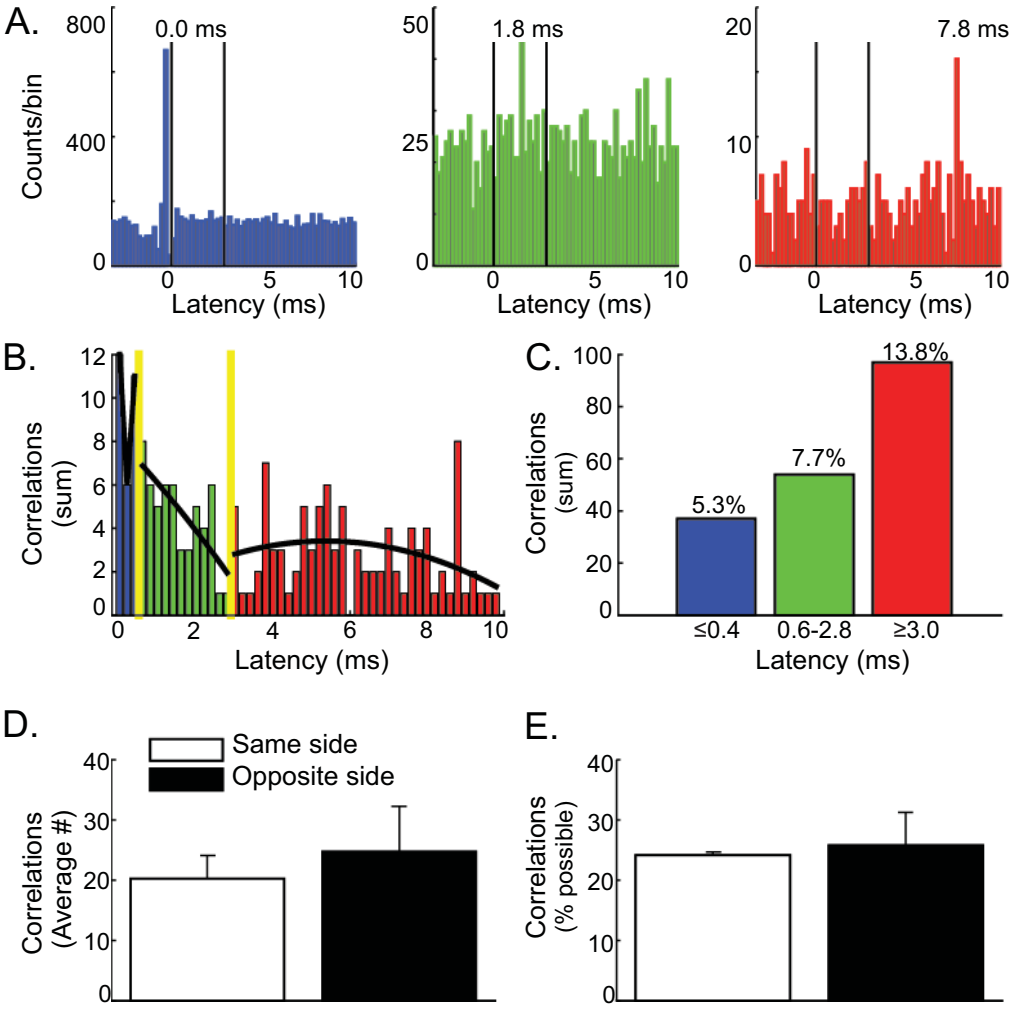
A.
0.0 ms
1.8 ms
7.8 ms
Counts/bin
Latency (ms)
B.
Correlations (sum)
Latency (ms)
C.
Correlations (sum)
5.3%
7.7%
13.8%
≤0.4
0.6-2.8
≥3.0
Latency (ms)
D.
Same side
Opposite side
Correlations (Average #)
E.
Correlations (% possible)

Figure 10

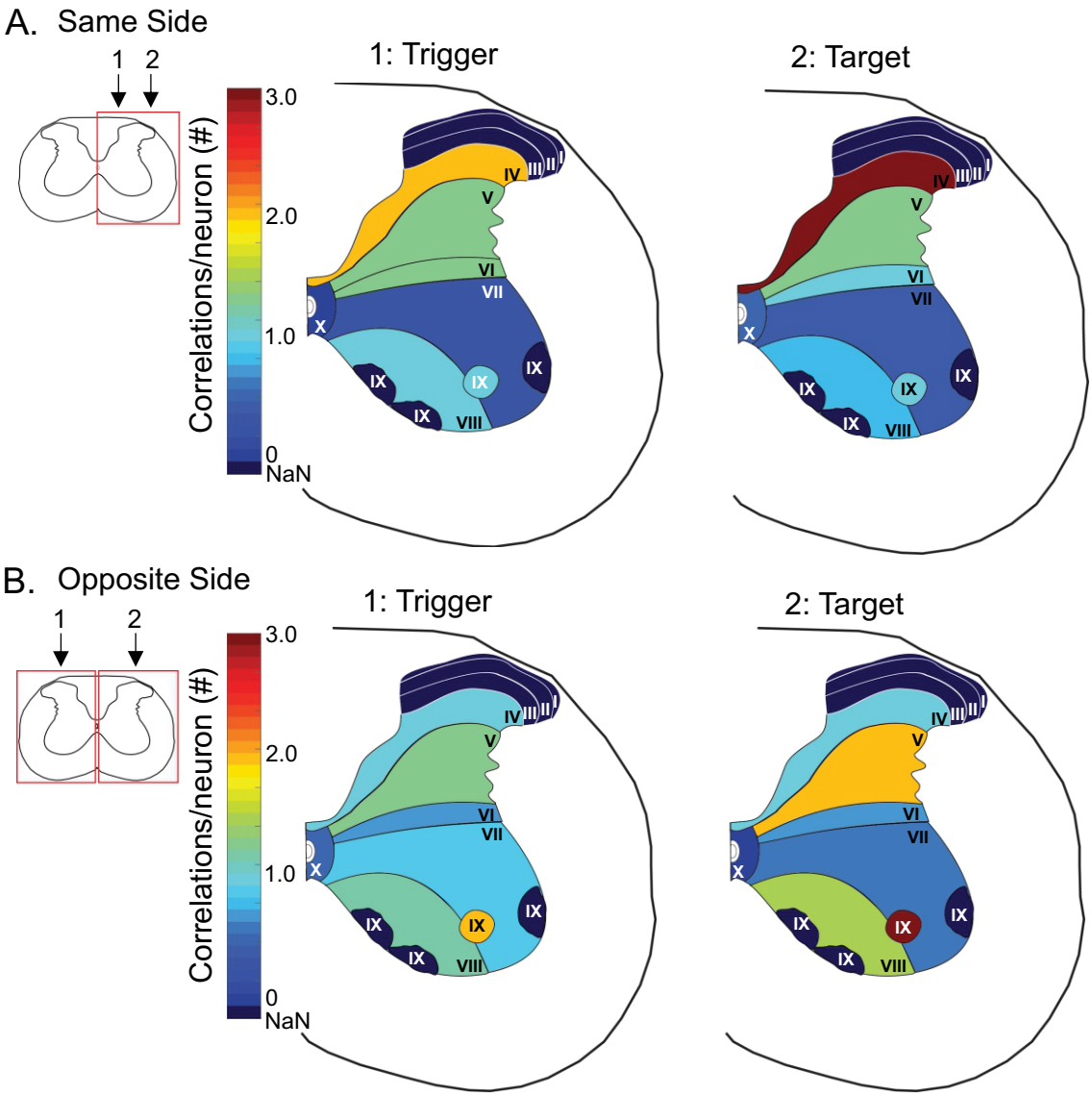
A. Same Side
1 2
1: Trigger
2: Target
Correlations/neuron (#)
3.0
2.0
1.0
0
NaN
I II III IV V VI VII VIII IX X
B. Opposite Side
1 2
1: Trigger
2: Target
Correlations/neuron (#)
3.0
2.0
1.0
0
NaN
I II III IV V VI VII VIII IX X

Table 1.

Dish no.	*Contents*	*Time*	*Volume/1 tray*
1	dH_2O	5 min	150mL/dish
2	dH_2O	5 min	150mL/dish
3*	1% $(NH_4)_2S$	5 min	48mL/tray
4*#	0.125% H_2O_2	5 min	48mL/tray
5	dH_2O	5 min	150mL/dish
6	dH_2O	5 min	150mL/dish
7*	1% ascorbic acid	5 min	48mL/tray
8	dH_2O	5 min	150mL/dish
9	dH_2O	5 min	150mL/dish
10*#	**Developer**	8 min	
	25% acacia		16mL
	2% hydroquinone, 5% citric acid		16mL
	1% $AgNO_2$		16mL
			48mL/tray
11	dH_2O	Quick rinse	150mL/dish
12	dH_2O	Quick rinse	150mL/dish
13	dH_2O	Quick rinse	150mL/dish
14	1% $Na_2S_2O_4$. $2H_2O$	3-4 min	150mL/dish
15	dH_2O	Quick rinse	150mL/dish

Store in dH_2O at 4°C until ready to mount on charged slides, then counterstain, and cover with mounting medium.

(*) Place solution in a 12-well tray.

(#) Light sensitive solutions.

☐ Change solution every 3 times.

▒ Change solutions every time.